

Gauge-Fixed Wannier Wave-Functions for Fractional Topological Insulators

Yang-Le Wu,¹ N. Regnault,^{1,2} and B. Andrei Bernevig¹

¹*Department of Physics, Princeton University, Princeton, NJ 08544*

²*Laboratoire Pierre Aigrain, ENS and CNRS, 24 rue Lhomond, 75005 Paris, France*

We propose an improved scheme to construct many-body trial wave functions for fractional Chern insulators (FCI), using one-dimensional localized Wannier basis. The procedure borrows from the original scheme on a continuum cylinder, but is adapted to finite-size lattice systems with periodic boundaries. It fixes several issues of the continuum description that made the overlap with the exact ground states insignificant. The constructed lattice states are translationally invariant, and have the correct degeneracy as well as the correct relative and total momenta. Our prescription preserves the (possible) inversion symmetry of the lattice model, and is isotropic in the limit of flat Berry curvature. By relaxing the maximally localized hybrid Wannier orbital prescription, we can form an orthonormal basis of states which, upon gauge fixing, can be used in lieu of the Landau orbitals. We find that the exact ground states of several known FCI models at $\nu = 1/3$ filling are well captured by the lattice states constructed from the Laughlin wave function. The overlap is higher than 0.99 in some models when the Hilbert space dimension is as large as 3×10^4 in each total momentum sector.

PACS numbers: 73.43.-f, 71.10.Fd, 03.65.Vf, 03.65.Ud

I. INTRODUCTION

The Chern insulator¹ is the first and simplest example of a topological insulator. It is defined by a non-zero Chern number of the occupied bands. It exhibits an integer Hall conductance similar to the integer quantum Hall effect but at zero overall magnetic field. Recently, several groups added interactions to the one-body topological (Chern) insulator problem and reported²⁻⁷ strongly-correlated phases similar to the Fractional Quantum Hall (FQH) effect. These fractional Chern insulators (FCI) have a partially filled band with non-zero Chern number and develop, similar to the FQH case, strongly correlated topological phases at specific values of ν of the filling factor.

At filling $\nu = 1/q$ ($q = 3, 5$ for fermions^{2-5,7}, $q = 2, 4$ for bosons⁶), a phase similar to the Laughlin state⁸ has been observed in numerical studies through several signatures. First, the system has q -fold quasi-degenerate ground states at filling $\nu = 1/q$, separated by a finite energy gap from higher excitations. Second, twisted boundary conditions drive spectral flow within the ground state manifold, showing a Hall conductance $\sigma_{xy} = e^2/(qh)$. Third, the excitations from the topological ground state resemble the FQH quasiholes,^{4,7} identified by the counting⁹ of low-lying levels in the gapped energy and entanglement spectra.¹⁰

Despite the similarity of the emergent features, the FCI and the FQH effects are hosted by substantially different systems. The FQH effects are typically observed in two-dimensional electron gas. This continuum system allows a holomorphic description, and the variational trial wave functions can be characterized by the asymptotic behavior when particles approach each other.^{11,12} In sharp contrast, the Chern insulators are defined on a discrete lattice, and its continuum limit is different from the FQH effect.^{13,14} This obstructs attempts to build model wave

functions using the asymptotic behavior.

An open question is thus *to what extent and in what form the FCI can be described by the FQH physics*. In this paper we provide a generic scheme to compare FQH and FCI wave functions at finite size. In particular, we address the fermionic FCI phase at filling $\nu = 1/3$ and clarify its relation to the Laughlin state.

The first step in this direction was made by Qi in Ref. 15. The one-dimensional maximally localized Wannier states are plane waves localized in the direction perpendicular to propagation. They form an alternative basis in a topological flat band, and they resemble the Landau orbitals in the lowest Landau level (LLL) in the continuum. The central, elegant idea of Ref. 15 is to exploit this similarity and transcribe FQH wave functions written in the second-quantized form to the FCI system. The two-dimensional (2D) fractional topological insulator (FTI) system was similarly analyzed using decoupled FQH states in the Wannier basis.

Upon closer inspection, the original proposal suffers from several issues that prevent direct application of this scheme to make contact with existing numerical studies. The formalism in Ref. 15 was built upon a smooth gauge in the continuum. This poses technical challenges for numerical implementation on a finite-size lattice, and conceptually, the one-dimensional (1D) *maximally* localized Wannier states are orthogonal to each other *only in the continuum limit*. The non-orthogonality at finite size spoils the translational invariance of the constructed many-body states. More importantly, the maximally localized Wannier orbital to LLL mapping in Ref. 15 is a mapping between the basis states of two *separate* systems. The two sets of basis states have *independent gauge freedoms*. Merely introducing a 1D relabeling of the Wannier states is not enough to properly fix the mapping from a Chern insulator to the LLL. A naive implementation of the formulas in Ref. 15 results in variational states very

low overlaps (lower than 0.04 for a system of 8 particles on a 6×4 lattice) with the exact diagonalization ground states of the two-orbital model discussed therein.

In this paper, we build upon Ref. 15 and provide an improved prescription for constructing FCI wave functions using gauge-fixed (non-maximally) localized Wannier states, with large overlap with the exact diagonalization ground states. Our procedure is defined on a lattice of finite size with periodic boundary conditions in both directions. We do not need gauge smoothing, and we trade maximal localization for the orthogonality between the 1D localized Wannier states at finite size. We explicitly fix the phase choice of the Wannier states so that it best matches that of the Landau orbitals. Our prescription keeps both the center-of-mass translational symmetry and the inversion symmetry at the many-body level, and it implements the folding rule⁹ that accounts for the total momenta of the degenerate FCI ground states on a torus. We also show that, in our prescription, using the Wannier bases localized in either x or y directions produces the same set of many-body states in the limit of flat Berry curvature.

As a numerical test, we construct the Laughlin state for several FCI models at filling $\nu = 1/3$. In all cases, the lattice Laughlin states have very high overlap with the ground states, and their entanglement spectra share the same gapped structure. The overlap for the best FCI models found so far⁷ reaches 0.99 for a system of 8 particles on a 6×4 lattice, of which the Hilbert space dimension is as large as 3×10^4 in each total momentum sector. Our results provide the first *direct, quantitative* evidence that the fractionalized phase in Chern insulators at $\nu = 1/3$ can be well approximated by the Laughlin state.

The paper is organized as follows. In Sec. II we discuss the many-body translational symmetries¹⁶ of the torus FQH states in the continuum. We construct a recombined set of degenerate FQH states that allow a direct mapping to the lattice. Sec. III summarizes with the basic properties of the 1D localized Wannier states on a lattice. Except for a few subtleties, this discussion is similar to the one in Ref. 15.

In Sec. IV describes the Wannier construction of the many-body FQH states on a lattice. We elaborate upon the *phase* choice of the 1D localized Wannier states. We show that the resulting many-body states are translationally invariant in both directions. We also demonstrate that the counting of the q -fold states in each momentum sector agrees with the counting rule proposed in Ref. 9. Eq. (70) provides an explicit and ready-to-use formula to rewrite *any FQH wave function* in a given Chern insulator model.

Sec. V shows that our prescription preserves inversion symmetry on the many-body level when such symmetry exists at the single-particle level. Sec. VI presents the numerical verification that the ground states of various FCI models are well approximated by the Laughlin state constructed using our prescription. We also examine how

close our phase choice for the Wannier basis is from the absolute ideal by a brute-force optimization. Sec. VII examines the isotropy of the Wannier construction. We prove that the many-body lattice states constructed using the Wannier bases localized in either direction are the same in the limit of flat Berry curvature. The isotropy in the presence of curvature fluctuations is tested numerically. Sec. VIII concludes the paper and discusses a few future directions.

II. FQH TRANSLATIONAL SYMMETRIES

It is instructive to review the many-body translational symmetries of the FQH system in the continuum. We begin by recapitulating the main results of the PRL¹⁶ by Haldane.

We study the problem of N_e electrons moving on a *twisted* torus with a perpendicular magnetic field. The twisted torus can be represented by a parallelogram with opposite edges identified. We set up a Cartesian coordinate system (\tilde{x}, \tilde{y}) , with orthonormal basis vectors (\hat{e}_x, \hat{e}_y) . The tilde over \tilde{x} and \tilde{y} emphasizes the continuous nature of these variables. We consider the torus spanned by $\mathbf{L}_1 = L_1 \hat{e}_x$ and $\mathbf{L}_2 = L_2 \hat{e}_y$ (see Fig. 1).⁵⁶ Here, L_1 and L_2 are the length of the two fundamental cycles of the torus, and the unit vector \hat{e}_v is defined by $\hat{e}_v = \sin \theta \hat{e}_x + \cos \theta \hat{e}_y$, where the twist angle $\theta \in (0, \pi)$ is the angle between the two fundamental cycles. The rectangular torus corresponds to $\theta = \pi/2$. We introduce the normal unit vector $\hat{e}_z \equiv \hat{e}_x \times \hat{e}_y$, and define the reciprocal primitive vectors

$$\mathbf{G}_1 = 2\pi \hat{e}_x / (L_1 \sin \theta), \quad \mathbf{G}_2 = 2\pi (\hat{e}_y - \cot \theta \hat{e}_x) / L_2. \quad (1)$$

They satisfy $\mathbf{G}_a \cdot \mathbf{L}_b = 2\pi \delta_{ab}$ for $a, b \in \{1, 2\}$.

The torus is pierced by a magnetic field in the $-\hat{e}_z$ direction, $\mathbf{B} = \nabla \times \mathbf{A} = B \hat{e}_z$ with $B < 0$. The Hamiltonian of the interacting electrons reads

$$H = \sum_i \frac{[-i\hbar \nabla_i - e\mathbf{A}(\tilde{\mathbf{r}}_i)]^2}{2m} + \sum_{i < j} V(\tilde{\mathbf{r}}_i - \tilde{\mathbf{r}}_j). \quad (2)$$

We denote by $e < 0$ the charge of the electron. The magnetic length is $l_B = \sqrt{\hbar / (eB)}$. The total number of fluxes N_ϕ penetrating the torus has to be an integer, given by $L_1 L_2 \sin \theta = 2\pi l_B^2 N_\phi$. We define $N = \text{GCD}(N_e, N_\phi)$, where GCD stands for the Greatest Common Divisor. Then $p \equiv N_e / N$ and $q \equiv N_\phi / N$ are coprime.

The magnetic translation operator of a single particle is defined by $T(\mathbf{a}) = e^{-i\mathbf{a} \cdot \mathbf{K} / \hbar}$, where $\mathbf{K} = -i\hbar \nabla - e\mathbf{A}(\tilde{\mathbf{r}}) + e\mathbf{B} \times \tilde{\mathbf{r}}$ is the guiding center momentum of the i -th particle. We pick Landau gauge $\mathbf{A}(\tilde{x}, \tilde{y}) = B\tilde{x} \hat{e}_y$, and impose periodic (not twisted) boundary conditions $T(\mathbf{L}_a) = 1$, $a = 1, 2$. The wave functions $\langle \tilde{x}, \tilde{y} | j \rangle$ of the N_ϕ single-particle states in the LLL are given by

$$\phi_j(\tilde{x}, \tilde{y}) = \frac{1}{(\sqrt{\pi}L_2l_B)^{1/2}} \sum_n^{\mathbb{Z}} \exp \left[2\pi(j + nN_\phi) \frac{\tilde{x} + i\tilde{y}}{L_2} - i \frac{\pi}{N_\phi} \frac{L_1 e^{-i\theta}}{L_2} (j + nN_\phi)^2 \right] e^{-\tilde{x}^2/(2l_B^2)}. \quad (3)$$

where the state index j is an integer defined modulo N_ϕ .

We can decompose the translation operator of the i -th electron, $T_i(\mathbf{a})$, into a relative part and a center-of-mass part, $T_i(\mathbf{a}) = T_{\text{rel},i}(\mathbf{a})T_{\text{cm}}(\mathbf{a}/N_e)$, where

$$T_{\text{rel},i}(\mathbf{a}) = T_i(\mathbf{a}) \prod_j^{N_e} T_j(-\frac{\mathbf{a}}{N_e}), \quad T_{\text{cm}}(\mathbf{a}) = \prod_j^{N_e} T_j(\mathbf{a}). \quad (4)$$

Here and hereafter throughout the paper, we use shorthand notation for products and summations:

$$\prod_i^M \equiv \prod_{i=0}^{M-1}, \quad \sum_i^M \equiv \sum_{i=0}^{M-1}. \quad (5)$$

We are particularly interested in the following translation operators and we define the shorthand notations

$$\begin{aligned} T_{\text{rel},i}^x &= T_{\text{rel},i}(p\mathbf{L}_1), & T_{\text{rel},i}^y &= T_{\text{rel},i}(p\mathbf{L}_2), \\ T_{\text{cm}}^x &= T_{\text{cm}}(\mathbf{L}_1/N_\phi), & T_{\text{cm}}^y &= T_{\text{cm}}(\mathbf{L}_2/N_\phi). \end{aligned} \quad (6)$$

Thanks to the periodic boundary condition, we can drop the particle index i from the relative translation operators, since $T_{\text{rel},i}^x = [(T_{\text{cm}}^x)^q]^\dagger$ and $T_{\text{rel},i}^y = [(T_{\text{cm}}^y)^q]^\dagger$ do not depend on the particle index.

The operators T_{rel}^x and T_{cm}^y , and of course T_{rel}^y being a power of T_{cm}^y , commute with each other and the Hamiltonian H .¹⁶ We use them to block-diagonalize the Hamiltonian into momentum sectors labeled by two-dimensional (2D) wave numbers (κ_x, κ_y) in an $N \times N_\phi$ Brillouin zone, defined by the eigenvalues⁵⁷

$$T_{\text{rel}}^x = e^{i2\pi\kappa_x/N}, \quad T_{\text{cm}}^y = e^{-i2\pi\kappa_y/N_\phi}. \quad (7)$$

The operator T_{cm}^x commutes with T_{rel}^x and H , but not with T_{cm}^y :

$$T_{\text{cm}}^y T_{\text{cm}}^x = T_{\text{cm}}^x T_{\text{cm}}^y e^{-i2\pi p/q}. \quad (8)$$

Therefore, the many-body energy eigenstates can be grouped into q -fold center-of-mass multiplets; the q states in each multiplet can be transversely by successive applications of T_{cm}^x and they share the same energy and the value of κ_x and $\kappa_y \bmod N$.

We set the cyclotron energy to infinity and focus on the states in the LLL. In this approximation, the many-body Hilbert space is spanned by the occupation-number basis states (Slater determinants) constructed from the LLL states $|j\rangle$, and the projected interacting Hamiltonian is given in Appx. A. We use the curly braces $\{\cdot\}$ to denote a list of quantum numbers for the N_e electrons. For succinctness, we always omit the electron indices from $\{\cdot\}$ and related expressions.

Now we are in a position to establish a concrete representation of the many-body translation algebra. The basis states in the LLL are $|\{j\}\rangle \equiv |j_0, j_1, \dots, j_{N_e-1}\rangle$ with an implied anti-symmetrization. The action of the many-body translation operators reads⁹

$$\begin{aligned} T_{\text{rel}}^x |\{j\}\rangle &= |\{j - q\}\rangle, & T_{\text{rel}}^y |\{j\}\rangle &= e^{i2\pi \sum j/N} |\{j\}\rangle, \\ T_{\text{cm}}^x |\{j\}\rangle &= |\{j + 1\}\rangle, & T_{\text{cm}}^y |\{j\}\rangle &= e^{-i2\pi \sum j/N_\phi} |\{j\}\rangle. \end{aligned} \quad (9)$$

Here the sum $\sum j$ runs over all the particles, and the state $|\{j + l\}\rangle$ is obtained from $|\{j\}\rangle$ by shifting the j quantum number of each particle by l . As expected, the relative and the center-of-mass translations are related by the periodic boundary conditions, $T_{\text{rel}}^x = [(T_{\text{cm}}^x)^q]^\dagger$, $T_{\text{rel}}^y = [(T_{\text{cm}}^y)^q]^\dagger$.

A. Recombination of the q -Fold States

It has been suggested that the FCI with $|C| = 1$ on an $N_x \times N_y$ lattice corresponds to a FQH system with flux $N_\phi = N_x N_y$.^{9,15} We now look for an alternative representation of the many-body translational symmetries with a Brillouin zone commensurate to the lattice system, in preparation for the analysis of the translational symmetry of the Wannier construction in Sec. IV C. We emphasize that we are still working in the continuum and we are merely providing another representation of the center-of-mass translation algebra. The integers N_x and N_y should be understood as a factorization of N_ϕ at this stage.

Following Ref. 9, we define the integers $N_{0x} = \text{GCD}(N_e, N_x)$, $N_{0y} = \text{GCD}(N_e, N_y)$, and $p_x = N_e/N_{0x}$, $p_y = N_e/N_{0y}$, $q_x = N_x/N_{0x}$, $q_y = N_y/N_{0y}$. Obviously p_x, q_x are coprime, so are p_y, q_y . Less obviously, $q_x q_y$ divides q ,⁹ and thus p, q_x are coprime, so are p, q_y . We define the translation operators⁵⁸

$$S_x = (T_{\text{cm}}^x)^{q/q_x}, \quad R_y = (T_{\text{cm}}^y)^{q_x}. \quad (10)$$

They commute with each other and the Hamiltonian H . Therefore, we can use (S_x, R_y) , instead of $(T_{\text{rel}}^x, T_{\text{cm}}^y)$, to block-diagonalize the Hamiltonian into momentum sectors. Since $(S_x)^{q_x} = (T_{\text{rel}}^x)^\dagger$, the new set of 2D wave numbers defined by (S_x, R_y) takes value from an $(Nq_x) \times (N_{0x}N_y)$ Brillouin zone [as opposed to the $N \times N_\phi$ Brillouin zone of Eq. (9)].

Notice that S_x operates within the q -fold multiplet. Successive applications of S_x break the multiplet into non-overlapping orbits. The states in each orbit have the same R_y eigenvalue due to $[S_x, R_y] = 0$. The orbit

structure can be revealed by the eigenvalues of T_{cm}^y , as they are distinct for the q states. Plugging Eq. (10) into Eq. (8), we have

$$T_{\text{cm}}^y S_x = S_x T_{\text{cm}}^y e^{-i2\pi p/q_x}, \quad (11)$$

$$T_{\text{cm}}^x R_y = R_y T_{\text{cm}}^x e^{i2\pi p/(q/q_x)}. \quad (12)$$

From Eq. (11), every orbit of S_x has the same length q_x . The total number of orbits is thus q/q_x . From Eq. (12), for $r \in [0 .. q/q_x)$, $(T_{\text{cm}}^x)^r$ brings any given state in the q -fold multiplet to q/q_x distinct states discriminated by R_y eigenvalues, and thus belonging to q/q_x different orbits of S_x . This covers *each* of the orbits exactly *once*.

We can recombine the q -fold states to form simultaneous eigenstates of S_x and R_y . We start the construction from an arbitrary energy eigenstate $|\Psi\rangle$ in the q -fold multiplet diagonal in $(T_{\text{rel}}^x, T_{\text{cm}}^y)$, labeled by $\kappa_x \in [0 .. N)$ and $\kappa_y \in [0 .. N_y)$. The usual, relative y -momentum which labels the eigenvalue of T_{rel}^y can be easily obtained as $\kappa_y \bmod N$. For the Laughlin case at filling $\nu = 1/3$, $|\Psi\rangle$ is just one of the threefold degenerate states on the torus. The q states can be regrouped into the orbits of S_x , labeled by r :

$$\left\{ (S_x)^m (T_{\text{cm}}^x)^r |\Psi\rangle \mid m \in [0 .. q_x) \right\}, \quad r \in [0 .. q/q_x). \quad (13)$$

We can recombine the q_x states in each orbit into q_x eigenstates of S_x . Within the multiplet, ince $(S_x)^{q_x} = (T_{\text{rel}}^x)^\dagger = e^{-i2\pi\kappa_x/N}$, we have

$$(S_x)^{q_x} = e^{-i2\pi q_x (\kappa_x + sN_e)/(Nq_x)}. \quad (14)$$

Note that the values of $e^{i2\pi(\kappa_x + sN_e)/(Nq_x)}$ are distinct for $s \in [0 .. q_x)$, thanks to p, q_x being coprime. We define the $q_x \times (q/q_x)$ states

$$|\Psi; s, r\rangle = \frac{1}{\sqrt{q_x}} \sum_m^{q_x} e^{i2\pi m(\kappa_x + sN_e)/(Nq_x)} (S_x)^m (T_{\text{cm}}^x)^r |\Psi\rangle, \quad (15)$$

for $s \in [0 .. q_x)$ and $r \in [0 .. q/q_x)$. These states are orthonormal, and they are simultaneous eigenstates of S_x and R_y in the $(Nq_x) \times (N_{0x}N_y)$ Brillouin zone,⁵⁹

$$\begin{aligned} S_x |\Psi; s, r\rangle &= e^{-i2\pi(\kappa_x + sN_e)/(Nq_x)} |\Psi; s, r\rangle, \\ R_y |\Psi; s, r\rangle &= e^{-i2\pi(\kappa_y + rN_e)/(N_{0x}N_y)} |\Psi; s, r\rangle. \end{aligned} \quad (16)$$

The $q_x \times (q/q_x)$ states are related by center-of-mass translations, namely

$$\begin{aligned} T_{\text{cm}}^x |\Psi; s, r\rangle &= |\Psi; s, r+1\rangle, \\ T_{\text{cm}}^y |\Psi; s, r\rangle &= e^{-i2\pi(\kappa_y + rN_e)/N_\phi} |\Psi; s-1, r\rangle. \end{aligned} \quad (17)$$

In terms of amplitudes, the second equation above can be written as [using Eq. (9)]

$$\begin{aligned} e^{-i2\pi \sum j/N_\phi} \langle \{j\} | \Psi; s, r \rangle \\ = e^{-i2\pi(\kappa_y + rN_e)/N_\phi} \langle \{j\} | \Psi; s-1, r \rangle. \end{aligned} \quad (18)$$

Incidentally, we note that $|\Psi; s, r\rangle$ is periodic under $s \rightarrow s + q_x$, but it acquires a phase when $r \rightarrow r + q/q_x$ [since $(T_{\text{cm}}^x)^{q/q_x} = S_x$ as defined in Eq. (10)]

$$|\Psi; s, r + q/q_x\rangle = e^{-i2\pi(\kappa_x + sN_e)/(Nq_x)} |\Psi; s, r\rangle. \quad (19)$$

B. Translational Symmetries in Amplitudes

We now consider the manifestation of the translation symmetries in the amplitudes $\langle \{j\} | \Psi; s, r \rangle$. The action of S_x and R_y on the basis states $|\{j\}\rangle$ reads

$$\begin{aligned} S_x |\{j\}\rangle &= |\{j + q/q_x\}\rangle, \\ R_y |\{j\}\rangle &= e^{-i2\pi \sum j/(N_{0x}N_y)} |\{j\}\rangle. \end{aligned} \quad (20)$$

Therefore, from the first equation above we have

$$e^{-i2\pi(\kappa_x + sN_e)/(Nq_x)} \langle \{j\} | \Psi; s, r \rangle = \langle \{j - q/q_x\} | \Psi; s, r \rangle, \quad (21)$$

while from the second, we find that the amplitude $\langle \{j\} | \Psi; s, r \rangle$ vanishes unless

$$\sum j = \kappa_y + rN_e \bmod N_{0x}N_y. \quad (22)$$

The last two equations above summarize the information that we need from the FQH side to establish the translational invariance of the FCI many-body wave functions to be constructed in Sec. IV on an $N_x \times N_y$ lattice.

III. HYBRID LOCALIZED WANNIER STATES

We now proceed to establish the hybrid Wannier basis in a Chern band on a lattice. The ultimate goal is to construct 1D localized Wannier states which are plane waves in the second direction (hybrid). Such states mimic the Landau orbitals $|j\rangle$. We begin by reviewing the construction and the properties of the 1D maximally localized Wannier states.¹⁷⁻¹⁹

Consider a 2D band insulator with N_b orbitals per unit cell, indexed by α . We assume lattice translational symmetry and periodic boundary conditions. Denote the primitive translation vectors by \mathbf{b}_1 and \mathbf{b}_2 , with $\hat{e}_z \cdot (\mathbf{b}_1 \times \mathbf{b}_2) > 0$. Then the Bravais lattice is indexed by $x\mathbf{b}_1 + y\mathbf{b}_2$, with $(x, y) \in \mathbb{Z}^2$ (be to differentiated from $(\tilde{x}, \tilde{y}) \in \mathbb{R}^2$ in the continuum.) We pick the principal region to be $(x, y) \in [0 .. N_x) \times [0 .. N_y)$. The momentum space is given by the reciprocal lattice \mathbf{k} . We label points in the momentum space by wave numbers $(k_x, k_y) \in \mathbb{Z}^2$, defined by $k_x = \mathbf{k} \cdot \mathbf{b}_1$ and $k_y = \mathbf{k} \cdot \mathbf{b}_2$. The single-particle orbitals can be written as $|x, y, \alpha\rangle$, or $|k_x, k_y, \alpha\rangle$ in the momentum space.

The energy eigenstates are Bloch waves. We focus on a single, isolated band $|k_x, k_y\rangle$, which will be fractionally filled in the many-body construction. For now we only focus on the one-band problem. Generalization to the 2D FTI problem is straightforward as that problem decouples in the Wannier basis. The wave function of the

Bloch band is $u_\alpha(k_x, k_y) = \langle k_x, k_y, \alpha | k_x, k_y \rangle$. We assume periodic boundary condition in *both* k_x and k_y directions, $|k_x + l_x N_x, k_y + l_y N_y, n\rangle = |k_x, k_y, n\rangle$, for $l_x, l_y \in \mathbb{Z}$. We set the first Brillouin zone to $[0 .. N_x) \times [0 .. N_y)$.

We denote the position of an orbital α relative to its unit cell coordinate by $\epsilon_\alpha^x \mathbf{b}_1 + \epsilon_\alpha^y \mathbf{b}_2$, where $(\epsilon_\alpha^x, \epsilon_\alpha^y) \in \mathbb{R}^2$ are the relative displacements of the orbitals within an unit cell. Taking into account the periodic boundary, we can define the (exponentiated) position operators

$$\hat{x} = \sum_{x,y} \sum_{\alpha} |x, y, \alpha\rangle e^{-i2\pi(x+\epsilon_\alpha^x)/N_x} \langle x, y, \alpha|, \quad (23)$$

and similarly \hat{y} . Here the integers (x, y) are summed over the Bravais lattice points in the principal region of the torus, and α is summed over all N_b orbitals.

Using the projector to the occupied band

$$P = \sum_{k_x, k_y} |k_x, k_y\rangle \langle k_x, k_y|, \quad (24)$$

we can define the projected position operators $\hat{\mathcal{X}} = P\hat{x}P$ and $\hat{\mathcal{Y}} = P\hat{y}P$. In the momentum space, they take the form

$$\begin{aligned} \hat{\mathcal{X}} &= \sum_{k_x, k_y} |k_x, k_y\rangle \mathcal{A}_x(k_x, k_y) \langle k_x + 1, k_y|, \\ \hat{\mathcal{Y}} &= \sum_{k_x, k_y} |k_x, k_y\rangle \mathcal{A}_y(k_x, k_y) \langle k_x, k_y + 1|, \end{aligned} \quad (25)$$

where (k_x, k_y) is summed over the first Brillouin zone, and $\mathcal{A}_{x,y}(k_x, k_y)$ are the (exponentiated) Berry connections given by

$$\begin{aligned} \mathcal{A}_x(k_x, k_y) &= \langle k_x, k_y | \hat{x} | k_x + 1, k_y \rangle \\ &= \sum_{\alpha} e^{-i2\pi\epsilon_\alpha^x/N_x} u_\alpha^*(k_x, k_y) u_\alpha(k_x + 1, k_y), \\ \mathcal{A}_y(k_x, k_y) &= \langle k_x, k_y | \hat{y} | k_x, k_y + 1 \rangle \\ &= \sum_{\alpha} e^{-i2\pi\epsilon_\alpha^y/N_y} u_\alpha^*(k_x, k_y) u_\alpha(k_x, k_y + 1). \end{aligned} \quad (26)$$

Notice that the Berry connections depend on the embedding of the lattice and its orbitals in real space, as does the Berry curvature.⁶⁰ The link to the usual continuum definition of the Berry connections is explicitly demonstrated in Appx. F. We emphasize that the definition of the exponentiated discrete Berry connections does not require a smooth gauge.

A. Localization and Orthogonality

Thanks to the translational invariance, we can view the 2D system as N_y decoupled 1D subsystems labeled by the momentum k_y . The position operator $\hat{\mathcal{X}}$ operates within each subsystem and is diagonal in k_y . At each value of k_y , the eigenstates of this operator are the

closest analogue to the states $|x, k_y, \alpha\rangle$ that we can construct within the occupied bands; they are the maximally localized Wannier state for the 1D subsystem.^{17–19} The eigenvalue of $\hat{\mathcal{X}}$ is the (exponentiated) Wannier center position in the \mathbf{b}_1 direction.

Ref. 15 proposed to build FQH wave functions using the maximally localized Wannier orbitals as one body basis with a one-to-one mapping into the LLL orbitals. A major issue at finite size, however, is that the N_x eigenstates of the projected position operator at each value of k_y are *not orthogonal* due to the *non-unitarity* of the projected position operator at finite N_x . This point is demonstrated in Appx. B.

Gram-Schmidt orthogonalization is not a suitable solution, as it mixes the Wannier states localized in different unit cells, thereby spoiling the translational invariance. The proper resolution is to keep only the *phase* part of the exponentiated Berry connection and use the alternative, unitary projected position operators to define the 1D localized Wannier states. Specifically, we define the unitary connections⁶¹

$$A_a(k_x, k_y) = \mathcal{A}_a(k_x, k_y) / |\mathcal{A}_a(k_x, k_y)|, \quad a = x, y, \quad (27)$$

and the unitary projected position operators

$$\hat{X} = \sum_{k_x, k_y} |k_x, k_y\rangle A_x(k_x, k_y) \langle k_x + 1, k_y|, \quad (28)$$

$$\hat{Y} = \sum_{k_x, k_y} |k_x, k_y\rangle A_y(k_x, k_y) \langle k_x, k_y + 1|. \quad (29)$$

Technically, the eigenstates of these operators are not *maximally* localized (they are almost so), but this is a small price to pay for the orthogonality.

If there is more than one occupied band, such in the case of the quantum spin Hall (QSH) effect and 2D topological insulators, the prescription for obtaining orthonormal orbitals is to perform a singular value decomposition (SVD) of the non-Abelian exponentiated Berry connection into $V\Sigma W^\dagger$, and use VW^\dagger in place of the Berry connection to define the projected position operators.¹⁸ Specifically, if the occupied bands are denoted by $|k_x, k_y, n\rangle$, we replace the matrix $\langle k_x, k_y, m | k_x + 1, k_y, n \rangle$ (of indices m, n) by its SVD when defining the projected position operator \hat{X} .¹⁹

Thanks to the gauge periodicity in both k_x and k_y , we can define the unitary Wilson loops

$$W_x(k_y) = \prod_{k_x} A_x(k_x, k_y), \quad W_y(k_x) = \prod_{k_y} A_y(k_x, k_y).$$

For later convenience, we introduce $\lambda_x(k_y)$ and $\lambda_y(k_x)$ defined by

$$[\lambda_x(k_y)]^{N_x} = W_x(k_y), \quad [\lambda_y(k_x)]^{N_y} = W_y(k_x). \quad (30)$$

We pick $\lambda_x(k_y)$ to be the N_x -th root with argument angle in $(-2\pi/N_x, 0]$, and $\lambda_y(k_x)$ to be the N_y -th root

with argument angle in $(-2\pi/N_y, 0]$. We can interpret $\lambda_y(k_x)$ and $\lambda_y(k_x)$ as the ‘‘average’’ phase (connection) of the Wilson loop evenly distributed to each bond along the loop. In general, for more than one occupied band, $\lambda_x(k_y)$ and $\lambda_y(k_x)$ are obtained from the sets of eigenvalues of the corresponding Wilson loop matrices.

The eigenvalues and the eigenstates of \widehat{X} can be found easily, due to its decoupling into N_y blocks labeled by k_y . Each block \widehat{X}_{k_y} is an $N_x \times N_x$ matrix in the Bloch basis. The N_x eigenvalues of \widehat{X}_{k_y} are given by the N_x -th roots of $W_x(k_y)$,¹⁹

$$\widehat{X}_{k_y}|X, k_y\rangle = \Lambda_x(X, k_y)|X, k_y\rangle, \quad (31)$$

where $\Lambda_x(X, k_y) = e^{-i2\pi X/N_x} \lambda_x(k_y)$, indexed by $X \in [0 \dots N_x)$. The eigenstate belonging to the eigenvalue $\Lambda_x(X, k_y)$ can be written

$$|X, k_y\rangle = \frac{e^{i\Phi_y(X, k_y)}}{\sqrt{N_x}} \times \sum_{k_x} e^{-i2\pi k_x X/N_x} \left\{ \frac{[\lambda_x(k_y)]^{k_x}}{\prod_{\kappa}^{k_x} A_x(\kappa, k_y)} \right\} |k_x, k_y\rangle. \quad (32)$$

Recall from Eq. (5) that we use the shorthand

$$\prod_{\kappa}^{k_x} A_x(\kappa, k_y) \equiv \prod_{\kappa=0}^{k_x-1} A_x(\kappa, k_y). \quad (33)$$

Since the curly-braced prefactor in Eq. (32) is unitary, these states inherit at finite size the orthonormality of $|k_x, k_y\rangle$ through the Fourier transform. These orthogonal Wannier orbitals are not maximally localized for the finite-size lattice, but quickly become so as the number of sites N_x increases. They exhibit a gauge freedom, $\Phi_y(X, k_y) \in \mathbb{R}$, which is a phase to be specified in Sec. IV B.

The center of the 1D localized Wannier state is given by

$$\langle X, k_y | \widehat{x} | X, k_y \rangle = \Lambda_x(X, k_y) \left[\frac{1}{N_x} \sum_{k_x} |\mathcal{A}_x(k_x, k_y)| \right], \quad (34)$$

where the bracketed factor is a positive real number. Therefore, we can interpret

$$\chi^{X, k_y} = -\frac{N_x}{2\pi} \arg[\Lambda_x(X, k_y)] = X - \frac{1}{2\pi} \arg[W_x(k_y)] \quad (35)$$

as the center of the maximally localized Wannier function, where we pick the branch of the argument function with $\arg(z) \in (-2\pi, 0]$ to make $\chi^{X, k_y} \in [X, X+1)$. We place the X -th unit cell over $[X, X+1)$. As expected, in each unit cell there are N_y Wannier centers, corresponding to the N_y values of k_y .

For a flat-band Hamiltonian with no band dispersion, such as the single-particle part of the FCI Hamiltonians

in Ref. 7, the Wannier states are actually single-particle energy eigenstates of the lowest, fractionally filled band. This qualifies the set of all the 1D localized Wannier states $\{|X, k_y\rangle\}$ as a single-particle basis for constructing the many-body trial states for the FCI, which lie entirely in the lowest band, in the same spirit as the LLL projected FQH wave functions.

B. Gauge Freedom

In the language of Ref. 18, the construction of eigenstates in Eq. (32) can be interpreted as transforming the Bloch states with an arbitrary phase factor to the ‘‘parallel transport’’ (pt) gauge, in which

$$|k_x, k_y\rangle_{\text{pt}} = \frac{[\lambda_x(k_y)]^{k_x}}{\prod_{\kappa}^{k_x} A_x(\kappa, k_y)} |k_x, k_y\rangle, \quad (36)$$

and the 1D localized Wannier states are just Fourier transform of the Bloch states $|k_x, k_y\rangle_{\text{pt}}$. Despite the name, technically the phase of $|k_x, k_y\rangle_{\text{pt}}$ contains not only the parallel transport $\prod_{\kappa}^{k_x} A_x(\kappa, k_y)$ from $|0, k_y\rangle$, it also contains a rotation to accommodate the Wilson loop $W_x(k_y)$.

Under the gauge transform

$$|k_x, k_y\rangle \rightarrow e^{i\eta(k_x, k_y)} |k_x, k_y\rangle, \quad (37)$$

the Wilson line transforms by

$$\prod_{\kappa}^{k_x} A_x(\kappa, k_y) \rightarrow e^{-i\eta(0, k_y)} \prod_{\kappa}^{k_x} A_x(\kappa, k_y) e^{i\eta(k_x, k_y)}, \quad (38)$$

and thus the Wannier state transforms by

$$|X, k_y\rangle \rightarrow e^{i\eta(0, k_y)} |X, k_y\rangle. \quad (39)$$

The reason for the appearance of $e^{i\eta(k_x, k_y)}$ with only $k_x = 0$ is obvious: the parallel transport gauge [Eq. (36)] depends only on the initial condition at $k_x = 0$ and the gauge-invariant Wilson loop $W_x(k_y)$. Had we chosen to start the parallel transport from k_x^0 , the Wannier state would acquire a phase $e^{i\eta(k_x^0, k_y)}$ upon the gauge transform. The full gauge freedom of the Wannier states is kept in the phase $e^{i\Phi_y(X, k_y)}$. Due to the X -dependency, this is much larger than the gauge freedom in $e^{i\eta(0, k_y)}$.

In Ref. 15, a similar gauge transformation formula was derived in a different, smooth gauge in the continuum limit that is *not* periodic in the k_y direction. However, as detailed in Appx. F3, we find in that case a gauge transformation formula that is fundamentally different from the one given in Ref. 15: due to the absence of periodic boundary condition in the k_y direction in the setup of Ref. 15, a gauge transformation with a non-trivial winding may shift the 1D localized Wannier state to another unit cell, changing the X index.

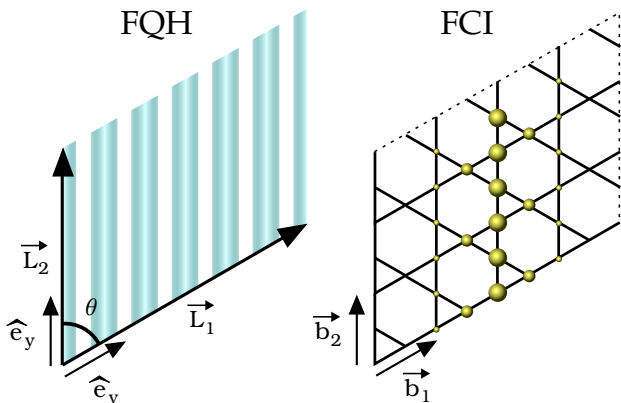


FIG. 1: Single-particle orbitals in the lowest Landau level (LLL) and the Chern band. In the left panel we show the Landau orbitals in the LLL on a torus. The two fundamental cycles are marked by \mathbf{L}_1 and \mathbf{L}_2 , and the twist angle is labeled by θ . The Landau orbitals are plane waves in the \hat{e}_y direction that are localized in the direction perpendicular to propagation. In the right panel we show a 1D Wannier state localized in the \mathbf{b}_1 direction and in the lowest band of the Kagome lattice model. The size of the spheres depicts the weights of the Wannier state on each lattice site.

Incidentally, we point out that any gauge fixing in the k_y direction at $k_x \neq 0$ is futile, as the “parallel transport” construction would effectively override any gauge choice at $k_x \neq 0$. This is reflected by the independence of Eq. (39) from $e^{i\eta(k_x, k_y)}$ with $k_x \neq 0$.

We emphasize that the phase factor $e^{i\Phi_y(X, k_y)}$, or the single-particle gauge for $|k_x, k_y\rangle$, do *not* affect the localization of the Wannier state, but they do affect essentially the similarity with the LLL. We will discuss the choice of $e^{i\Phi_y(X, k_y)}$ in Sec. IV B.

C. Connection to the Lowest Landau Level

Ultimately, we want to bridge the physics of a partially filled band with a Chern number $C = \pm 1$ and that of the spinless FQH effects in the LLL on a continuum torus. (Unless noted otherwise, in this paper we specialize to Chern number $|C| = 1$.)

As illustrated in Fig. 1, at the single-particle level, both the Wannier states $|X, k_y\rangle$ in a Chern band and the Landau-gauge orbitals $|j\rangle$ in the LLL are plane waves localized in the direction perpendicular to wave propagation. Building upon the correspondence between the center lines of the localized states, Ref. 15 proposed a linear relabeling of the Wannier states. The resulting 1D label is analogous to the LLL state index j . We now examine this relabeling of the Wannier states in more details. As we will see, the original prescription lacks a few ingredients that are essential for a concrete numerical implementation of the scheme.

First, we need to specify the torus geometry in the continuum. The number of fluxes in the corresponding

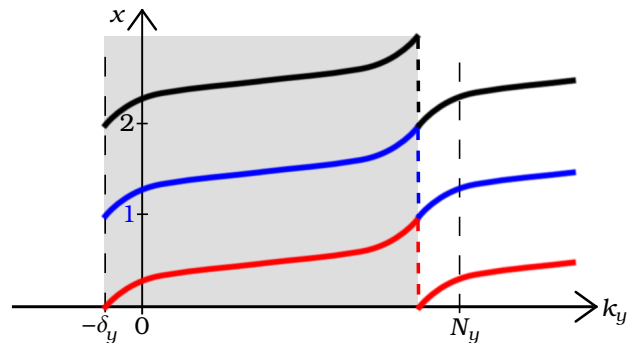


FIG. 2: The principal Brillouin zone for $C = +1$. Plotted are the flows of the Wannier center position $\chi^{X, k_y} = X - \arg[W_x(k_y)]/(2\pi)$ [Eq. (35)] as a function of k_y , color-coded according to the unit cell index X . The movement of the Wannier center in each unit cell is monotonic in the principal Brillouin zone $Ck_y + \delta_y \in [0 \dots N_y)$ (marked by the gray shade), but not monotonic in the Brillouin zone $k_y \in [0 \dots N_y)$.

LLL problem is given by $N_\phi = N_x N_y$.^{9,15} We want the continuum torus to take the same shape as the lattice system with periodic boundaries. The aspect ratio L_1/L_2 is set to⁶²

$$\frac{L_1}{L_2} = \frac{N_x |\mathbf{b}_1|}{N_y |\mathbf{b}_2|}. \quad (40)$$

The only remaining parameter is the twist angle θ between \mathbf{L}_1 and \mathbf{L}_2 (defined in Sec. II). For brevity, we want to map both $C = 1$ and $C = -1$ Chern bands to the LLL with a magnetic field in the $-\hat{e}_z$ direction as studied in Sec. II. For $C = 1$, we put \mathbf{L}_1 and \mathbf{L}_2 in the direction of \mathbf{b}_1 and \mathbf{b}_2 , respectively. For $C = -1$, we need to “flip” the fundamental parallelogram. This corresponds to choosing the twist angle $\theta = \pi - \langle \mathbf{b}_1, \mathbf{b}_2 \rangle$, where $\langle \mathbf{b}_1, \mathbf{b}_2 \rangle \in (0, \pi)$ is the angle between \mathbf{b}_1 and \mathbf{b}_2 . This choice of θ is justified numerically in Sec. VIB.

We now make a detailed comparison between the LLL orbitals $|j\rangle$ and the Wannier orbitals $|X, k_y\rangle$. In the LLL, the center coordinate $L_1 j / N_\phi$ of orbital $|j\rangle$ in the \mathbf{b}_1 direction is a monotonically increasing function of j , and the $j = 0$ orbital is centered along the line $x = 0$. In the Chern band, the unitary Wilson loop $W_x(k_y)$ is a pure phase; when k_y changes, it winds around the unit circle at the origin of the complex plane. In the continuum limit, $W_x(k_y)$ has winding number $C = \pm 1$ when k_y goes around a single Brillouin zone. Assume for the moment that the winding motion of $W_x(k_y)$ on the unit circle is *unidirectional* (clockwise when $C = 1$ and counterclockwise when $C = -1$) when k_y increase from 0 to N_y , i.e. there is no “zigzag” pattern of going back-and-forth anywhere. In this case, when the k_y Brillouin zone boundary is *properly* chosen, $\arg[W_x(k_y)] \in (-2\pi, 0]$ depends *monotonically* on k_y .

The proper choice of the Brillouin zone is illustrated in Fig. 2. We start the k_y Brillouin zone from the point where $W_x(k_y)$ is closest to 1 in the lower half of the complex plane. The specific prescription is the following.

We pick the branch of $\arg[W_x(k_y)]$ that takes value in $(-2\pi, 0]$. We define the shift $\delta_y \in [0 .. N_y)$ as the cardinality of the set

$$\left\{ k_y \in [0 .. N_y) \mid \arg[W_x(k_y)] > \arg[W_x(0)] \right\}. \quad (41)$$

Then, for $Ck_y + \delta_y \in [0 .. N_y)$, $\arg[W_x(k_y)]$ depends *monotonically* on k_y ; $Ck_y + \delta_y$ labels the Wannier centers in an unit cell sequentially in ascending order of the center position χ^{X, k_y} . We refer to the set of k_y given by

$$Ck_y + \delta_y \in [0 .. N_y) \quad (42)$$

as the ‘‘principal Brillouin zone’’ (pBZ). We introduce the 1D label of Wannier states

$$j^{X, k_y} = XN_y + Ck_y + \delta_y \quad (43)$$

with $Ck_y + \delta_y \in [0 .. N_y)$. We need to shift k_y back to the pBZ *before* performing the mapping. Thanks to the explicit choice of the domain for k_y , the mapping $(X, k_y) \rightarrow j$ is invertible. In the presence of ‘‘zigzag’’ patterns in $W_x(k_y)$, we stick to the above j^{X, k_y} formula, and take δ_y as a variational parameter. This simple dependence on k_y is necessary for the translational invariance of the FQH-analog wave functions, as we will see in Sec. IV C. In the rest of this paper we will focus on the case without ‘‘zigzag’’ patterns.

The phase factor $e^{i\Phi_y(X, k_y)}$ is subject to periodicity constraints. Since in the LLL $|j\rangle = |j + N_\phi\rangle$, the Wannier states $|X, k_y\rangle$ and $|X + N_x, k_y\rangle$ are mapped to the same LLL state. This mandates the gauge periodicity in X , i.e. $|X, k_y\rangle = |X + N_x, k_y\rangle$. Eq. (32) then leads to

$$e^{i\Phi_y(X, k_y)} = e^{i\Phi_y(X + N_x, k_y)}. \quad (44)$$

The periodic gauge of the Bloch state in the k_y direction, i.e. $|k_x, k_y\rangle = |k_x, k_y + N_y\rangle$, requires that

$$e^{i\Phi_y(X, k_y)} = e^{i\Phi_y(X, k_y + N_y)}. \quad (45)$$

It should be noted that the analogy between the Wannier states and the LLL states is not exact even in the continuum limit, due to the inevitable fluctuations in the Berry curvature. For example, if the Berry curvature is not uniform in the y direction, the Wannier centers χ^{X, k_y} are not distributed evenly over each unit cell, in contrast to the uniform distribution of the LLL orbitals. This is in line with the comparison between the LLL and the Chern band made in Refs. 20,21.

IV. WANNIER CONSTRUCTION OF FQH STATES ON A LATTICE

We now turn to the construction of model wave functions in a fractional Chern insulator defined on an $N_x \times N_y$ lattice. We consider finding model wave functions

that approximate the ground states of generic density-density interaction with translational invariance, namely

$$V_{\text{lat}} = \sum_{(\mu, \nu, \delta)} \sum_{\mathbf{r}} \psi_{\mathbf{r}+\delta, \mu}^\dagger \psi_{\mathbf{r}, \nu}^\dagger \psi_{\mathbf{r}, \nu} \psi_{\mathbf{r}+\delta, \mu}, \quad (46)$$

Here δ is the unit cell displacements between neighboring orbitals μ and ν . The sum (μ, ν, δ) is over all distinct (up to lattice translation) orbital pairs within some interaction range. The Bravais lattice coordinate $\mathbf{r} = (x, y) \in \mathbb{Z}^2$ is summed over the principal region of the torus. We refer the reader to Ref. 7 for a series of examples with concrete choices of (μ, ν, δ) . Longer range interactions can also be implemented, but our experience is that they diminish the strength of the FQH-like state.

In the flat-band limit of the single band approximation^{4,7}, the interacting Hamiltonian is just the projected density-density interaction $PV_{\text{lat}}P$:

$$H_{\text{lat}} = \frac{1}{N_\phi} \sum_{\{\mu, \nu, \delta\}} \sum_{\mathbf{k}_1 \mathbf{k}_2 \mathbf{k}_3 \mathbf{k}_4} \delta'_{\mathbf{k}_1 + \mathbf{k}_2, \mathbf{k}_3 + \mathbf{k}_4} e^{-i(\mathbf{k}_1 - \mathbf{k}_4) \cdot \delta} \times u_\mu^*(\mathbf{k}_1) u_\nu^*(\mathbf{k}_2) u_\nu(\mathbf{k}_3) u_\mu(\mathbf{k}_4) \psi_{\mathbf{k}_1}^\dagger \psi_{\mathbf{k}_2}^\dagger \psi_{\mathbf{k}_3} \psi_{\mathbf{k}_4}. \quad (47)$$

Here $\mathbf{k}_n = (k_{x,n}, k_{y,n})$, $n = 1, 2, 3, 4$, are summed over the first Brillouin zone, and the primed Kronecker- δ allows umklapp processes $\mathbf{k}_1 + \mathbf{k}_2 = \mathbf{k}_3 + \mathbf{k}_4 \pmod{(N_x, N_y)}$.

Based on the physics of the FQH, we expect that the Hamiltonian in Eq. (47) could have a topological ground state at filling $\nu = 1/q$ that resembles the Laughlin state. The Laughlin state expansion in non-interacting many-body states is known and hence all we need for a model FCI state is an appropriate map between the FCI single-particle orbitals and those of the LLL. The relevance of these trial wave functions to the actual FCI ground state is demonstrated in Sec. VI. We now examine the details of this construction.

For a flat-band single-particle lattice Hamiltonian, the many-body Hilbert space is spanned by the Slater determinant states $|\{X, k_y\}\rangle$. The 1D index j^{X, k_y} defined in Eq. (43) provides a formal mapping between the many-body basis states $|\{X, k_y\}\rangle$ on the lattice and $|\{j\}\rangle$ in the continuum. The lattice analogue of $|\Psi; s, r\rangle$ states can be constructed:

$$|\Psi; s, r\rangle_{\text{lat}} = \sum_{\{X, k_y\}} |\{X, k_y\}\rangle \langle \{j^{X, k_y}\} | \Psi; s, r \rangle, \quad (48)$$

where $\langle \{j^{X, k_y}\} | \Psi; s, r \rangle$ are the FQH amplitudes of the states defined in Eq. (15), and $\{X, k_y\}$ is summed over all N_e -particle configurations in the Wannier basis.

Naively, this seems to be the end of the story. However, the state $|\Psi; s, r\rangle_{\text{lat}}$ defined above is *not* covariant under a single-particle gauge transform on $|X, k_y\rangle$, as the continuum states $|j\rangle$ do *not* transform accordingly. We have to fix the phase $e^{i\Phi_y(X, k_y)}$ of the Wannier states $|X, k_y\rangle$ in conformity with the phase of the $|j\rangle$ states. This is not surprising: following Ref. 15, up to now we have only established a mapping between the state *labels*

(X, k_y) and j , rather than a mapping between the actual states. In the following, we seek the guidelines for choosing $e^{i\Phi_y(X, k_y)}$ based on the similarity with the LLL. If we do not properly fix the $e^{i\Phi_y(X, k_y)}$ phase, the overlaps with the exact ground states can be tiny.

A. Connection between Wannier States

For the LLL orbitals $|j\rangle$ defined in Eq. (3), we find in Appx. A that the adjacent orbitals satisfy

$$\langle j|e^{-i\mathbf{G}_2\cdot\tilde{\mathbf{r}}}|j+1\rangle = e^{-|\mathbf{G}_2|^2 l_B^2/4} \in \mathbb{R}_+. \quad (49)$$

Here, $\mathbf{G}_2 = 2\pi(\hat{e}_y - \cot\theta\hat{e}_x)/L_2$ is the reciprocal lattice vector defined in Eq. (1) in Sec. II, and the position operator $\tilde{\mathbf{r}}$ takes values in the continuum. We can interpret $e^{-i\mathbf{G}_2\cdot\tilde{\mathbf{r}}}$ as a translation by $-\mathbf{G}_2$ in the momentum space.

This condition spells out the gauge choice of the LLL orbitals. In the continuum limit, it gives the parallel transport between the $|j\rangle$ and $|j+1\rangle$ orbitals. We need to find a consistent gauge for the Wannier states. Recall that \hat{Y} implements translation in the momentum space along k_y , which is the direction reciprocal to \mathbf{b}_2 . Therefore, on a lattice, the quantity analogous to $\langle j|e^{-i\mathbf{G}_2\cdot\tilde{\mathbf{r}}}|j+1\rangle$ is the connection between adjacent Wannier states

$$\langle X, k_y|\hat{Y}|X', k'_y\rangle. \quad (50)$$

Here, in the same spirit as the orthogonality fix for $|X, k_y\rangle$, we use the *unitary* projected position operator \hat{Y} , defined in Eq. (29), and (X', k'_y) is the label of the Wannier state *next* to $|X, k_y\rangle$, defined by

$$j^{X', k'_y} = j^{X, k_y} + C. \quad (51)$$

Plugging in the definition of j^{X, k_y} in Eq. (43), we find $k'_y = k_y + 1 \bmod N_y$. If going from k_y to $k_y + 1$ crosses the boundary of the principal Brillouin zone [Eq. (42)], the Wannier centers (X, k_y) and (X', k'_y) are located in different unit cells ($X' = X + C$), otherwise they are in the same unit cell ($X' = X$). Notice that for $|C| > 1$, Eq. (51) breaks the $N_x N_y$ Wannier states into $|C|$ groups, and it implies a $|C|$ -layer FQH analogy.²²

We can calculate the Wannier connection $\langle X, k_y|\hat{Y}|X', k'_y\rangle$ by expanding the Wannier states in Bloch basis using Eq. (32). Since the operator \hat{Y} is diagonal in k_x , the two Bloch basis expansions is reduced into a single sum over k_x . Consider a generic term k_x in the sum. The A_x factors from the Wannier states and the A_y factor from \hat{Y} can be collected into a Wilson line going along $(0, k_y + 1)(k_x, k_y + 1)(k_x, k_y)(0, k_y)$, which equals $A_y(0, k_y)$ times the Wilson loop around the path shown in Fig. 3. The λ_x factors from the Wannier states are $[\lambda_x(k_y + 1)/\lambda_x(k_y)]^{k_x}$. If the two Wannier states are not in the same unit cell, they must be in adjacent unit cells $X' = X + C$ [due to Eq. (51)], and we have another factor $e^{i2\pi k_x C/N_x}$.

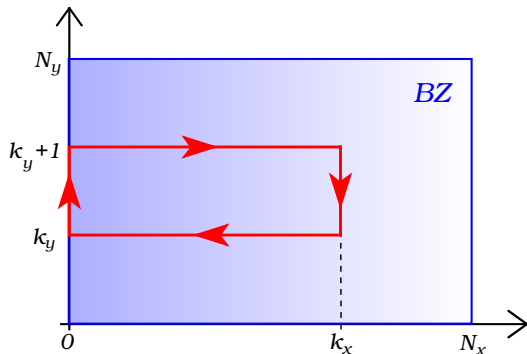


FIG. 3: The loop $(0, k_y)(0, k_y + 1)(k_x, k_y + 1)(k_x, k_y)(0, k_y)$ in the $N_x \times N_y$ lattice Brillouin zone. The Wilson loop around this path is defined in Eq. (54) as $W_{\blacksquare}(k_x, k_y)$. Notice that at $k_x = N_x$, the connections at the two vertical edges cancel each other due to periodic boundary, leading to $W_{\blacksquare}(N_x, k_y) = W_x(k_y)/W_x(k_y + 1)$.

Putting all these together, for (X', k'_y) defined in Eq. (51), we have the expression

$$\langle X, k_y|\hat{Y}|X', k'_y\rangle = \frac{e^{i\Phi_y(X', k'_y)}}{e^{i\Phi_y(X, k_y)}} A_y(0, k_y) \mathcal{U}_y(k_y), \quad (52)$$

where the gauge-invariant quantity $\mathcal{U}_y(k_y)$ is defined as

$$\mathcal{U}_y(k_y) = \frac{1}{N_x} \sum_{k_x} \frac{W_{\blacksquare}(k_x, k_y)}{\overline{W_{\blacksquare}}(k_x, k_y)}. \quad (53)$$

Here, $W_{\blacksquare}(k_x, k_y)$ is the unitary Wilson loop in Fig. 3,

$$W_{\blacksquare}(k_x, k_y) = \frac{\prod_{\kappa}^{k_x} A_x(\kappa, k_y)}{\prod_{\kappa}^{k_x} A_x(\kappa, k_y + 1)} \frac{A_y(k_x, k_y)}{A_y(0, k_y)}, \quad (54)$$

while $\overline{W_{\blacksquare}}(k_x, k_y) = [\mu_x(k_y)]^{k_x}$ is given by $\mu_x(k_y)$ defined over the principal Brillouin zone [pBZ, the set of κ satisfying $C\kappa + \delta_y \in [0 .. N_y)$],

$$\mu_x(k_y) = \begin{cases} \frac{\lambda_x(k_y)}{\lambda_x(k_y + 1)} & \text{if } k_y + 1 \in \text{pBZ}, \\ e^{i2\pi C/N_x} \frac{\lambda_x(k_y)}{\lambda_x(k_y + 1)} & \text{otherwise.} \end{cases} \quad (55)$$

We emphasize that the above definition requires first shifting k_y back to the pBZ. The two cases in Eq. (55) correspond to whether or not going from k_y to $k_y + 1$ crosses the boundary of the pBZ.

We now try to understand $\mu_x(k_y)$ and $\overline{W_{\blacksquare}}(k_x, k_y)$ physically. Without loss of generality, we consider the case of $C = +1$. Since $[\lambda_x(k_y)]^{N_x} = W_x(k_y)$ [Eq. (30)], we have for both cases of Eq. (55),

$$[\mu_x(k_y)]^{N_x} = \left[\frac{\lambda_x(k_y)}{\lambda_x(k_y + 1)} \right]^{N_x} = W_{\blacksquare}(N_x, k_y). \quad (56)$$

Now we need to take the N_x -th root of this equation. Special care needs to be taken with the branch choice. Recall

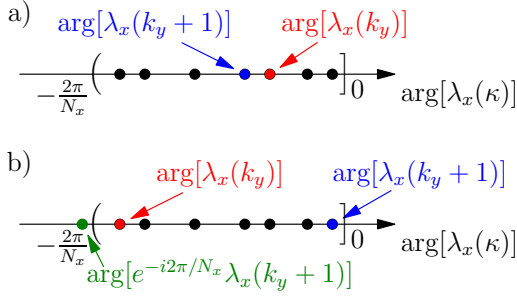


FIG. 4: Flow of $\arg[\lambda_x(\kappa)]$ in the interval $(-2\pi/N_x, 0]$. The solid dots represents the N_y values of $\arg[\lambda_x(\kappa)]$ for the N_y Wannier centers in each unit cell. Here we show the case of $C = +1$: $\arg[\lambda_x(\kappa)]$ is a monotonically decreasing function of κ in the pBZ. Panel a) When k_y and $k_y + 1$ can be put in the principal Brillouin zone simultaneously, we have $\arg[\lambda_x(k_y)/\lambda_x(k_y + 1)] \in (0, 2\pi/N_x)$. Panel b) When going from k_y to $k_y + 1$ crosses the boundary of the principal Brillouin zone, we have $\arg[e^{i2\pi/N_x}\lambda_x(k_y)/\lambda_x(k_y + 1)] \in (0, 2\pi/N_x)$. Summarizing both cases, we have $\arg[\mu_x(k_y)] \in (0, 2\pi/N_x)$, for $\mu_x(k_y)$ defined in Eq. (55).

from Sec. III A that $\arg[\lambda_x(\kappa)]$ lies in $(-2\pi/N_x, 0]$ by definition. Since we assume the absence of “zigzag” patterns in the winding of $W_x(\kappa)$, the motion of $\arg[\lambda_x(\kappa)]$ in the interval $(-2\pi/N_x, 0]$ must be monotonic when $\kappa \in$ pBZ, and $\arg[\lambda_x(\kappa)]$ jumps from the left boundary of the interval to the right boundary when κ crosses the boundary of the pBZ. As illustrated in Fig. 4, for all values of k_y , we have $\arg[\mu_x(k_y)] \in (0, 2\pi/N_x)$. On the other hand, since the phase angle of the Wilson loop is given by the curvature enclosed in the loop, the argument angle $\arg[W_{\blacksquare}(N_x, k_y)] \in [0, 2\pi)$ is the total curvature enclosed in the N_x plaquettes in the row between k_y and $k_y + 1$. Then, the N_x -th root of Eq. (56) gives

$$\arg[\mu_x(k_y)] = \frac{1}{N_x} \arg[W_{\blacksquare}(N_x, k_y)], \quad (57)$$

Therefore the argument angle $\arg[\overline{W}_{\blacksquare}(k_x, k_y)] = k_x \arg[\mu_x(k_y)]$ is k_x/N_x times the total curvature enclosed in the N_x plaquettes in the row between k_y and $k_y + 1$. When the curvature is constant across the N_x plaquettes at k_y , we have $\overline{W}_{\blacksquare}(k_x, k_y) = W_{\blacksquare}(k_x, k_y)$. The phase of each term in $\mathcal{U}_y(k_y)$ [Eq. (53)] can hence be interpreted as a measure of curvature fluctuations in the k_x direction.

B. Phase Fixing: Explicit Prescription

Compared with $\langle j|e^{-i\mathbf{G}_2 \cdot \tilde{\mathbf{r}}}|j+1\rangle \in \mathbb{R}_+$ in the LLL [Eq. (49)], a major difference in the Chern band is that the connection $\langle X, k_y|\hat{Y}|X', k'_y\rangle$ between the Wannier states *cannot* be gauge fixed to a real number. To see this, we take the product of Eq. (52) over all (X, k_y) . Thanks to the periodicity of $e^{i\Phi_y(X, k_y)}$ [Eqs. (44)

and (45)], the product takes a simple form:

$$\prod_X \prod_{k_y} \langle X, k_y|\hat{Y}|X', k'_y\rangle = \left[W_y(0) \prod_{k_y} \mathcal{U}_y(k_y) \right]^{N_x}, \quad (58)$$

Without further constraints from symmetry, the expression on the right hand side is a complex, rather than a positive real number. Even if we ignore the curvature fluctuations, in general we still *cannot* make all $\langle X, k_y|\hat{Y}|X', k'_y\rangle \in \mathbb{R}_+$. This is fundamentally different from the LLL [Eq. (49)].

Hence, we relax this condition and look for $e^{i\Phi_y(X, k_y)}$ that makes the *phase* of $\langle X, k_y|\hat{Y}|X', k'_y\rangle$ independent from X and k_y .⁶³ This phase is given by the N_ϕ -th root of the right hand side of Eq. (58). Define the phase $U_y(k_y) = \mathcal{U}_y(k_y)/|\mathcal{U}_y(k_y)|$. Similar to the phase $\lambda_y(k_x)$ for the connection $A_y(k_x, k_y)$ [Eq. (30)], we can define a phase ω_y with argument angle in $(-\pi/N_y, \pi/N_y]$ by

$$(\omega_y)^{N_y} = \prod_{\kappa} U_y(\kappa). \quad (59)$$

Then, to have the phase of $\langle X, k_y|\hat{Y}|X', k'_y\rangle$ independent from X and k_y , we can use

$$\langle X, k_y|\hat{Y}|X', k'_y\rangle = \lambda_y(0) \omega_y |\mathcal{U}_y(k_y)|. \quad (60)$$

Here, we have picked a specific branch of the N_ϕ -th root of (the phase of) Eq. (58). We could have picked another gauge by putting on the right hand side of Eq. (60) an extra factor $e^{i2\pi w/N_\phi}$, with $w \in (0 .. N_\phi)$. However, this makes no difference to the resulting set of many-body states $\{|\Psi; s, r\rangle_{\text{lat}}\}$ [Eq. (48)]. The reason is the following. Without loss of generality, we consider the effect of this extra factor $e^{i2\pi w/N_\phi}$ in the case with $C > 0$. When we gauge fix the Wannier states one by one, using Eq. (60) but with an extra $e^{i2\pi w/N_\phi}$ between each pair of adjacent Wannier states, the Wannier state $|X, k_y\rangle$ receives an extra factor $e^{i2\pi w j^{X, k_y}/N_\phi}$. Therefore, the many-body state in Eq. (48) becomes

$$|\Psi; s, r\rangle_{\text{lat}}^w = \sum_{\{X, k_y\}} |\{X, k_y\}\rangle e^{i2\pi w \sum j^{X, k_y}/N_\phi} \langle \{j^{X, k_y}\}|\Psi; s, r\rangle, \quad (61)$$

Plugging in Eq. (18), we find

$$|\Psi; s, r\rangle_{\text{lat}}^w = e^{i2\pi w(\kappa_y + rN_e)/N_\phi} |\Psi; s + w, r\rangle_{\text{lat}}. \quad (62)$$

The w -dependence is reduced to an overall phase factor, and a shift in the s index, which can be absorbed by a reshuffling of s . Therefore, we can safely set w to zero, and use Eq. (60) to fix the phase of the Wannier states.

Plugging this prescription into Eq. (52), we find

$$e^{i\Phi_y(X', k'_y) - i\Phi_y(X, k_y)} = \frac{\lambda_y(0)}{A_y(0, k_y)} \frac{\omega_y}{U_y(k_y)}. \quad (63)$$

Notices that the quantities on the right hand side are all unitary. Together with the initial condition $e^{i\Phi_y(0,0)} = 1$, Eq. (63) recursively specifies the choice of $e^{i\Phi_y(X,k_y)}$ for all the N_ϕ states. Thanks to Eqs. (30) and (59), this choice of $e^{i\Phi_y(X,k_y)}$ does not depend on X , and we can drop the X argument and write $e^{i\Phi_y(k_y)}$ instead. We note that any choice of $e^{i\Phi_y(k_y)}$ without an X -dependence *that is periodic in k_y* can be achieved by simply modifying the gauge of the single-particle Bloch states along $k_x = 0$. This changes the phase of the Wannier states by $e^{i\eta(0,k_y)}$ as shown in Eq. (39).

C. Translational Invariance

We now examine the translational symmetry of the many-body states $|\Psi; s, r\rangle$. For the moment we do not

specialize to the phase choice in Eq. (63) and consider the constraint from translational invariance on a generic $e^{i\Phi_y(X,k_y)}$.

Define the N_e -particle center-of-mass translation operators on the lattice

$$\begin{aligned} T_{\text{lat,cm}}^x &= \sum_{\{x,y,\alpha\}} |\{x+1, y, \alpha\}\rangle \langle \{x, y, \alpha\}|, \\ T_{\text{lat,cm}}^y &= \sum_{\{x,y,\alpha\}} |\{x, y+1, \alpha\}\rangle \langle \{x, y, \alpha\}|. \end{aligned} \quad (64)$$

The action on the wave function of the many-body lattice state $|\Psi; s, r\rangle_{\text{lat}}$ defined in Eq. (48) is found to be

$$\langle \{X, k_y\} | T_{\text{lat,cm}}^x | \Psi; s, r \rangle_{\text{lat}} = e^{i \sum [\Phi_y(X, k_y) - \Phi_y(X-1, k_y)]} \langle \{X-1, k_y\} | \Psi; s, r \rangle_{\text{lat}}, \quad (65)$$

$$\langle \{X, k_y\} | T_{\text{lat,cm}}^y | \Psi; s, r \rangle_{\text{lat}} = e^{-i2\pi \sum k_y / N_y} \langle \{X, k_y\} | \Psi; s, r \rangle_{\text{lat}}, \quad (66)$$

where \sum means summation over all the N_e phases of different quantum numbers $\{X, k_y\}$ of the N_e electron wave function. The translational invariance in the y direction is already apparent: Eq. (22) dictates that the non-vanishing components of $\langle \{X, k_y\} | \Psi; s, r \rangle_{\text{lat}}$ have the same value of $\sum k_y = C[\kappa_y + (r - \delta_y)N_e] \bmod N_y$. This is the total momentum K_y . The prefactor in Eq. (66) is the same for all the non-vanishing components, i.e. the wave function is translationally invariant in the y direction. The situation in the x direction is more involved. Plugging Eqs. (21) and (43) into Eq. (65), we have

$$\langle \{X, k_y\} | T_{\text{lat,cm}}^x | \Psi; s, r \rangle_{\text{lat}} = e^{-i2\pi(\kappa_x + sN_e)/N_x} e^{i \sum [\Phi_y(X, k_y) - \Phi_y(X-1, k_y)]} \langle \{X, k_y\} | \Psi; s, r \rangle_{\text{lat}}. \quad (67)$$

In general, the exponential prefactor is different for each component (Slater determinants of different sets $\{X, k_y\}$), spoiling the translational invariance. To restore this symmetry, $e^{i\Phi_y(X, k_y) - i\Phi_y(X-1, k_y)}$ has to be *independent* from X and k_y . Translational invariance is part of the main reason why we also have asked for the phase of $\langle X, k_y | \hat{Y} | X', k'_y \rangle$ to be independent from X and k_y in the previous section. The periodic boundary condition on $e^{i\Phi_y(X, k_y)}$ then guarantees that the exponential prefactor is an N_x -th root of unity, and thus the state recovers translational invariance in the x direction.

D. Total Momenta and the Folding Picture

We now consider the phase choice given in Sec. IV B. Plugging Eq. (63) into Eq. (67), we have

$$\begin{aligned} \langle \{X, k_y\} | T_{\text{lat,cm}}^x | \Psi; s, r \rangle_{\text{lat}} \\ = e^{-i2\pi(\kappa_x + sN_e)/N_x} \langle \{X, k_y\} | \Psi; s, r \rangle_{\text{lat}}, \end{aligned} \quad (68)$$

where the relative momentum κ_x of the FQH state $|\Psi\rangle$ is defined by the eigenvalue of the relative translation oper-

ator T_{rel}^x in Eq. (7). Hence the FQH-analogue many-body wave functions $\langle \{X, k_y\} | \Psi; s, r \rangle_{\text{lat}}$ constructed through the Wannier functions using the above prescription are indeed translationally invariant. The total momentum of the N_e particles in state $|\Psi; s, r\rangle_{\text{lat}}$ is given by the wave numbers

$$\begin{aligned} K_x &= \kappa_x + sN_e \bmod N_x, \\ K_y &= C[\kappa_y + (r - \delta_y)N_e] \bmod N_y. \end{aligned} \quad (69)$$

Ref. 9 obtained the counting for FCI model states from the corresponding counting for FQH model states by first folding the $N \times N$ relative Brillouin zone down to $N_{0x} \times N_{0y}$, and then unfolding to the $N_x \times N_y$ lattice Brillouin zone. We now show that our procedure precisely reproduces this folding picture.

First consider the case $C = +1$. Recall that $\text{GCD}(N_e, N_x) = N_{0x}$, $N_x = q_x N_{0x}$, $\text{GCD}(N_e, N_y) = N_{0y}$, $N_y = q_y N_{0y}$. For $s \in [0 .. q_x)$, the q_x values of K_x are all distinct and can be written as $\kappa_x + t_x N_{0x} \bmod N_x$ with $t_x \in [0 .. q_x)$. This clearly implements the folding rule in the x direction. In the y direction, for $r \in [0 .. q/q_x)$, the q/q_x values of K_y form nothing

but a $q/(q_x q_y)$ -fold replica of the q_y values of $\kappa_y + t_y N_{0x} \bmod N_y$ with $t_y \in [0 .. q_y)$. This corresponds to the folding rule in the y direction, producing $q/(q_x q_y)$ states in each momentum sector. The shift parameter δ_y can be absorbed into r and thus only reshuffles the order of K_y values. For the case of $C = -1$, the minus sign from C in K_y [Eq. (69)] can be absorbed as a reshuffling of r . This is explained in details later, in Eq. (79). The results are thus in full agreement with Ref. 9.

In Ref. 23, the generalized Pauli principle^{11,12} was invoked through the Wannier mapping¹⁵ to determine the *total* number of Moore-Read FCI quasihole states. Using

our updated formalism, the number of quasihole states in each momentum sector could be found as well, and it is in agreement with the earlier results obtained in Ref. 23.

E. Many-Body Amplitudes in the Bloch Basis

We are now in a position to give the final formula for the amplitudes of the many-body lattice states constructed from the FQH states $|\Psi; s, r\rangle$,

$$\langle \{k_x, k_y\} | \Psi; s, r \rangle_{\text{lat}} = \prod \left\{ \frac{(\omega_y)^{k_y}}{\prod_{\kappa}^{k_y} U_y(\kappa)} \frac{[\lambda_y(0)]^{k_y}}{\prod_{\kappa}^{k_y} A_y(0, \kappa)} \frac{[\lambda_x(k_y)]^{k_x}}{\prod_{\kappa}^{k_x} A_x(\kappa, k_y)} \right\} \frac{1}{\sqrt{N_x^{N_e}}} \sum_{\{X\}} e^{-i2\pi \sum k_x X / N_x} \langle \{j^{X, k_y}\} | \Psi; s, r \rangle. \quad (70)$$

Here the product outside the curly braces is over the (k_x, k_y) configurations of the N_e particles, and $\langle \{j^{X, k_y}\} | \Psi; s, r \rangle$ are the many-body amplitudes of the recombined FQH states [Eq. (15)].

The above formula is the central result of this paper. This prescription is not limited to a specific model wave function. It applies to *any* FQH state that can be expressed in a second-quantized basis; a real-space wave function is not actually needed. We note that the absolute value of each component in the Bloch basis does not depend on the gauge choice of the Wannier states, thanks to the X -independence of $e^{i\Phi_y(X, k_y)}$.

V. INVERSION SYMMETRY

Although not a vital element of a topological phase, the inversion symmetry is respected by FQH model wave functions. Many Chern insulator models are inversion symmetric as well. For such models, the acceptable many-body wave functions for a *featureless* liquid state must respect inversion symmetry. To this end, in the following we specialize to inversion-symmetric Chern insulators and show that our construction always preserves inversion symmetry on the many-body level.

A. Inversion Symmetry of the FQH States

First we briefly discuss the FQH inversion symmetry in the continuum. Inversion is implemented by the unitary operator \mathcal{P} :

$$\mathcal{P}|\tilde{x}, \tilde{y}\rangle = |-\tilde{x}, -\tilde{y}\rangle. \quad (71)$$

Evidently $\mathcal{P}^2 = 1$. Using the definition of $\langle \tilde{x}, \tilde{y} | j \rangle$ in Eq. (3), we can show that the annihilation operator Ψ_j of

state $|j\rangle$ satisfies $\mathcal{P}\Psi_j\mathcal{P} = \Psi_{-j}$, and thus the occupation-number basis states satisfy

$$\mathcal{P}|\{j\}\rangle = | \{-j\} \rangle. \quad (72)$$

It is straight-forward to show that the FQH Hamiltonian H commutes with \mathcal{P} , and that inversion flips the direction of translation operators,

$$\mathcal{P}T\mathcal{P} = T^\dagger, \quad (73)$$

where T can be any of single-particle or many-body translation operator, such as T_{cm}^x , S_x , or R_y .

Inversion does not commute with the relative translation operators. Therefore, in general the operator \mathcal{P} mixes different center-of-mass multiplets. However, the ground state energy level in an Abelian topological phase is populated exclusively by the q -fold degenerate ground state, and the operator \mathcal{P} must operate within the q -fold center-of-mass multiplet, since $[H, \mathcal{P}] = 0$.

Consider the action of \mathcal{P} on the state $|\Psi\rangle$ that we pick from the q -fold ground states. This state has total momentum (κ_x, κ_y) . By the above argument, κ_x must be inversion symmetric, while κ_y changes to $-\kappa_y$ under inversion. Inversion on $|\Psi\rangle$ can be compensated by a center-of-mass translation. We can find a unique $t \in [0 .. q)$ such that

$$tN_e = -2\kappa_y \bmod N_\phi. \quad (74)$$

Then, $|\Psi\rangle$ must be an eigenstate of $\mathcal{P}(T_{\text{cm}}^x)^t$. This composite operator satisfies $[\mathcal{P}(T_{\text{cm}}^x)^t]^2 = 1$ thanks to Eq. (73), and thus the eigenvalue ζ_Ψ has to be ± 1 :

$$\mathcal{P}|\Psi\rangle = \zeta_\Psi (T_{\text{cm}}^x)^t |\Psi\rangle. \quad (75)$$

We move on to discuss the recombined states $|\Psi; s, r\rangle$. Plugging Eq. (75) into Eq. (15), we have

$$\begin{aligned} & \mathcal{P}|\Psi; s, r\rangle \\ &= \frac{1}{\sqrt{q_x}} \sum_m^{q_x} e^{i2\pi m(\kappa_x + sN_e)/(Nq_x)} (S_x)^{-m} (T_{\text{cm}}^x)^{t-r} \zeta_\Psi |\Psi\rangle \\ &= \zeta_\Psi |\Psi; \bar{s}, \bar{r}\rangle, \end{aligned} \quad (76)$$

Here \bar{r} is defined by

$$\bar{r} = t - r, \quad (77)$$

and $\bar{s} \in [0 .. q_x)$ by

$$-(\kappa_x + sN_e) = \kappa_x + \bar{s}N_e \pmod{Nq_x}. \quad (78)$$

It is easy to show that there exists a unique value of $\bar{s} \in [0 .. q_x)$ satisfying the above constraint. From $\bar{r} = t - r$, we can show that

$$-(\kappa_y + rN_e) = \kappa_y + \bar{r}N_e \pmod{N_0xN_y}. \quad (79)$$

In components, Eq. (76) reads

$$\langle \{-j\} | \Psi; s, r \rangle = \zeta_\Psi \langle \{j\} | \Psi; \bar{s}, \bar{r} \rangle. \quad (80)$$

B. Inversion Operator on the Lattice

We now extend the inversion operator \mathcal{P} to the lattice. As shown in Appx. C 1, the exponentiated position operators transforms under inversion by

$$\mathcal{P}\hat{x}\mathcal{P} = \hat{x}^\dagger, \quad \mathcal{P}\hat{y}\mathcal{P} = \hat{y}^\dagger. \quad (81)$$

Since the single-particle Hamiltonian is inversion symmetric, the unitary operator \mathcal{P} must take the Bloch state $|k_x, k_y\rangle$ to $|-k_x, -k_y\rangle$, up to a k -dependent phase factor $e^{i\xi_{k_x, k_y}}$ ⁶⁴

$$|-k_x, -k_y\rangle = e^{i\xi_{k_x, k_y}} \mathcal{P}|k_x, k_y\rangle. \quad (82)$$

Considering that $\mathcal{P}^2 = 1$, we have

$$e^{-i\xi_{k_x, k_y}} = e^{i\xi_{-k_x, -k_y}}. \quad (83)$$

These phase factors constitute the inversion sewing matrix; the explicit expressions can be found in Appx. C 1. Since we work in periodic gauge, the phase factor must be periodic as well,

$$e^{i\xi_{k_x + mN_x, k_y + nN_y}} = e^{i\xi_{k_x, k_y}}, \quad (84)$$

for $m, n \in \mathbb{Z}$. If both N_x and N_y are even, there are four points (\bar{k}_x, \bar{k}_y) in the Brillouin zone that are inversion symmetric (up to a reciprocal vector), namely $(0, 0)$, $(N_x/2, 0)$, $(0, N_y/2)$, and $(N_x/2, N_y/2)$. Thanks to Eqs. (83) and (84), we have $e^{i\xi_{k_x, k_y}} = \pm 1$ if (k_x, k_y) is inversion symmetric, and $e^{i\xi_{k_x, k_y}}$ at these points are just the inversion eigenvalues of the lowest band. The periodic boundary condition is crucial in relating $e^{i\xi_{k_x, k_y}}$ to inversion eigenvalue if $(k_x, k_y) \neq (0, 0)$.

C. Inversion Symmetry of the Connections

We now look for the implication of the inversion symmetry in the Berry connection and the Wilson loop. The Berry connection satisfies

$$\begin{aligned} \mathcal{A}_x(k_x, k_y) &= \langle k_x, k_y | \mathcal{P}^2 \hat{x} \mathcal{P}^2 | k_x + 1, k_y \rangle \quad (85) \\ &= e^{i\xi_{k_x, k_y} - i\xi_{k_x+1, k_y}} \langle -k_x, -k_y | \hat{x}^\dagger | -k_x - 1, -k_y \rangle \\ &= e^{i\xi_{k_x, k_y} - i\xi_{k_x+1, k_y}} [\mathcal{A}_x(-k_x - 1, -k_y)]^*, \end{aligned}$$

or for the unitary connections,

$$A_x(k_x, k_y) A_x(-k_x - 1, -k_y) = e^{i\xi_{k_x, k_y} - i\xi_{k_x+1, k_y}}, \quad (86)$$

$$A_y(k_x, k_y) A_y(-k_x, -k_y - 1) = e^{i\xi_{k_x, k_y} - i\xi_{k_x, k_y+1}}. \quad (87)$$

These are the lattice versions of the transformation of the Berry connections in the continuum [Eq. (73) in Ref. 24.]

We now derive the lattice version of some well-known inversion properties of the Wilson loop.²⁴ Due to the periodicity of the phase factors $e^{i\xi_{k_x, k_y}}$, the unitary discrete Wilson loop satisfies

$$W_x(k_y) W_x(-k_y) = W_y(k_x) W_y(-k_x) = 1. \quad (88)$$

Therefore, at inversion symmetric momentum (\bar{k}_x, \bar{k}_y) , we have

$$W_x(\bar{k}_y) = \pm 1, \quad W_y(\bar{k}_x) = \pm 1. \quad (89)$$

At inversion symmetric \bar{k}_y , the Wannier center must be either on the Bravais lattice, or at a mid-bond point of the Bravais lattice.

If N_x is even, we can go farther and express $W_x(\bar{k}_y)$ as a product of the two inversion eigenvalues at \bar{k}_y .²⁵

$$W_x(\bar{k}_y) = \prod_{\kappa}^{N_x/2} A_x(\kappa, \bar{k}_y) A_x(-\kappa - 1, \bar{k}_y) \quad (90)$$

$$= e^{i\xi_{0, \bar{k}_y} - i\xi_{N_x/2, \bar{k}_y}}. \quad (91)$$

Similarly, if N_y is even, we can show that

$$W_y(\bar{k}_x) = e^{i\xi_{\bar{k}_x, 0} - i\xi_{\bar{k}_x, N_y/2}}. \quad (92)$$

For the moment, we consider the continuum limit with large and even N_x, N_y . Ref. 24 showed that the product of the four inversion eigenvalues at $(k_x, k_y) = (0, 0)$, $(N_x/2, 0)$, $(0, N_y/2)$, and $(N_x/2, N_y/2)$ is equal to $(-1)^C = -1$ for $|C| = 1$. Therefore, in addition to Eq. (88), we now have

$$W_x(0) W_x(N_y/2) = W_y(0) W_y(N_x/2) = -1. \quad (93)$$

The case where N_x or N_y is odd needs special treatment, as we will see soon.

These properties of the Wilson loop strongly constrain the shift parameter δ_y for the Wannier-LLL mapping introduced in Sec. III C. Recall that we pick the argument angle $\arg[W_x(k_y)] \in (-2\pi, 0]$. The shift $\delta_y \in [0 .. N_y)$ is

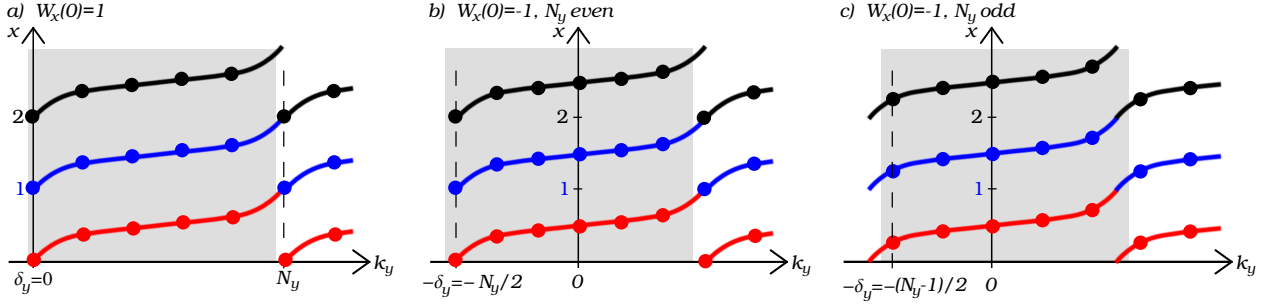


FIG. 5: The shift parameter δ_y fixed by inversion for $C = +1$. The three panels correspond to the three cases in Eq. (94). Compared with Fig. 2, here we highlight the discrete nature of the finite-size system. The wave number k_y takes N_y discrete values in each Brillouin zone. The solid dots represents the N_y Wannier centers in each unit cell, colored coded by the unit cell index X . The gray shade shows the principal Brillouin zone $Ck_y + \delta_y \in [0 .. N_y)$.

defined as the number of $W_x(k_y)$ with $\arg[W_x(k_y)] > \arg[W_x(0)]$. We have shown that the Wilson loops $W_x(k_y)$ come in complex-conjugate pairs at momenta coupled by inversion, and in particular, $W_x(0) = \pm 1$. As illustrated in Fig. 5, with inversion, the shift δ_y is fixed to

$$\delta_y = \begin{cases} 0 & \text{if } W_x(0) = 1; \\ N_y/2 & \text{if } W_x(0) = -1 \text{ and } N_y \text{ even;} \\ (N_y - 1)/2 & \text{if } W_x(0) = -1 \text{ and } N_y \text{ odd.} \end{cases} \quad (94)$$

A key quantity in our gauge choice Eq. (63) for the Wannier states is $\lambda_y(0)\omega_y$. We now examine the constraint from inversion symmetry on it. Since $[\lambda_y(0)]^{N_y} = W_y(0)$ [Eq. (30)] and $W_y(0)$ is fixed by inversion symmetry to ± 1 , we have

$$[\lambda_y(0)]^{2N_y} = 1. \quad (95)$$

As shown in Appx. C2, the curvature fluctuations are also subject to the inversion symmetry,

$$U_y(k_y)U_y(-k_y - 1) = 1. \quad (96)$$

Recall from Eq. (59) that $(\omega_y)^{N_y} = \prod_{\kappa}^{N_y} U_y(\kappa)$. We can recombine the U_y factors in $[\prod_{\kappa}^{N_y} U_y(\kappa)]^2$ into pairs, and get

$$(\omega_y)^{2N_y} = 1. \quad (97)$$

Combining this with Eq. (95), we have

$$[\lambda_y(0)\omega_y]^{2N_y} = 1. \quad (98)$$

D. Inversion Symmetry of the Wannier States

In Appx. C3, we find the action of the inversion operator \mathcal{P} on the Wannier states $|X, k_y\rangle$:

$$\begin{aligned} & e^{i\xi_0, k_y} e^{-i\Phi_y(X, k_y)} \mathcal{P}|X, k_y\rangle \\ &= \begin{cases} e^{-i\Phi_y(-X, -k_y)} | -X, -k_y\rangle & \text{if } W_x(k_y) = 1, \\ e^{-i\Phi_y(-X-1, -k_y)} | -X-1, -k_y\rangle & \text{otherwise.} \end{cases} \end{aligned} \quad (99)$$

Considering that we place the X -th unit cell over the interval $[X, X + 1)$, this rule of transformation is not surprising: for example, inversion takes an on-site Wannier state centered at $x = 2 + 0$ to a state centered at $x = -2 + 0$, while it takes a Wannier state centered at $x = 2 + 0.3$ to $x = -3 + 0.7$, to be in $[X, X + 1)$.

In Sec. IV B, we make the gauge choice with $e^{i\Phi_y(X, k_y)}$ independent from X . We now drop the X argument and write $e^{i\Phi_y(k_y)}$. This enables us to further simplify the $e^{i\Phi_y(k_y)}$ factors in Eq. (99). The starting point is the recursive definition of $e^{i\Phi_y(k_y)}$ in Eq. (63). Define the shorthand notation

$$\tilde{A}_y(k_y) = A_y(0, k_y)U_y(k_y). \quad (100)$$

Then Eq. (63) could be rewritten as

$$e^{i\Phi_y(k_y+1) - i\Phi_y(k_y)} = \frac{\lambda_y(0)\omega_y}{\tilde{A}_y(k_y)}, \quad (101)$$

thanks to the periodicity of $e^{i\Phi_y(k_y)}$ in k_y . We would now like to relate, by recursion of Eq. (101), $e^{i\Phi_y(k_y)}$ with $e^{i\Phi_y(-k_y)}$. The result would be a product of $\lambda_y(0)\omega_y/\tilde{A}_y(\kappa)$ along the path connecting $-k_y$ to k_y . Thanks to the periodicity of $e^{i\Phi_y(k_y)}$ in k_y , we can focus on the first Brillouin zone $k_y \in [0 .. N_y)$. Since $-k_y \leq k_y$, successive application of Eq. (101) leads to

$$\begin{aligned} e^{i\Phi_y(0, k_y) - \Phi_y(0, -k_y)} &= \prod_{\kappa=-k_y}^{k_y-1} \frac{\lambda_y(0)\omega_y}{\tilde{A}_y(\kappa)} \\ &= [\lambda_y(0)\omega_y]^{2k_y} \left/ \prod_{\kappa=0}^{k_y-1} \tilde{A}_y(\kappa)\tilde{A}_y(-\kappa-1) \right. \end{aligned} \quad (102)$$

The product of \tilde{A}_y factors in the rewritten form on the second line shows the inversion symmetry structure explicitly: from the inversion symmetry structure of $A_y(k_x)$ in Eq. (87) and that of $U_y(k_y)$ in Eq. (96), we have

$$\tilde{A}_y(k_y)\tilde{A}_y(-k_y - 1) = e^{i\xi_0, k_y - i\xi_0, k_y+1}. \quad (103)$$

Plugging this into Eq. (102), we get the relative phase between the Wannier states which are inversion partners

$$e^{i\Phi_y(k_y) - i\Phi_y(-k_y)} = e^{i\xi_{0,k_y} - i\xi_{0,0}} [\lambda_y(0) \omega_y]^{2k_y}. \quad (104)$$

Therefore, the inversion operation on the Wannier states [Eq. (99)] can be simplified to

$$\begin{aligned} e^{i\xi_{0,0}} [\lambda_y(0) \omega_y]^{-2k_y} \mathcal{P}|X, k_y\rangle \\ = \begin{cases} |-X, -k_y\rangle & \text{if } W_x(k_y) = 1, \\ |-X - 1, -k_y\rangle & \text{otherwise.} \end{cases} \end{aligned} \quad (105)$$

This concludes our analysis of the action of inversion on the one-body states.

E. Inversion Symmetry of the Many-Body States

When the one-body model is inversion symmetric, we require the FCI many-body wave functions on lattice to inherit the inversion symmetry of the FQH states on a torus. First we check whether the inversion transformation is compatible with the Wannier-LLL mapping on the *index* level. Under inversion, the LLL state index transforms by $j \rightarrow -j \bmod N_\phi = N_x N_y$, while as shown in Eq. (105), the Wannier state index transforms by

$$(X, k_y) \rightarrow \begin{cases} (-X, -k_y) & \text{if } W_x(k_y) = 1, \\ (-X - 1, -k_y) & \text{otherwise.} \end{cases} \quad (106)$$

In Appx. C 4, we show that the 1D index j^{X,k_y} defined by Eq. (43) transforms by

$$j^{X,k_y} \rightarrow \begin{cases} -j^{X,k_y} - 1 & \text{if } W_x(0) = -1 \text{ and } N_y \text{ odd;} \\ -j^{X,k_y} & \text{otherwise.} \end{cases} \quad (107)$$

Note that for a given system, all the j^{X,k_y} indices obey the *same* transformation rule. The transformation in the first case is *not* a good FQH symmetry on the single-particle level. However, on the many-body level, a simultaneous change j to $-j - 1$ for *all particles* is a good symmetry, implemented by $\mathcal{PT}_{\text{cm}}^x$.

Finally, we are ready to investigate the inversion symmetry of the many-body lattice state $|\Psi; s, r\rangle_{\text{lat}}$ defined in Eq. (48). Plugging Eqs. (105) and (107) into the Wannier-LLL mapping in Eq. (48), we can get the inverted amplitudes on the FQH side. Then, we can apply Eq. (80) and relate it to another state in the q -fold multiplet and map it back to the lattice. This identifies the inversion partner of the many-body lattice state and obtains the many-body matrix elements of the lattice operator \mathcal{P} in the q -dimensional subspace. The details are presented in Appx. C 5, while the gist is the following. The q lattice states $|\Psi; s, r\rangle_{\text{lat}}$ come in inversion pairs:

$$\mathcal{P}|\Psi; s, r\rangle_{\text{lat}} \propto \begin{cases} |\Psi; \bar{s}, \bar{r} - 1\rangle_{\text{lat}} & \text{if } W_x(0) = -1 \text{ and } N_y \text{ odd;} \\ |\Psi; \bar{s}, \bar{r}\rangle_{\text{lat}} & \text{otherwise.} \end{cases} \quad (108)$$

Here the indices (\bar{s}, \bar{r}) are defined conjugate to (s, r) , in Eqs. (77) and (78). Recall that the total momentum of the N_e particles in state $|\Psi; s, r\rangle$ is given by $(K_x, K_y) = [\kappa_x + sN_e, C\kappa_y + C(r - \delta_y)N_e] \bmod (N_x, N_y)$ [Eq. (69)]. The total momentum of its inversion partner given in the above equation is $(-K_x, -K_y) \bmod (N_x, N_y)$, as anticipated and shown in Appx. C 5.

To summarize, our construction of lattice wave functions indeed preserves on the many-body level the inversion symmetry of the host Chern insulator. In contrast, the gauge and the original construction in Ref. 15 does not preserve inversion symmetry unless $W_y(0) = 1$, as shown in Appx. G.

VI. NUMERICAL TESTS

We perform the Wannier construction in the five fermionic lattice models studied previously at filling $\nu = 1/3$: the checkerboard lattice model,²⁶ the Haldane model on the honeycomb lattice,¹ a two-orbital model that resembles half (spin-up) of the mercury-telluride two-dimensional topological insulator,²⁷ the Kagome lattice model with spin-orbit coupling between nearest neighbors,²⁸ and the spin-polarized ruby lattice model.²⁹ For each model, we use the parameter set specified previously^{4,7} and focus on the lattice sizes and aspect ratios where the system has a threefold quasi-degenerate ground state in numerics well separated from the excited states. These are all inversion symmetric models, for which we list the values of $W_x(0)$, $W_y(0)$, and C for each model in Table I.

We obtain the ‘‘Laughlin’’ FCI states on the lattice using the formalism described in this paper, i.e. replacing $|\Psi\rangle$ in Eqs. (15) and (70) by the Laughlin FQH states on the torus in the continuum. The threefold Laughlin FQH states are obtained by numerically diagonalizing the FQH model Hamiltonian with only the first pseudopotential, $V_m = \delta_{m,1}$. Details of the continuum FQH Hamiltonian can be found in Appx. A. As detailed in Sec. III C, the continuum torus for the FQH calculations has the same aspect ratio as the lattice system, and the twist angle θ of the five models are given in the last column of Table I. The three Laughlin states are exact replicas except for a

TABLE I: Values of the Chern number C , the Wilson loops $W_x(0)$ and $W_y(0)$, and the twist angle θ of the corresponding FQH torus, for the five lattice models at the studied parameters.

Model	C	$W_x(0)$	$W_y(0)$	θ
Checkerboard	-1	+1	-1	$\pi/2$
Haldane	-1	+1	-1	$\pi/3$
Kagome	+1	+1	+1	$\pi/3$
Ruby	-1	-1	+1	$\pi/3$
Two-orbital	+1	-1	-1	$\pi/2$

shift in the total momentum κ_y . As shown in Sec. II A, they can be recombined into $|\Psi; s, r\rangle$ and then mapped to the lattice using the Wannier basis. We will refer to the resulting lattice states as the Laughlin FCI states, as opposed to the Laughlin FQH states in the continuum.

For all of the five models, we find that the Laughlin FCI states are indeed translationally invariant and inversion symmetric. In contrast, if we follow the prescription in Ref. 15, the resulting many-body states break the inversion symmetry for the checkerboard lattice model, the two-orbital model, and the Haldane model. As explained in Appx. G, the issue responsible for this is that the Wilson loop $W_y(0)$ equals -1 in these models at the studied parameter set.

A. Overlap

The relevance of the Laughlin FCI states can be checked by computing the overlap with the ground states obtained from exact diagonalization of the FCI models at filling $\nu = 1/3$.^{4,7}

The number and momenta of Laughlin FCI states (shown in Sec. IV D) match those of the exact ground states obtained by exact diagonalization. When both N_x and N_y are divisible by 3, all of the threefold states have total momentum zero. In such cases with more than one state in a certain momentum sector, the states can mix and we do not have a one-one correspondence between the two groups of states to compute the overlaps. Instead, we first build the projector into the subspace spanned by the exact diagonalization states, then the projector into the subspace spanned by the Laughlin FCI states, and finally, we define the overlap to be the trace of the product of the two projectors, divided by the dimension of the subspace, i.e.

$$\frac{1}{3} \sum_i \sum_{s,r} \left| \text{lat} \langle \text{ED}; i | \Psi; s, r \rangle_{\text{lat}} \right|^2, \quad (109)$$

where $|\text{ED}; i\rangle_{\text{lat}}$, $i = 1, 2, 3$ are the threefold ground states obtained from exact diagonalization, and the indices (s, r) are summed over the threefold Laughlin FCI states in the same momentum sector. This naturally generalizes the usual definition of overlap as the absolute square of the inner product. When the Laughlin FCI states appear at different momenta, we take the usual overlap with the exact diagonalization states.

Shown in Fig. 6 against the Hilbert space dimension are the overlap values between the Laughlin FCI states obtained by the Wannier construction and the exact ground states at filling $\nu = 1/3$, of the five models on a lattice of size 4×3 , 5×3 , 6×3 , 7×3 , and 6×4 . The only exception is the two-orbital model: it does not have a *gapped* threefold quasi-degenerate ground state when $N_y = 3$.⁷ At 6×3 the threefold states have the same total momentum, and thus there is only one overlap value for each model. At other lattice sizes, two of the threefold states

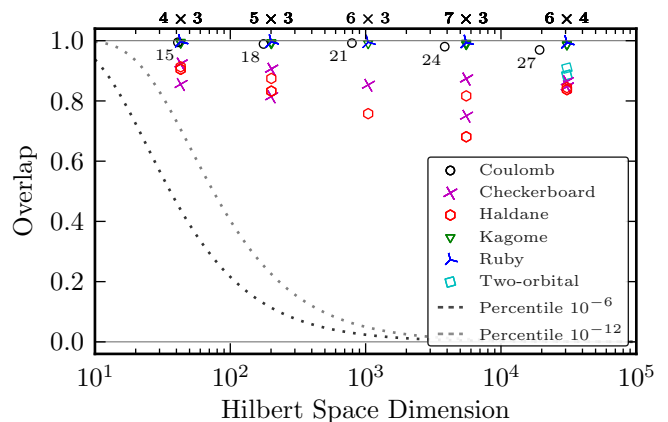


FIG. 6: Overlap between variational states and the exact ground states. The size of the lattice is labeled by $N_x \times N_y$ at top. The plot includes the checkerboard lattice model (purple crosses), the Haldane model (red hexagons), the Kagome lattice model (green triangles), the ruby lattice model (blue Y-shapes), and the two-orbital model (cyan squares). The Wannier construction is performed using the $|X, k_y\rangle$ basis. At 6×3 , the three states in a multiplet are in the same momentum sector, and thus there is one overlap value for each model. At other lattice sizes, two out of the three states have identical overlap due to inversion symmetry. Also shown is the overlap between the FQH ground state of the Coulomb interaction at filling $\nu = 1/3$ and the Laughlin model state, denoted by black circles and labeled by the number of flux N_ϕ . As a baseline, we also plot the top 10^{-6} and 10^{-12} percentiles (gray lines) of the overlap values *between random unit vectors* as a function of the Hilbert space dimension. The overlap axis range is set to $[0, 1]$ to contrast with Fig. 7.

form an inversion pair and have the same overlap value. Also shown in Fig. 6 are the overlap values between the Laughlin state and the FQH ground state of the Coulomb interaction on a torus with unity aspect ratio, pierced by $N_\phi = 15, 18, 21, 24, 27$ fluxes.

We find that at comparable Hilbert space sizes, the overlap for the Kagome lattice model and the ruby lattice model are comparable with or *even higher* than the overlap for the Coulomb interaction in the continuum, while the overlap for the Haldane model, the two-orbital model, and the checkerboard lattice model have slightly lower overlap than the Coulomb interaction. We note one possible reason for the higher overlaps in the FCI systems. The lattice interactions used in the FCI models are Hubbard interactions between the nearest neighbors. Their short-ranged nature is preserved by the mapping to the LLL via the *localized* Wannier states, and thus the FCI interaction in the Wannier/LLL basis maybe be closer to the Laughlin pseudopotential Hamiltonian, compared with the long-range Coulomb interaction in the continuum.

We emphasize that the overlap with the Laughlin FCI state should be interpreted in the context of the size of the Hilbert space. In Appx. H we find that the probability for two random complex unit vectors in a space of

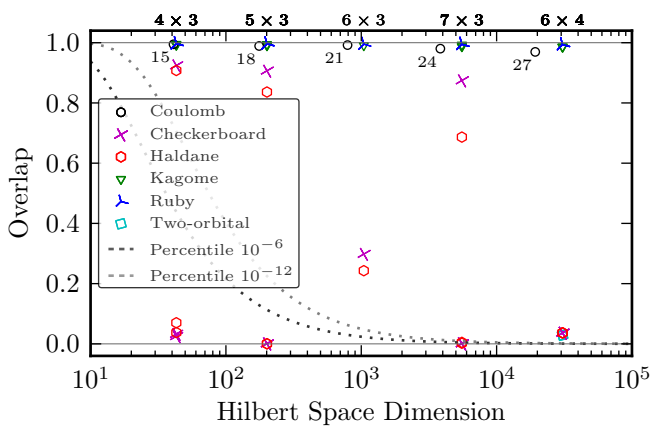


FIG. 7: Overlaps between variational states and the exact ground states using the prescription in Ref. 15. Inversion breaking for the checkerboard lattice model and the Haldane model is clearly visible at 4×3 , and present (although not discernible in this figure) at other lattice sizes. Inversion breaking for these models is also present at 7×3 and 6×4 , even though obscured by the finite resolution of the plot. The inversion symmetry of the two-orbital model at 6×4 is also broken.

dimension d to have an overlap larger than a given value is *exponentially small* at large d . This is illustrated in Fig. 6 by the plot of the top 10^{-6} and 10^{-12} percentile values of the overlap between random vectors, as a function of the Hilbert space dimension.

We observe a slight decreasing trend in the overlap as the system size increases, much slower than the exponential decay of the random overlap. There is also an upward kink when going from 7×3 to 6×4 for the checkerboard lattice and the Haldane models. This agrees with the finding in Ref. 4 that the topological phase is more stable when the aspect ratio is closer to unity.

We have also tested the performance of the proposal in Ref. 15. While the original proposal was given in the continuum limit $N_x, N_y \rightarrow \infty$ (formulated using derivatives such as $\langle k_x, k_y | \partial_{k_x} | k_x, k_y \rangle$) and on a cylinder, as detailed in Appx. G, we extend this proposal to handle finite-size lattice models with multiple sublattices and periodic boundaries, but do not change the gauge used there. We repeat the overlap calculations using this alternative prescription. The results are compiled in Fig. 7. The overlap values for the Kagome lattice model and the ruby lattice model are comparable with those calculated using our proposal. However, the overlap values for the checkerboard lattice model, the two-orbital model (which is the model in the original discussion¹⁵), and the Haldane model are much lower than the values obtained from our prescription. At 6×4 , the overlap values for these three models fall below 0.04. Also, the constructed many-body states break the inversion symmetry in these models. The culprit is explained in Appx. F 3 and Appx. G. In short, when $W_y(0) \neq 1$, the gauge choice $a_y = 0$ used in Ref. 15 does not mimic the behavior of the LLL or

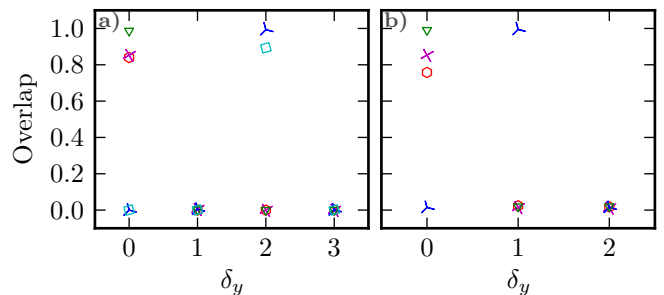


FIG. 8: Overlaps between the Laughlin FCI states and the exact diagonalization states, as a function of the shift parameter δ_y in the Wannier-LLL mapping. Please refer to the legend and caption of Fig. 6 for the annotation of scatter symbols. The left (right) panel shows the calculations on a 6×4 (6×3) lattice. For clarity, for each model at each δ_y we show the average overlap of the threefold states. The two-orbital model is not included in the 6×3 calculation, as it does not have a gapped topological ground state at this lattice size. The values of δ_y that produce significant overlaps are in full agreement with Eq. (94).

bitals: enforcing $a_y = 0$ in the interior of the Brillouin zone mandates that the connection on the Brillouin zone boundary has to take care of the gauge-invariant Wilson loop, and deviates from $a_y = 0$. The prescription in Ref. 15 does not properly handle the cases where the Wilson loop $W_y(0)$ is not unity, which include the above three lattice models at the studied parameters, as shown in Table I.

B. Mapping Parameters Revisited

In the previous section, the shift parameter δ_y for the Wannier-LLL mapping and the twist angle θ of the continuum torus used in the FQH calculations were set according to the discussions in Sec. III C. We now revisit the choice of δ_y and θ by checking explicitly how it affects the overlaps with the FCI ground states.

First we perform the Wannier constructions for the five models using the θ angle specified in Table I, but we vary the shift parameter δ_y over $[0 .. N_y)$. In Fig. 8, we show the dependence of the overlaps on δ_y for 6×4 and 6×3 lattices. At $N_y = 4$ (even), for the three models with $W_x(0) = +1$, namely (see Table I), the Kagome lattice model, the checkerboard lattice model, and the Haldane model, the Laughlin FCI states have significant overlaps with the exact diagonalization ground states only at $\delta_y = 0$; for the two models with $W_x(0) = -1$, namely, the ruby lattice model and the two-orbital model, the significant overlaps appear at $\delta_y = 2 = N_y/2$. At $N_y = 3$ (odd), the significant overlaps for the three models with $W_x(0) = +1$ are still at $\delta_y = 0$, but for the ruby lattice models with $W_x(0) = -1$, the peak in overlap is shifted to $\delta_y = 1 = (N_y - 1)/2$.⁶⁵ The above results are in full agreement with the choice of δ_y in Eq. (94).

We now put δ_y to the values specified by Eq. (94), but

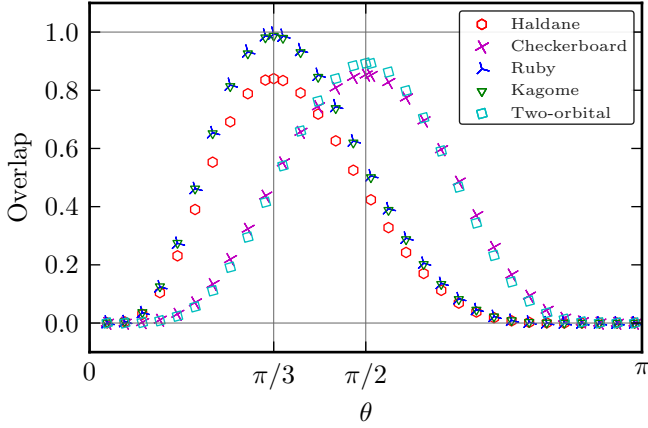


FIG. 9: Overlaps between the Laughlin FCI states and the exact diagonalization states on a 6×4 lattice, as a function of the twist angle θ of the continuum torus for the FQH calculations. For clarity, for each model at each δ_y we show the average overlap of the threefold states. For each model, a peak in overlap is clearly visible at the value of θ given in Table I, in accordance with the discussion in Sec. III C.

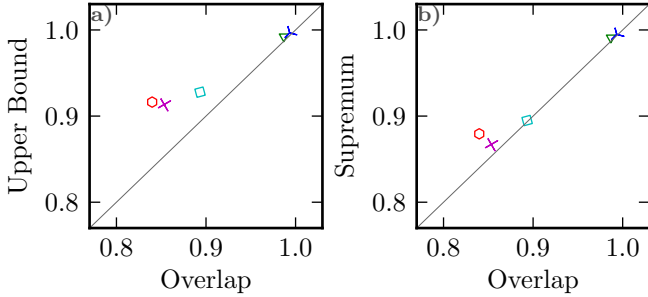


FIG. 10: Overlap optimization for the Laughlin lattice states by tuning the single-particle gauge. The calculations are performed on a 6×4 lattice. Please refer to the legend and caption of Fig. 6 for the annotation of scatter symbols. Shown in a) is the overlap upper bound (110) obtained by removing the relative phase at each component between the exact ground state and the Laughlin lattice state, against the actual overlap. Shown in b) is the supremum (the least upper bound) of the overlap, obtained by a brute force optimization of the single-particle gauge of the Bloch states, against the actual overlap.

vary the twisted angle θ of the continuum torus for FQH calculations. The overlaps as a function of θ are shown in Fig. 9. For each of the five models, we find a clear peak in overlap centered around the value of θ suggested in Sec. III C, as shown in Table I. This confirms that our choice of the twist angle θ is appropriate.

C. Gauge Optimization

As detailed in Sec. IV B, the phase choice $e^{i\Phi_y(X, k_y)}$ of the Wannier basis is based on the similarity with the LLL orbital behavior. There are other possible alterna-

tive gauge choices. We now try to understand how close our gauge fixing procedure gets to several brute-force optimized gauges.

We first examine the limit where the phases of the Slater determinant weights in the variational trial states are tuned to match perfectly with the phases in the exact diagonalization ground states. Eq. (70) shows that the *absolute value* of each component $\langle \{k_x, k_y\} | \Psi; s, r \rangle_{\text{lat}}$ of the many-body state in the Bloch basis does not depend on the parallel-transport gauge in the k_x direction, nor on the gauge choice of the Wannier states if we limit ourselves to a set of $e^{i\Phi_y(X, k_y)}$ phases that have no real X dependence. Inspired by this, we remove the relative phase from the Bloch-basis overlap formula between the Laughlin lattice state $|\Psi; s, r\rangle_{\text{lat}}$ and the corresponding exact diagonalization ground state $|\text{ED}; s, r\rangle$, and calculate

$$\left[\sum_{\{k_x, k_y\}} \left| \langle \text{lat} | \text{ED}; s, r \rangle \langle \{k_x, k_y\} | \Psi; s, r \rangle_{\text{lat}} \right|^2 \right]. \quad (110)$$

This real number serves as *an upper bound* to the actual overlap. It neglects the phases of the Slater determinant weights in the many-body wave functions.⁶⁶ In Fig. 10a), the numerical values of this upper bound are shown against the overlap values from our prescription for the five lattice models. We find that the upper bound is still far from unity for the three under-performing models, namely, the checkerboard lattice model, the Haldane model, and the two-orbital model. This can be interpreted in two possible ways: The X dependence of $e^{i\Phi_y(X, k_y)}$ may be essential for the three models, or, the ground states of the three models may be simply more complicated than the Laughlin lattice states. Our results are not sufficient to distinguish between the two scenarios.

The upper bound is higher than the actual overlaps from our prescription, which would naively suggest that our prescription is not optimal. This is not true. To reach the upper bound calculated in Eq. (110), we need to tune the phases of all the Slater determinant weights in the many-body state. The number of such phases is on the order of $(N_x N_y)$ -choose- N_e . We in no way have the freedom to tune these phases independently. The most we are allowed to do is tune the phases of the $N_x N_y$ Wannier states independently. The *least* upper bound, i.e. the supremum, is hence found by tuning the single-particle gauge to reach maximum overlap. In general, this variational overlap value cannot reach the upper bound in Eq. (110).

The actual supremum can be found by a brute-force optimization. We introduce $N_x \times N_y$ variational gauge degrees of freedom $e^{i\Upsilon_{k_x, k_y}}$ for the Bloch states $|k_x, k_y\rangle$. This transforms the Bloch amplitudes by

$$\langle \{k_x, k_y\} | \Psi; s, r \rangle_{\text{lat}} \Rightarrow e^{-i \sum \Upsilon_{k_x, k_y}} \langle \{k_x, k_y\} | \Psi; s, r \rangle_{\text{lat}}.$$

We optimize the average overlap with the threefold exact ground states by tuning these $N_x N_y$ parameters. As

explained in Sec. III B, $e^{i\Upsilon_{0,k_y}}$ covers the degrees of freedom carried by the Wannier phase choice $e^{i\Phi_y(k_y)}$. We are not able to perform the optimization on $e^{i\Phi_y(X,k_y)}$ with non-trivial X -dependence due to the prohibiting computational complexity. We use the Nelder-Mead (downhill simplex) algorithm³⁰ to find the local overlap maximum around our prescription. The convergence threshold is 10^{-4} on the overlap (output) and the phase angles of the gauge transform (input).

In Fig. 10b), the suprema are shown against the overlap values from our prescription. Comparing with Fig. 10a), we find that the supremum is much lower than the upper bound (110) for the three under-performing models. This reduction is not surprising, since the variational degrees of freedom are far fewer than the number of many-body amplitudes. The proximity of the data points to the diagonal line in Fig. 10b) suggests that our prescription is very close to the optimal one if we refrain from introducing X -dependent phases in $|X, k_y\rangle$. From the values of $e^{i\Upsilon_{k_x,k_y}}$ at the supremum, we find that to improve our prescription, we need to move slightly away from the parallel transport gauge [Sec. III B] in the k_x direction. This may be attributed to the curvature fluctuations. We leave explorations in this direction for future work.

D. Entanglement Spectrum

Overlap only provides an overall, sometimes inaccurate^{31,32} estimate on the similarity between two states. To compare the correlations in the Laughlin FCI states and the ground states, we now turn to their particle entanglement spectra.

First introduced by Li and Haldane,¹⁰ the entanglement spectrum examines the information imprinted in a many-body state. By effectively performing a spectral decomposition of the many-body state, the entanglement spectrum reveals the excitations supported by the state. Of particular interest in our study is the particle entanglement spectrum (PES), which encodes the characteristics of the quasihole excitations from the ground state.³³ We divide the N_e particles into two groups A and B of N_A and N_B particles respectively, trace out the degrees of freedom carried by the particles in B , and examine of the negative logarithm of the eigenvalues of the reduced density matrix ρ_A .

The Laughlin FQH state exhibits a highly non-trivial pattern in the PES:^{9,10,33} In each momentum sector, the number of entanglement levels at finite entanglement energy matches the counting of the Laughlin quasiholes of N_A particles in qN_e fluxes. The total number of levels, i.e. the number of non-zero modes of the reduced density matrix, is much smaller than the dimension of the reduced density matrix.

The PES of various FCI ground states at filling $\nu = 1/3$ has a low entanglement energy structure similar to the PES of the Laughlin state.^{4,7,9} It also displays a non-

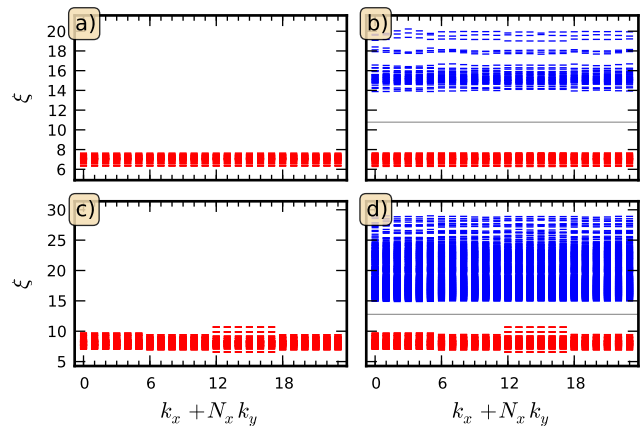


FIG. 11: Particle entanglement spectrum of the Kagome lattice model of $N = 8$ particles on the $N_x \times N_y = 6 \times 4$ lattice. Shown in a) and b) are the spectra of the Laughlin FCI state and the exact ground state, respectively, with $N_A = 3$. Shown in c) and d) are the corresponding spectra with $N_A = 4$. In each momentum sector, we calculate the number of admissible configurations n , and color the lowest n entanglement energy levels in red and the rest in blue. The structure shown in the left panel exhibits the defining characteristic of the Laughlin state.

universal high entanglement energy structure separated by an entanglement gap from the Laughlin-like structure. The number of levels below the gap at each total momentum matches the number of quasiholes folded to the lattice Brillouin zone.⁹ An ideal Laughlin state in the FCI would exhibit an infinite entanglement gap.

For the Laughlin FCI model state obtained from the Wannier construction, we find a large number of zero modes in the reduced density matrix – corresponding to an infinite entanglement gap. The number of the finite entanglement energy levels is given exactly by the counting of Laughlin quasiholes folded to the lattice Brillouin zone. Writing the Laughlin FQH state in the Wannier basis is just a unitary transformation. Thus it does not modify the rank of the reduced density matrix, and it preserves the entanglement spectrum of the Laughlin FQH state. An example is shown in Fig. 11. The entanglement energy levels below the gap of the exact diagonalization ground state exhibit almost identical structure in the spectra of the Laughlin FCI state and the ground state. The Laughlin FCI state captures a very important feature of the correlations in the FCI ground states. This further corroborates the proposal^{4,9} that the quasihole counting in the PES can be interpreted as a signature of a FQH-type of topological phase.

VII. ISOTROPY/NEMATICITY OF THE WANNIER CONSTRUCTION

An undesirable feature of the Wannier construction is that it seems to explicitly break the isotropy between the

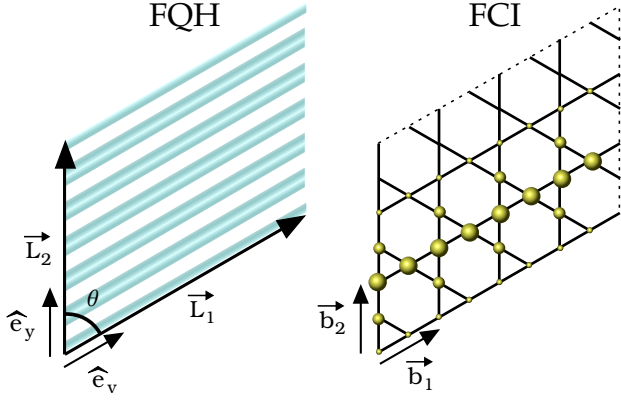


FIG. 12: Single-particle orbitals in the lowest Landau level (LLL) and the Chern band in the alternative gauge choice. In the left panel we show the Landau orbitals in the LLL on a torus. The two fundamental cycles are marked by \mathbf{L}_1 and \mathbf{L}_2 , and the twist angle is labeled by θ . The Landau orbitals are plane waves in the \hat{e}_v direction that are localized in the direction perpendicular to propagation. In the right panel we show a 1D Wannier state localized in the \mathbf{b}_2 direction and in the lowest band of the Kagome lattice model. The size of the spheres depicts the weights of the Wannier state on each lattice site.

two axes of the lattice system when the original Hamiltonian is not fourfold rotationally symmetric.⁶⁷ The formalism singles out one direction in the 2D lattice along which the single-particle states (both on lattice and in the LLL) localize. The two alternative choices of localizing along the x/y direction are not guaranteed to produce the same set of q -fold many-body states for the FCI.

In the following, we show that the weights of the corresponding Bloch-basis Slater determinants in the two sets of many-body states constructed from the two alternatives have the same absolute value, but the phases may differ. However, in the limit of flat curvature, the two alternatives produce exactly the same set of q -fold many-body states. (In this paper we do not explore other possible localization directions of the Wannier basis.)

So far we have been using single-particle states $|X, k_y\rangle$

that are plane waves in the \hat{e}_y direction. We now examine the alternative choice of using single-particle states $|Y, k_x\rangle$ that are *localized* in the \hat{e}_y direction, and the corresponding alternative basis in the LLL.

A. FQH States in a Rotated Gauge

We look for a one-body basis in the LLL that are localized in the \hat{e}_y direction, as illustrated in Fig. 12. The “natural” gauge in this case is aligned along the \hat{e}_v direction. We setup a rotated coordinate system (\tilde{u}, \tilde{v}) with the \tilde{v} axis pointing in the direction of \hat{e}_v :

$$\begin{aligned}\tilde{u}(\tilde{x}, \tilde{y}) &= \tilde{x} \cos \theta - \tilde{y} \sin \theta, \\ \tilde{v}(\tilde{x}, \tilde{y}) &= \tilde{x} \sin \theta + \tilde{y} \cos \theta,\end{aligned}\quad (111)$$

where θ is the angle between the two fundamental cycles of the torus. Then the new gauge is the Landau gauge in the rotated coordinates $\mathbf{A}'(\tilde{x}, \tilde{y}) = B \tilde{u}(\tilde{x}, \tilde{y}) \hat{e}_v$. This is related to the original Landau gauge $\mathbf{A} = B \tilde{x} \hat{e}_y$ by the gauge transform $\mathbf{A}' - \mathbf{A} = \nabla \chi$, with $\nabla = (\partial_{\tilde{x}}, \partial_{\tilde{y}})$ and

$$\chi(\tilde{x}, \tilde{y}) = \frac{B}{2} [\tilde{u}(\tilde{x}, \tilde{y}) \tilde{v}(\tilde{x}, \tilde{y}) - \tilde{x} \tilde{y}]. \quad (112)$$

Since the guiding-center momentum is gauge-covariant, the guiding-center translation operator in the primed gauge is given by

$$T'_i(\mathbf{a}) = e^{ie\chi/\hbar} T_i(\mathbf{a}) e^{-ie\chi/\hbar}. \quad (113)$$

From this we can obtain the primed variants of the many-body translation operators discussed earlier.

We denote by $|j\rangle'_v$ and ${}_v\langle j|$ the single-particle states in this gauge that satisfy the guiding-center periodic boundary conditions $T'_i(\mathbf{L}_1) = T'_i(\mathbf{L}_2) = 1$. The prime highlights the alternative gauge choice \mathbf{A}' , while the superscript v emphasizes that this state is propagating in the \hat{e}_v direction (and localized in the \hat{e}_y direction). The wave functions of these states resemble those in the unprimed gauge [Eq. (3)],

$$\phi_j^{v'}(\tilde{x}, \tilde{y}) = \frac{1}{(\sqrt{\pi} L_1 l_B)^{1/2}} \sum_n \exp \left[-2\pi(j + nN_\phi) \frac{\tilde{u}(\tilde{x}, \tilde{y}) + i\tilde{v}(\tilde{x}, \tilde{y})}{L_1} + i \frac{\pi}{N_\phi} \frac{L_2 e^{i\theta}}{L_1} (j + nN_\phi)^2 \right] e^{-[\tilde{u}(\tilde{x}, \tilde{y})]^2 / (2l_B^2)}. \quad (114)$$

The state $|j\rangle'_v$ is localized along the line $\tilde{y} = \tilde{x} \cot \theta + jL_2/N_\phi$. The center line moves in the *positive* \hat{e}_y direction when we increase j .

The Slater determinant basis $|\{j\}\rangle'_v$ for the N_e -electron Hilbert space generates a representation of the many-

body translation operators. In particular, we find

$$\begin{aligned}T_{\text{rel}}^{x'} |\{j\}\rangle'_v &= e^{-i2\pi \sum j/N} |\{j\}\rangle'_v, \\ T_{\text{rel}}^{y'} |\{j\}\rangle'_v &= |\{j - q\}\rangle'_v, \\ T_{\text{cm}}^{x'} |\{j\}\rangle'_v &= e^{i2\pi \sum j/N_\phi} |\{j\}\rangle'_v, \\ T_{\text{cm}}^{y'} |\{j\}\rangle'_v &= |\{j + 1\}\rangle'_v.\end{aligned}\quad (115)$$

In contrast to the unprimed transformations in Eq. (9), the translations in the \mathbf{L}_1 (rather than \mathbf{L}_2) direction are diagonal, and the eigenvalues of the diagonal operators differ by a complex conjugate.

We can diagonalize the interaction system with the help of the many-body translational symmetries. For obvious reasons the eigenstates are just the gauge-transform of the states discussed in Sec. II A. Recall the state $|\Psi\rangle$ diagonal in $(T_{\text{rel}}^x, T_{\text{cm}}^y)$ with wave number (κ_x, κ_y) . Denote by $|\Psi\rangle'$ the gauge-transformed state. Then we have

$$\begin{aligned} T_{\text{rel}}^{x'}|\Psi\rangle' &= e^{i2\pi\kappa_x/N}|\Psi\rangle', \\ T_{\text{cm}}^{y'}|\Psi\rangle' &= e^{-i2\pi\kappa_y/N_\phi}|\Psi\rangle'. \end{aligned} \quad (116)$$

And the simultaneous eigenstates of S'_x , R'_y , and the Hamiltonian can be constructed from $|\Psi\rangle'$ in a parallel manner to the construction of $|\Psi; s, r\rangle$ state in Sec. II A. The result is of course given by the gauge transform $|\Psi; s, r\rangle'$.

We can express the $|\Psi; s, r\rangle'$ states by the amplitudes $\langle\{j\}|\Psi; s, r\rangle'$. We emphasize that

$$\langle\{j\}|\Psi; s, r\rangle' \neq \langle\{j\}|\Psi; s, r\rangle, \quad (117)$$

because the single-particle state $|j\rangle'_v$ is *not* the gauge transform of the state $|j\rangle$. We now seek a link between the two unequal amplitudes in Eq. (117). First, we can transform $|j\rangle'_v$ back to the unprimed gauge, using $\chi(\tilde{x}, \tilde{y})$ given by Eq. (112). The resulting states $|j\rangle_v$ are given by the wave function

$$\phi_j^v(\tilde{x}, \tilde{y}) = e^{i[\tilde{x}\tilde{y} - \tilde{u}(\tilde{x}, \tilde{y})\tilde{v}(\tilde{x}, \tilde{y})]/(2l_B^2)} \phi_j^{v'}(\tilde{x}, \tilde{y}). \quad (118)$$

These state are still propagating in the \hat{e}_v direction, as signified by the super/sub-script v . We thus arrive at an alternative single-particle basis $|j\rangle_v$ of the LLL in the Landau gauge.

Thanks to the invariance of the inner product under the gauge transform, the many-body amplitudes satisfy

$$\langle\{j\}|\Psi; s, r\rangle' = \langle\{j\}|\Psi; s, r\rangle. \quad (119)$$

The last ingredient is the expansion of the state $|j\rangle_v$ in the $|j\rangle$ basis. We have already seen some hint from the two representations of the many-body translation operators. Comparing Eq. (9) and Eq. (115), we find that the

Slater determinant state formed by a *Fourier series* of the Landau orbitals $|m\rangle$ transforms in the same way as $|\{j\}\rangle_v$ under the many-body translation operators. We can actually prove that

$$|j\rangle_v = \frac{e^{i(\frac{\pi}{4} - \frac{\theta}{2})}}{\sqrt{N_\phi}} \sum_m^{N_\phi} e^{-i2\pi jm/N_\phi} |m\rangle. \quad (120)$$

This behavior under a Fourier transform is expected of the shifted Gaussian form of the single-particle wave function. The details are presented in Appx. D.

B. Alternative Wannier Construction

The Wannier basis $|Y, k_x\rangle$ localized in the \hat{e}_y direction (see Fig. 12) can be obtained trivially from $|X, k_y\rangle$ by exchanging all x and y and replacing C by $-C$. Using this substitution rule, we can define δ_x , ω_x , $U_x(k_x)$ alongside their sub- y counterparts.

We link the $|Y, k_x\rangle$ state to the LLL orbital $|j^{Y, k_x}\rangle'_v$. The index mapping is given by

$$j_v^{Y, k_x} = YN_x - Ck_x + \delta_x. \quad (121)$$

Here we put a subscript v to distinguish it from the j^{X, k_y} mapping defined earlier. Then we can transcribe the FQH states $|\Psi; s, r\rangle'$ to the lattice. The resulting many-body lattice states $|\Psi; s, r\rangle'_{\text{lat}}$ are translationally invariant. Despite the name, the new lattice states $|\Psi; s, r\rangle'_{\text{lat}}$ are *not the gauge transform* of the states $|\Psi; s, r\rangle_{\text{lat}}$, since they are constructed from different Wannier mappings not related by any gauge transform on a lattice at zero magnetic field. We emphasize that only in the LLL does the prime denote the rotated Landau gauge.

The total momenta of $|\Psi; s, r\rangle'_{\text{lat}}$ are given by

$$\begin{aligned} K_x &= C[\kappa_x + (s + \delta_x)N_e] \bmod N_x, \\ K_y &= \kappa_y + rN_e \bmod N_y. \end{aligned} \quad (122)$$

The counting of the q states in each total momentum sector is exactly the same as the counting of the unprimed lattice states. The amplitudes in the Bloch basis are given by

$$\langle\{k_x, k_y\}|\Psi; s, r\rangle'_{\text{lat}} = \prod \left\{ \frac{(\omega_x)^{k_x}}{\prod_{\kappa}^{k_x} U_x(\kappa)} \frac{[\lambda_x(0)]^{k_x}}{\prod_{\kappa}^{k_x} A_x(\kappa, 0)} \frac{[\lambda_y(k_x)]^{k_y}}{\prod_{\kappa}^{k_y} A_y(k_x, \kappa)} \right\} \frac{1}{\sqrt{N_y}^{N_e}} \sum_{\{Y\}} e^{-i2\pi \sum k_y Y/N_y} \langle\{j_v^{Y, k_x}\}|\Psi; s, r\rangle'. \quad (123)$$

By comparison, recall that

$$\langle\{k_x, k_y\}|\Psi; s, r\rangle_{\text{lat}} = \prod \left\{ \frac{(\omega_y)^{k_y}}{\prod_{\kappa}^{k_y} U_y(\kappa)} \frac{[\lambda_y(0)]^{k_y}}{\prod_{\kappa}^{k_y} A_y(0, \kappa)} \frac{[\lambda_x(k_y)]^{k_x}}{\prod_{\kappa}^{k_x} A_x(\kappa, k_y)} \right\} \frac{1}{\sqrt{N_x}^{N_e}} \sum_{\{X\}} e^{-i2\pi \sum k_x X/N_x} \langle\{j^{X, k_y}\}|\Psi; s, r\rangle. \quad (70)$$

C. Lattice Amplitudes

Now we are ready to check the isotropy/nematicity of the lattice states obtained by the Wannier constructions.

To avoid the unnecessary clutter, here we focus on the simplest case with $C = +1$ and $\delta_x = \delta_y = 0$. The generic case is treated in Appx. E and the conclusion is the same.

In this case, the Wannier mappings are reduced to

$$j^{X,k_y} = XN_y + k_y, \quad j_v^{Y,k_x} = YN_x - k_x. \quad (124)$$

Recall from Sec. III C the subtle point that the above mapping holds only if (k_x, k_y) is in the principal Brillouin zone, in this case $(-N_x .. 0] \times [0 .. N_y)$. To minimize the trouble, we set all the N_e momenta in $\{k_x, k_y\}$ on the left hand side of Eqs. (70) and 123 to the principal Brillouin

zone.

Note that the fractional factors enclosed by the curly braces in those equations are invariant under a shift of Brillouin zones: for example, $(\omega_x)^{k_x} / \prod_{\kappa}^{k_x} U_x(\kappa)$ does not change if we shift $k_x \rightarrow k_x + N_x$. Therefore, we can always pull (k_x, k_y) back to the first Brillouin zone $[0 .. N_x) \times [0 .. N_y)$ when evaluating the prefactors in the curly braces.

Thanks to $C = +1$, $\delta_x = \delta_y = 0$, the dependence of (K_x, K_y) on (s, r) is identical for both $|\Psi; s, r\rangle_{\text{lat}}$ and $|\Psi; s, r\rangle'_{\text{lat}}$. Hence we try to relate the $\langle \{j\} | \Psi; s', r' \rangle'$ and $\langle \{j\} | \Psi; s, r \rangle$ with

$$(s', r') = (s, r). \quad (125)$$

We first plug the Fourier transform in Eq. (120) into Eq. (119). We can rewrite each sum over m in the Fourier transform as a double sum over all unit cells X and all l_y points in the principal Brillouin zone $[0, N_y)$. We find that

$$\langle \{j\} | \Psi; s', r' \rangle' = \frac{e^{i\gamma}}{\sqrt{N_\phi}^{N_e}} \sum_{\{X\}} e^{-i2\pi \sum k_x X / N_x} \sum_{\{l_y\}} e^{i2\pi \sum l_y Y / N_y} e^{-i2\pi \sum k_x l_y / N_\phi} \langle \{j^{X,l_y}\} | \Psi; s, r \rangle, \quad (126)$$

where $e^{i\gamma} = e^{-iN_e(\frac{\pi}{4} - \frac{\theta}{2})}$ is a constant phase factor. Here we have used $e^{i2\pi XY N_x N_y / N_\phi} = 1$, thanks to $N_x N_y = N_\phi$ for $|C| = 1$. Therefore, we have

$$\frac{1}{\sqrt{N_y}^{N_e}} \sum_{\{Y\}} e^{-i2\pi \sum k_y Y / N_y} \langle \{j_v^{Y,k_x}\} | \Psi; s', r' \rangle' = e^{i\gamma} e^{-i2\pi \sum k_x k_y / N_\phi} \frac{1}{\sqrt{N_x}^{N_e}} \sum_{\{X\}} e^{-i2\pi \sum k_x X / N_x} \langle \{j^{X,k_y}\} | \Psi; s, r \rangle, \quad (127)$$

Here the sum over each Y produces a $\delta_{k_y, l_y}^{\text{mod } N_y}$. Since both k_y and l_y are limited to $[0 .. N_y)$, this is just δ_{k_y, l_y} and thus we can remove the sum over $\{l_y\}$. Putting the above equation into Eq. (123), we find that

$$\langle \{k_x, k_y\} | \Psi; s', r' \rangle'_{\text{lat}} = e^{i\gamma} \prod \left\{ \frac{(\omega_x)^{k_x}}{\prod_{\kappa}^{k_x} U_x(\kappa)} \frac{[\lambda_x(0)]^{k_x}}{\prod_{\kappa}^{k_x} A_x(\kappa, 0)} \frac{[\lambda_y(k_x)]^{k_y}}{\prod_{\kappa}^{k_y} A_y(k_x, \kappa)} e^{-i2\pi C k_x k_y / N_\phi} \right\} \frac{1}{\sqrt{N_x}^{N_e}} \sum_{\{X\}} e^{-i2\pi \sum k_x X / N_x} \langle \{j^{X,k_y}\} | \Psi; s, r \rangle. \quad (128)$$

The above equation holds (up to an inconsequential overall constant phase factor) for generic (C, δ_x, δ_y) values, as proved in Appx. E.

Disregarding the overall constant phase $e^{i\gamma}$, the only difference between $\langle \{k_x, k_y\} | \Psi; s', r' \rangle'_{\text{lat}}$ and $\langle \{k_x, k_y\} | \Psi; s, r \rangle_{\text{lat}}$ [Eq. (70)] is the phase enclosed by the curly braces. Therefore, the two alternative choices of the Wannier localization direction produce two sets of many-body lattice states with exactly the same absolute value for each Bloch-basis component,

$$\left| \langle \{k_x, k_y\} | \Psi; s', r' \rangle'_{\text{lat}} \right| = \left| \langle \{k_x, k_y\} | \Psi; s, r \rangle_{\text{lat}} \right|. \quad (129)$$

We now examine the phase part. Define the shorthand

notations for the phase prefactors in Eqs. (70) and (123):

$$e^{i\phi_{k_x, k_y}} \equiv \frac{(\omega_y)^{k_y}}{\prod_{\kappa}^{k_y} U_y(\kappa)} \frac{[\lambda_y(0)]^{k_y}}{\prod_{\kappa}^{k_y} A_y(0, \kappa)} \frac{[\lambda_x(k_y)]^{k_x}}{\prod_{\kappa}^{k_x} A_x(\kappa, k_y)},$$

$$e^{i\phi'_{k_x, k_y}} \equiv \frac{(\omega_x)^{k_x}}{\prod_{\kappa}^{k_x} U_x(\kappa)} \frac{[\lambda_x(0)]^{k_x}}{\prod_{\kappa}^{k_x} A_x(\kappa, 0)} \frac{[\lambda_y(k_x)]^{k_y}}{\prod_{\kappa}^{k_y} A_y(k_x, \kappa)}. \quad (130)$$

Intuitively, $e^{i\phi_{k_x, k_y}}$ comes from the parallel transport in the Brillouin zone along

$$(0, 0) \leftarrow (0, k_y) \leftarrow (k_x, k_y),$$

while the phase $e^{i\phi'_{k_x, k_y}}$ comes from the parallel transport along

$$(0, 0) \leftarrow (k_x, 0) \leftarrow (k_x, k_y).$$

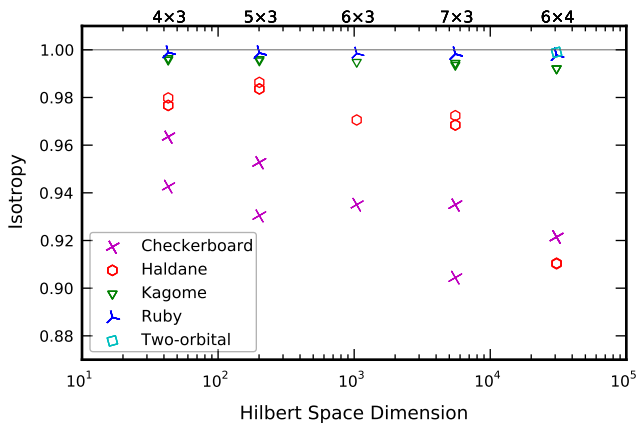


FIG. 13: Isotropy of the Wannier construction, measured by the overlap between the two sets of Laughlin lattice states constructing using the $|X, k_y\rangle$ and $|Y, k_x\rangle$ Wannier bases. Please refer to the caption and legend of Fig. 6 for the annotation of scatter groups and lines. Inversion symmetry symmetry can be observed similar to Fig. 6.

As these phases are not identical for all Slater determinants, the Wannier wave functions exhibit a certain degree of nematicity. However, in the limit of flat Berry curvature, we expect that the two different routes of parallel transport picks up a relative phase of $e^{i2\pi k_x k_y / N_\phi}$ for $C = 1$, which is canceled exactly by the $e^{-i2\pi k_x k_y / N_\phi}$ phase from the basis transform from $|j\rangle_v$ to $|j\rangle$.

The algebra indeed works out. As explained earlier, we can shift (k_x, k_y) to $[0 \dots N_x] \times [0 \dots N_y]$ when evaluating the phase prefactor. For flat curvature, we have $\omega_{x,y} = U_{x,y} = 1$, and the Wilson loop around the rectangle is

$$\prod_{\kappa}^{k_x} A_x(\kappa, 0) \prod_{\kappa}^{k_y} A_y(k_x, \kappa) \left[\prod_{\kappa}^{k_y} A_y(0, \kappa) \prod_{\kappa}^{k_x} A_x(\kappa, k_y) \right]^\dagger = e^{i2\pi C k_x k_y / N_\phi}. \quad (131)$$

Recall that $\lambda_x(k_y)$ and $\lambda_y(k_x)$ are related to the Wilson loops $W_x(k_y)$ and $W_y(k_x)$ by Eq. (30), and thus

$$\left[\frac{\lambda_y(k_x)}{\lambda_y(0)} \right]^{k_y} = \left[\frac{\lambda_x(0)}{\lambda_x(k_y)} \right]^{k_x} = e^{i2\pi C k_x k_y / N_\phi}. \quad (132)$$

Putting all these together, we find as claimed

$$e^{i\phi_{k_x, k_y}} = e^{i\phi'_{k_x, k_y}} e^{-i2\pi C k_x k_y / N_\phi}, \quad (133)$$

and thus the Wannier construction *is* indeed isotropic in the limit of flat Berry curvature:

$$|\Psi; s, r\rangle_{\text{lat}} \propto |\Psi; s', r'\rangle'_{\text{lat}}. \quad (134)$$

D. Numerical Check

Realistic lattice models inevitably introduce fluctuations in the Berry curvature. The fluctuations persist in the thermodynamic limit $N_e \rightarrow \infty$. We note

that the phase difference between $\langle \{k_x, k_y\} | \Psi; s, r \rangle'_{\text{lat}}$ and $\langle \{k_x, k_y\} | \Psi; s, r \rangle_{\text{lat}}$ does not vanish in the continuum limit if the curvature is not flat. It cannot be eliminated by any point group symmetry, either.

A detailed analysis of the impact on the isotropy of the Wannier construction is hard to carry out. But we can still examine the isotropy or nematicity numerically. We find strong isotropy in the five FCI models despite fluctuating Berry curvature. Shown in Fig. 13 is the isotropy measured by the overlap between the Laughlin lattice states constructed using the $|X, k_y\rangle$ and the $|Y, k_x\rangle$ Wannier bases. The isotropy is higher than 0.997 for the ruby lattice model and the two-orbital model at all system sizes checked. A decreasing trend is observable for the checkerboard lattice model and the Haldane model, but the slope is much slower than that of the overlap values with the exact ground states.

VIII. DISCUSSION AND CONCLUSION

In this paper, we have studied the Wannier construction of FQH states for fractional Chern insulators. Despite being first proposed more than a year ago¹⁵, no overlap studies with the exact diagonalization have been reported. If one did the comparison naively, low overlap would be obtained (see Fig. 7). We have proposed a new, related prescription which fixes several outstanding issues in Ref. 15. In particular, we highlight the gauge freedom in the 1D localized Wannier states and the restriction imposed by the Wilson loops. The key point is that the relative phase between adjacent Wannier states must follow the same pattern as the LLL orbitals in the Landau gauge, otherwise the states obtained from the FQH-FCI mapping are not relevant to the FCI problem.

We describe and justify in details a finite-size prescription for a generic lattice model with multiple sublattices. We provide an explicit, step-by-step recipe to construct the counterpart of any FQH wave function on a Chern insulator. Our prescription is tailored for the torus geometry to make contact with existing numerical studies. It preserves the full translational invariance in both directions, as well as the inversion symmetry. Moreover, in the limit of flat Berry curvature, the constructed many-body states are the same using the Wannier basis localized in either x or y direction.

We find the major obstacle to the Wannier construction to be the fluctuations in the Berry curvature. We try to accommodate the fluctuations in the localization direction in the gauge choice of the Wannier basis. The fluctuations in the other direction keeps the Wannier centers from evenly spaced like the LLL orbitals, and we find no way to ameliorates the situation without spoiling translational invariance. We have no real control over the nematicity developed from the curvature fluctuations. This complication from curvature is an important feature that sets the FCI apart from the FQH in the continuum.

In an earlier paper⁹, two of us discovered a folding rule

to relate the counting of the FQH states on a torus to the counting of the FCI states at each total momentum. It was established by arguing that the FCI phase on a lattice is in the same universality class as the FQH phase on a torus with δ -function lattice pinning potentials. In this paper, the Wannier construction reorganizes the degenerate FQH model states and produces a set of model lattice states. These states have exactly the same counting in each total momentum sector of the energy and the entanglement spectra as predicted by the counting rule in Ref. 9. This provides a concrete implementation of the folding rule that connects the FCI and the FQH effects.

We perform the Wannier construction for the Laughlin state numerically in the five lattice models known to support a fractionalized phase. We find that the model state obtained from the Wannier construction and the actual FCI ground state have consistently large overlap in all cases, and their entanglement spectra exhibit very similar structures. The many-body physics in Chern insulators at filling $\nu = 1/3$ is indeed a close parallel to the Laughlin-type of FQH physics in the continuum with a strong magnetic field.

Using these five examples, we demonstrate that our prescription for the single-particle gauge is at or very close to the local optimum in terms of the overlap with the exact ground states. We also show that our prescription has strong isotropy by checking the overlap between the many-body states constructed using the Wannier bases localized in either x or y direction.

Our results provide another comparison across the array of known FCI models. Among the five models that we have checked, the ground states of the Kagome lattice model and the ruby lattice model have the largest overlap with the Laughlin model state. This is consistent with the finding in Ref. 7 that these two models host the most stable Laughlin-type FCI phase among the five.

We note a few interesting directions for future work. Two of us recently studied the thin-torus limit of the FCI.³⁴ In that limit, the projected interaction is dominated by classical electrostatic terms and allows an exact or perturbative solution. This may provide a better understanding of the varied performance of the Wannier construction in different models.

In this paper we focus the numerical tests on the Laughlin state. The general formalism of the Wannier construction, however, is able to handle more complicated FQH states. Lattice analogs of composite fermion states³⁵ and non-Abelian FQH states such as Moore-Read³⁶ and Read-Rezayi states³⁷ have been identified in a few Chern insulators.^{7,9,23,38} Moreover, it was proposed that topological flat bands with Chern number $|C| \geq 2$ ³⁹⁻⁴³ may be understood as a multi-component FQH system.²² It would be interesting to see how well these states could be captured by some established FQH trial wave functions mapped to the lattice by the Wannier construction.

Time-reversal invariant fractional \mathbb{Z}_2 topological insulators have been constructed from two copies of FCI and

the field theory describing their low-energy excitations have been established.^{44,45} More recently, the algebraic structure of the projected density operators for topological insulators in three⁴⁶ or higher dimensions⁴⁷ have been studied. With necessary generalizations, the gauge-fixed Wannier construction may be useful for the study of the wave functions of these more complicated systems. In particular, the case of 2D FTI (quantum spin Hall) can be tackled similar to the FCI problem, as the FTI system becomes decoupled in the Wannier basis.

Another interesting approach to build trial wave functions for the FCI is the parton construction^{48,49}, initially pioneered by Wen^{50,51} to construct the FQH wave functions in the continuum. This alternative is plagued by a critical issue at the moment. To achieve fractional filling $\nu = 1/q$ of electrons, the number of partons in a fully filled band should be reduced accordingly. For the original FQH system, this is not a problem since the size of the parton LLL orbital increases automatically due to the decrease of charge. On a lattice, this change has to be put in by hand through a unit-cell enlargement. Refs. 48,49 discussed how to preserve the lattice symmetries in the electronic wave functions, but their solutions involve partonic bands that are *drastically different* from the original electronic band: even the band *topologies* may be totally different. It would be interesting to find a cure to this unsettling problem, to develop a concrete prescription for correct torus degeneracies, and to compare with the Wannier construction and the exact ground states.

IX. ACKNOWLEDGEMENTS

We wish to thank A. Alexandradinata, X. Dai, C. Fang, F.D.M. Haldane, X.L. Qi, and B. Yang for helpful comments and inspiring discussions. BAB was supported by Princeton Startup Funds, NSF CAREER DMR-095242, ONR-N00014-11-1-0635, DARPA-N66001-11-1-4110, Packard Foundation, Keck grant, and NSF-MRSEC DMR-0819860 at Princeton University. NR was supported by NSF CAREER DMR-095242, ONR-N00014-11-1-0635, Packard Foundation, and Keck grant. YLW was supported by NSF CAREER DMR-095242. BAB thanks Technion, Israel, and Ecole Normale Supérieure, Paris, for generous hosting during the stages of this work. YLW thanks the Institute of Physics, Chinese Academy of Sciences for hospitality.

Appendix A: FQH Projected Hamiltonian

In this Appendix we give the expression of the FQH interacting Hamiltonian projected to the lowest Landau level (LLL) on a twisted torus. This is a trivial generalization of the formula given in Ref. 52.

In the limit of large cyclotron energy, we keep in the Hilbert space only the states in the LLL. Since the kinetic

energy is fully quenched, the Hamiltonian is simply the projected density-density interaction term V .

Define the field operator ψ_j to annihilate the Landau orbital state $|j\rangle$. The LLL-projected density operator can be written in momentum space as

$$\rho_{\mathbf{q}} = \sum_{j_1, j_2} \langle j_1 | e^{-i\mathbf{q}\cdot\tilde{\mathbf{r}}} | j_2 \rangle \psi_{j_1}^\dagger \psi_{j_2} \quad (\text{A1})$$

$$= \int d\tilde{\mathbf{r}} e^{-i\mathbf{q}\cdot\tilde{\mathbf{r}}} \sum_{j_1, j_2} \phi_{j_1}^*(\tilde{\mathbf{r}}) \phi_{j_2}(\tilde{\mathbf{r}}) \psi_{j_1}^\dagger \psi_{j_2}, \quad (\text{A2})$$

where the reciprocal lattice vector \mathbf{q} is given by $\mathbf{q} = q_1 \mathbf{G}_1 + q_2 \mathbf{G}_2$ with $(q_1, q_2) \in \mathbb{Z}^2$, the continuous coordinate $\tilde{\mathbf{r}}$ is integrated over the principal region of the torus, and the orbital index j_1, j_2 are summed over $[0 .. N_\phi)$. Following the detailed steps laid out in Ref. 53, we can simplify the above formula and get

$$\rho_{\mathbf{q}} = e^{-|\mathbf{q}|^2 l_B^2 / 4} \sum_j^{N_\phi} e^{-i2\pi q_1(j+q_2/2)/N_\phi} \psi_j^\dagger \psi_{j+q_2}. \quad (\text{A3})$$

In the second-quantized form, the projected two-body interaction can be written as

$$V = \frac{1}{2L_1 L_2 \sin \theta} \sum_{\mathbf{q}} V_{\mathbf{q}} \rho_{-\mathbf{q}} \rho_{\mathbf{q}}, \quad (\text{A4})$$

where the reciprocal lattice vector $\mathbf{q} = q_1 \mathbf{G}_1 + q_2 \mathbf{G}_2$ is summed over the infinite grid $(q_1, q_2) \in \mathbb{Z}^2$. Plugging in $\rho_{\mathbf{q}}$, we find

$$V = \frac{1}{2L_1 L_2 \sin \theta} \sum_{\mathbf{q}} e^{-|\mathbf{q}|^2 l_B^2 / 2} V_{\mathbf{q}} \sum_{j_1}^{N_\phi} \sum_{j_2}^{N_\phi} e^{i2\pi q_1(j_1 - j_2 - q_2)/N_\phi} \psi_{j_1}^\dagger \psi_{j_2}^\dagger \psi_{j_2 + q_2} \psi_{j_1 - q_2}, \quad (\text{A5})$$

where $V_{\mathbf{q}} = \int d\mathbf{r} e^{-i\mathbf{q}\cdot\mathbf{r}} V(\mathbf{r})$ is the Fourier transform of the interaction potential $V(\mathbf{r})$.¹⁶ The Fourier coefficient $V_{\mathbf{q}}$ can be expressed in terms of the Haldane pseudopotentials V_m ,⁵⁴

$$V_{\mathbf{q}} = 4\pi l_B^2 \sum_{m=0}^{\infty} V_m L_m(|\mathbf{q}|^2 l_B^2), \quad (\text{A6})$$

where $L_m(x)$ are the Laguerre polynomials.

As a side note, we point out an interesting link between adjacent $|j\rangle$ orbitals. Combining Eqs. (A1) and (A3) at $\mathbf{q} = \mathbf{G}_2$, we find

$$\langle j | e^{-i\mathbf{G}_2 \cdot \tilde{\mathbf{r}}} | j+1 \rangle = e^{-|\mathbf{G}_2|^2 l_B^2 / 4} \in \mathbb{R}_+. \quad (\text{A7})$$

This can be viewed as the defining property of the particular gauge choice of $\phi_j(\tilde{\mathbf{r}})$ made in Eq. (3).

Appendix B: Orthogonality Problem

In this Appendix, we show that the eigenstates of the projected position operator $\hat{\mathcal{X}}$ at finite size are *not* orthogonal to each other due to the non-unitarity of the Berry connections.

For simplicity, we focus on the case of a single occupied band; the problem is generic for any number of occupied bands. In this case, the Berry connection $\mathcal{A}_x(k_x, k_y)$ is Abelian, and the project position operator in the x direction is given by Eq. (25):

$$\hat{\mathcal{X}} = \sum_{k_x, k_y} |k_x, k_y\rangle \mathcal{A}_x(k_x, k_y) \langle k_x + 1, k_y|, \quad (\text{B1})$$

where the Berry connection is defined as [Eq. (26)]

$$\mathcal{A}_x(k_x, k_y) = \sum_{\alpha} e^{-i2\pi \epsilon_{\alpha}^x / N_x} u_{m, \alpha}^*(k_x, k_y) u_{n, \alpha}(k_x + 1, k_y).$$

Generically, at finite size we have $|\mathcal{A}_x(k_x, k_y)| < 1$; only in the thermodynamic limit does this become an equality.

Since $\hat{\mathcal{X}}$ is diagonal in k_y , we can solve the eigenvalue problem at each k_y independently. The N_x eigenvalues of $\hat{\mathcal{X}}$ at k_y are

$$e^{-i2\pi X / N_x} D(k_y) \lambda_x(k_y), \quad (\text{B2})$$

labeled by $X \in [0 .. N_x)$. Here, the unitary phase factor $\lambda_x(k_y)$ is the N_x -th root of the *phase* part of the Wilson loop along a fixed k_y , defined in Eq. (30), while the positive real number $D(k_y)$ is the N_x -th root of the absolute value of the Wilson loop,

$$D(k_y) = \left| \prod_{\kappa}^{N_x} \mathcal{A}_x(\kappa, k_y) \right|^{1/N_x}. \quad (\text{B3})$$

The corresponding eigenstates are

$$|X, k_y\rangle = \mathcal{N}_{k_y} \sum_{k_x}^{N_x} e^{-i2\pi k_x X / N_x} \frac{[D(k_y) \lambda_x(k_y)]^{k_x}}{\prod_{\kappa}^{k_x} \mathcal{A}_x(\kappa, k_y)} |k_x, k_y\rangle,$$

and the normalization factor is given by

$$\mathcal{N}_{k_y} = \left\{ \sum_{k_x}^{N_x} \frac{[D(k_y)]^{2k_x}}{\prod_{\kappa}^{k_x} |\mathcal{A}_x(\kappa, k_y)|^2} \right\}^{-1/2}. \quad (\text{B4})$$

Therefore,

$$\begin{aligned} \langle X_1, k_y | X_2, k_y \rangle &= [\mathcal{N}_{k_y}]^* \mathcal{N}_{k_y} \\ &\times \sum_{k_x}^{N_x} e^{i2\pi k_x (X_1 - X_2)} \frac{[D(k_y)]^{k_x}}{\prod_{\kappa}^{k_x} |\mathcal{A}_x(\kappa, k_y)|}. \end{aligned} \quad (\text{B5})$$

Evidently, in general the Wannier states localized in different unit cells at each k_y are *not* orthogonal at finite size, preventing a nice mapping into the orthogonal LLL orbitals. The Wannier orbitals become orthogonal quickly in the thermodynamic limit due to the oscillatory nature of the sum, which averages to zero if $X_1 \neq X_2$.

Appendix C: Inversion Symmetry

1. Inversion Operator

We derive the inversion transformation of the exponentiated position operators \hat{x} and \hat{y} in Eq. (81) and provide an explicit expression for the sewing matrix elements $e^{i\xi_{k_x, k_y}}$ defined in Eq. (82).

By properly choosing the reference point in each unit cell, we can put the inversion centers on the Bravais lattice $(x, y) \in \mathbb{Z}^2$. Inversion takes the α orbital located at $(x + \epsilon_\alpha^x, y + \epsilon_\alpha^y)$ to $(-x - \epsilon_\alpha^x, -y - \epsilon_\alpha^y)$. For the insulator to be inversion symmetric, we must have an orbital at $(-x - \epsilon_\alpha^x, -y - \epsilon_\alpha^y)$ before taking inversion. So there must

exist a Bravais lattice shift $(\Delta_\alpha^x, \Delta_\alpha^y) \in \mathbb{Z}^2$ and sublattice displacements $(\epsilon_\beta^x, \epsilon_\beta^y) \in \mathbb{R}^2$ such that

$$\begin{aligned} -x - \epsilon_\alpha^x &= -x - \Delta_\alpha^x + \epsilon_\beta^x \\ -y - \epsilon_\alpha^y &= -y - \Delta_\alpha^y + \epsilon_\beta^y \end{aligned} \quad (\text{C1})$$

Note that $(\Delta_\alpha^x, \Delta_\alpha^y)$ depends only on α , not on β . Different orbitals β may share the same value of $(\epsilon_\beta^x, \epsilon_\beta^y)$. In orbital space, inversion is implemented by

$$\mathcal{P}|x, y, \alpha\rangle = \sum_\beta \mathbb{P}_{\alpha\beta} | -x - \Delta_\alpha^x, -y - \Delta_\alpha^y, \beta\rangle, \quad (\text{C2})$$

where the matrix \mathbb{P} is unitary and satisfies $\mathbb{P}^2 = 1$.

The position operator \hat{y} transforms under inversion

$$\mathcal{P}\hat{y}\mathcal{P} = \sum_{x,y} \sum_\alpha e^{-i2\pi(y+\epsilon_\alpha^y)/N_y} \sum_{\beta\gamma} \mathbb{P}_{\alpha\beta} | -x - \Delta_\alpha^x, -y - \Delta_\alpha^y, \beta\rangle \langle -x - \Delta_\alpha^x, -y - \Delta_\alpha^y, \gamma | \mathbb{P}_{\gamma\alpha} \quad (\text{C3})$$

$$= \sum_{x,y} \sum_\alpha e^{-i2\pi(-y-\Delta_\alpha^y+\epsilon_\alpha^y)/N_y} \sum_{\beta\gamma} \mathbb{P}_{\alpha\beta} |x, y, \beta\rangle \langle x, y, \gamma | \mathbb{P}_{\gamma\alpha} \quad (\text{C4})$$

$$= \sum_{x,y} \sum_{\beta\gamma} e^{i2\pi(y+\epsilon_\beta^y)/N_y} \left(\sum_\alpha \mathbb{P}_{\gamma\alpha} \mathbb{P}_{\alpha\beta} \right) |x, y, \beta\rangle \langle x, y, \gamma | \quad (\text{C5})$$

$$= \hat{y}^\dagger. \quad (\text{C6})$$

In the second step we changed the summation dummy index $(x, y) \rightarrow (-x - \Delta_\alpha^x, -y - \Delta_\alpha^y)$, and in the third step we made use of Eq. (C1). Similarly, we can show that $\mathcal{P}\hat{x}\mathcal{P} = \hat{x}^\dagger$. In momentum/orbital space, we have

$$\mathcal{P}|k_x, k_y, \alpha\rangle = \frac{1}{\sqrt{N_x N_y}} \sum_{x,y} e^{i2\pi(k_x x/N_x + k_y y/N_y)} \sum_\beta \mathbb{P}_{\alpha\beta} | -x - \Delta_\alpha^x, -y - \Delta_\alpha^y, \beta\rangle \quad (\text{C7})$$

$$= e^{-i2\pi(k_x \Delta_\alpha^x/N_x + k_y \Delta_\alpha^y/N_y)} \sum_\beta \mathbb{P}_{\alpha\beta} | -k_x, -k_y, \beta\rangle. \quad (\text{C8})$$

The sewing matrix elements

$$e^{i\xi_{k_x, k_y}} = \langle k_x, k_y | \mathcal{P} | -k_x, -k_y \rangle \quad (\text{C9})$$

can be expressed in terms of $\mathbb{P}_{\alpha\beta}$,

$$\begin{aligned} e^{i\xi_{k_x, k_y}} &= \sum_\alpha \sum_\beta e^{i2\pi(k_x \Delta_\alpha^x/N_x + k_y \Delta_\alpha^y/N_y)} \\ &\times u_\beta^*(k_x, k_y) \mathbb{P}_{\alpha\beta} u_\alpha(-k_x, -k_y). \end{aligned} \quad (\text{C10})$$

2. Inversion Symmetry in Curvature Fluctuations

We study the inversion property of the curvature fluctuation $U_y(k_y) = \mathcal{U}_y(k_y)/|\mathcal{U}_y(k_y)|$, where $\mathcal{U}_y(k_y)$ is defined in Eq. (53) as:

$$\mathcal{U}_y(k_y) = \frac{1}{N_x} \sum_{k_x} \frac{W_\blacksquare(k_x, k_y)}{\overline{W}_\blacksquare(k_x, k_y)}. \quad (\text{53})$$

First, we study the Wilson loop $W_\blacksquare(k_x, k_y)$. The inversion transformation of the Berry connection in Eqs. (86) and (87) relates $W_\blacksquare(k_x, k_y)$ to the Wilson loop around $(N_x - k_x, -k_y)(N_x, -k_y)(N_x, -k_y - 1)(N_x - k_x, -k_y - 1)(N_x - k_x, -k_y)$, except for the corner case $W_\blacksquare(0, k_y) = 1$. Due to the *loop* structure, all the sewing matrix elements cancel completely, and we have

$$W_\blacksquare(k_x, k_y) \frac{W_\blacksquare(N_x - k_x, -k_y - 1)}{W_\blacksquare(N_x, -k_y - 1)} = 1. \quad (\text{C11})$$

It is easy to check that the corner case $k_x = 0$ is incorporated as well.

Then we study the denominator $\overline{W}_\blacksquare(k_x, k_y) = [\mu_x(k_y)]^{k_x}$, with $\mu_x(k_y)$ defined by Eq. (55). We can prove that

$$\overline{W}_\blacksquare(k_x, k_y) = \overline{W}_\blacksquare(k_x, -k_y - 1). \quad (\text{C12})$$

Setting $k_x = N_x$ in Eq. (C11), we have [recall that

$$W_{\blacksquare}(0, -k_y - 1) = 1]$$

$$W_{\blacksquare}(N_x, k_y) = W_{\blacksquare}(N_x, -k_y - 1). \quad (\text{C13})$$

Using Eq. (57) to fix the branch choice, we can take the N_x -th root of this equation and get

$$\mu_x(k_y) = \mu_x(-k_y - 1). \quad (\text{C14})$$

Taking the k_x -th power of the above equation proves Eq. (C12).

Combine Eq. (C11) with Eq. (C12), we can show that the curvature fluctuation $\mathcal{U}_y(k_y)$ satisfy

$$\begin{aligned} [\mathcal{U}_y(k_y)]^* &= \frac{1}{N_x} \sum_{k_x}^{N_x} \frac{[W_{\blacksquare}(k_x, k_y)]^*}{[\overline{W}_{\blacksquare}(k_x, k_y)]^*} \\ &= \frac{1}{N_x} \sum_{k_x}^{N_x} \frac{W_{\blacksquare}(N_x - k_x, -k_y - 1)}{\overline{W}_{\blacksquare}(N_x, -k_y - 1) / \overline{W}_{\blacksquare}(k_x, -k_y - 1)} \\ &= \frac{1}{N_x} \sum_{k_x}^{N_x} \frac{W_{\blacksquare}(N_x - k_x, -k_y - 1)}{\overline{W}_{\blacksquare}(N_x, -k_y - 1) / \overline{W}_{\blacksquare}(k_x, -k_y - 1)} \\ &= \frac{1}{N_x} \sum_{k_x}^{N_x} \frac{W_{\blacksquare}(N_x - k_x, -k_y - 1)}{\overline{W}_{\blacksquare}(N_x - k_x, -k_y - 1)} \\ &= \mathcal{U}_y(-k_y - 1). \end{aligned} \quad (\text{C15})$$

Here we have used $W_{\blacksquare}(N_x, k_y) = \overline{W}_{\blacksquare}(N_x, k_y)$, which follows from the definition of $\overline{W}_{\blacksquare}(k_x, k_y) = [\mu_x(k_y)]^{k_x}$ and Eq. (56). This proves Eq. (96), namely,

$$U_y(k_y)U_y(-k_y - 1) = 1.$$

3. Inversion Transformation of the Wannier States

We prove the inversion transformation of $|X, k_y\rangle$ in Eq. (99).

Using $[\lambda_x(k_y)]^{N_x} = W_x(k_y)$ [Eq. (30)], we can rewrite the inversion transformation of $W_x(k_y)$ in Eq. (88) as

$$[\lambda_x(k_y)\lambda_x(-k_y)]^{N_x} = 1. \quad (\text{C16})$$

Taking the N_x -th root, we have

$$\lambda_x(k_y) = e^{-i2\pi n/N_x} / \lambda_x(-k_y), \quad (\text{C17})$$

where $n \in \mathbb{Z}$ is to be determined. Recall that *by definition*, both $\lambda_x(k_y)$ and $\lambda_x(-k_y)$ must have their argument angles in $(-2\pi/N_x, 0] \bmod 2\pi$. So there are the following two cases:

“**on-site**” If $W_x(k_y) = 1$, we have $\lambda_x(k_y) = \lambda_x(-k_y) = 1$, and thus

$$\lambda_x(k_y) = 1/\lambda_x(-k_y). \quad (\text{C18})$$

The Wannier centers are located on the Bravais lattice.

“**off-site**” If $W_x(k_y) \neq 1$, we have

$$\lambda_x(k_y) = e^{-i2\pi/N_x} / \lambda_x(-k_y), \quad (\text{C19})$$

since both $\lambda_x(k_y)$ and $\lambda_x(-k_y)$ have argument angle in $(-2\pi/N_x, 0) \bmod 2\pi$. In particular, for $W_x(k_y) = -1$, we have $\lambda_x(k_y) = \lambda_x(-k_y) = e^{-i\pi/N_x}$.

From the inversion transformation of the Berry connection $A_x(k_y)$ in Eq. (86) we can get

$$\prod_{\kappa}^{N_x} A_x(\kappa, k_y) \Big/ \prod_{\kappa}^{N_x - k_x} A_x(\kappa, k_y) = \prod_{\kappa = N_x - k_x}^{N_x - 1} A_x(\kappa, k_y) = e^{i\xi_{N_x - k_x, k_y}} e^{-i\xi_{N_x, k_y}} \Big/ \prod_{\kappa}^{k_x} A_x(\kappa, -k_y). \quad (\text{C20})$$

Therefore, we have the inversion transformation of the Wannier states

$$e^{i\xi_{0, k_y}} e^{-i\Phi_y(X, k_y)} \mathcal{P}|X, k_y\rangle = \frac{1}{\sqrt{N_x}} \sum_{k_x}^{N_x} e^{-i2\pi k_x X/N_x} \frac{[\lambda_x(k_y)]^{k_x}}{\prod_{\kappa}^{k_x} A_x(\kappa, k_y)} e^{i\xi_{N_x, k_y} - i\xi_{k_x, k_y}} |-k_x, -k_y\rangle \quad (\text{C21})$$

$$= \frac{1}{\sqrt{N_x}} \sum_{k_x}^{N_x} e^{i2\pi k_x X/N_x} \frac{[\lambda_x(k_y)]^{N_x - k_x}}{\prod_{\kappa}^{N_x - k_x} A_x(\kappa, k_y)} e^{i\xi_{N_x, k_y} - i\xi_{N_x - k_x, k_y}} |k_x, -k_y\rangle \quad (\text{C22})$$

$$= \frac{1}{\sqrt{N_x}} \sum_{k_x}^{N_x} e^{i2\pi k_x X/N_x} [\lambda_x(k_y)]^{-k_x} \frac{\prod_{\kappa}^{N_x} A_x(\kappa, k_y)}{\prod_{\kappa}^{N_x - k_x} A_x(\kappa, k_y)} e^{i\xi_{N_x, k_y} - i\xi_{N_x - k_x, k_y}} |k_x, -k_y\rangle \quad (\text{C23})$$

$$= \frac{1}{\sqrt{N_x}} \sum_{k_x}^{N_x} e^{-i2\pi k_x (-X)/N_x} \frac{[\lambda_x(k_y)]^{-k_x}}{\prod_{\kappa}^{k_x} A_x(\kappa, -k_y)} |k_x, -k_y\rangle \quad (\text{C24})$$

$$= \begin{cases} e^{-i\Phi_y(-X, -k_y)} |-X, -k_y\rangle & \text{if } W_x(k_y) = 1, \\ e^{-i\Phi_y(-X-1, -k_y)} |-X-1, -k_y\rangle & \text{otherwise.} \end{cases} \quad (\text{C25})$$

Here in the second step we performed a change of summation variable $k_x \rightarrow N_x - k_x$ and made use of the invariance of each term under $k_x \rightarrow k_x + N_x$, while in the last step we used Eqs. (C18) and (C19).

4. Inversion Transformation of the 1D Index

We prove the inversion transformation rule of j^{X,k_y} in Eq. (107), namely,

$$j^{X,k_y} \rightarrow \begin{cases} -j^{X,k_y} - 1 & \text{if } W_x(0) = -1 \text{ and } N_y \text{ odd;} \\ -j^{X,k_y} & \text{otherwise.} \end{cases} \quad (107)$$

We will use the inversion transformation of (X, k_y) in Eq. (106), namely,

$$(X, k_y) \rightarrow \begin{cases} (-X, -k_y) & \text{if } W_x(k_y) = 1, \\ (-X - 1, -k_y) & \text{otherwise.} \end{cases}$$

A discussion of the location of $W_x(k_y) = 1$ is thus necessary. At a generic k_y , due to the absence of any protection by symmetry, in general we can assume $W_x(k_y) \neq 1$. With inversion symmetry, We can safely assume that $W_x(k_y) = 1$ happens only at $k_y = 0$ or $\frac{N_y}{2}$, otherwise the flow of the Wannier center would exhibit “zigzag” patterns.

We only elaborate the proof for $C = +1$; the situation when $C = -1$ is completely analogous. We discuss the three cases of δ_y in Eq. (94) one by one, namely,

$$\delta_y = \begin{cases} 0 & \text{if } W_x(0) = 1; \\ N_y/2 & \text{if } W_x(0) = -1 \text{ and } N_y \text{ even;} \\ (N_y - 1)/2 & \text{if } W_x(0) = -1 \text{ and } N_y \text{ odd.} \end{cases}$$

Recall that the 1D label $j^{X,k_y} = XN_y + Ck_y + \delta_y$ is defined with $Ck_y + \delta_y \in [0 .. N_y)$. As emphasized in Sec. III C, before performing the mapping, we need to first shift k_y to the principal Brillouin zone (pBZ). The pBZ is defined by $Ck_y + \delta_y \in [0 .. N_y)$. The three cases for the shift parameter δ_y and the corresponding pBZ are illustrated in Fig. 5.

In the first case, $W_x(0) = 1$. In this case we have $\delta_y = 0$, and the principal Brillouin zone is pBZ = $[0 .. N_y)$. If $k_y = 0$, we have $W_x(0) = 1$ and $-k_y = 0 \in \text{pBZ}$, and thus under inversion

$$j^{X,0} = XN_y \rightarrow -XN_y = -j^{X,0}.$$

If $k_y \in (0 .. N_y)$, we have $W_x(k_y) \neq 1$ and $N_y - k_y \in \text{pBZ}$, and thus under inversion

$$\begin{aligned} j^{X,k_y} &= XN_y + k_y \\ &\rightarrow (-X - 1)N_y + N_y - k_y = -j^{X,k_y}. \end{aligned}$$

In the second case, $W_x(0) = -1$ and N_y is even. We have $\delta_y = \frac{N_y}{2}$, and pBZ = $[-\frac{N_y}{2} .. \frac{N_y}{2})$. Due to $|C| = 1$,

we have $W_x(-\frac{N_y}{2}) = -1/W_x(0) = 1$ [Eq. (93)]. If $k_y = -\frac{N_y}{2}$, we have $W_x(-\frac{N_y}{2}) = 1$ and $-N_y - k_y = -\frac{N_y}{2} \in \text{pBZ}$, and thus under inversion

$$\begin{aligned} j^{X,-\frac{N_y}{2}} &= XN_y - \frac{N_y}{2} + \frac{N_y}{2} \\ &\rightarrow -XN_y + \frac{N_y}{2} - \frac{N_y}{2} = -j^{X,-\frac{N_y}{2}}. \end{aligned}$$

If $k_y \in (-\frac{N_y}{2} .. \frac{N_y}{2})$, we have $W_x(k_y) \neq 1$ and $-k_y \in \text{pBZ}$, and thus under inversion

$$\begin{aligned} j^{X,k_y} &= XN_y + k_y + \frac{N_y}{2} \\ &\rightarrow (-X - 1)N_y + (-k_y) + \frac{N_y}{2} = -j^{X,k_y}. \end{aligned}$$

In the third case, $W_x(0) = -1$ and N_y is odd. We have $W_x(k_y) \neq 1$ and $\delta_y = \frac{N_y - 1}{2}$, and pBZ = $[-\frac{N_y - 1}{2} .. \frac{N_y - 1}{2})$ (illustrated in Fig. 5c). For any $k_y \in \text{pBZ}$, we have $-k_y \in \text{pBZ}$, and thus

$$\begin{aligned} j^{X,k_y} &= XN_y + k_y + \frac{N_y - 1}{2} \\ &\rightarrow (-X - 1)N_y + (-k_y) + \frac{N_y - 1}{2} = -j^{X,k_y} - 1. \end{aligned}$$

Summarizing the three cases, we have proved Eq. (107). We emphasize that for a given system [and thus given $W_x(0)$ and N_y], all the j^{X,k_y} indices obey the *same* transformation rule, but the transformation of (X, k_y) indices still comes in two cases [Eq. (106)].

5. Inversion Symmetry of the Many-Body States

We study the inversion operation on the many-body states $|\Psi; s, r\rangle_{\text{lat}}$. From Eq. (48) we have

$$\langle \{X, k_y\} \mathcal{P} | \Psi; s, r \rangle_{\text{lat}} = \sum_{\{X_1, k_{y,1}\}} \langle \{X, k_y\} \mathcal{P} | \{X_1, k_{y,1}\} \rangle \langle \{j^{X_1, k_{y,1}}\} | \Psi; s, r \rangle. \quad (C26)$$

Plugging into the above equation the inversion transformation of the Wannier states in Eq. (105), the sum over $(X_1, k_{y,1})$ reduces to a *single term*, with $(X_1, k_{y,1})$ equals either $(-X, -k_y)$ or $(-X - 1, -k_y)$, depending on the condition in Eq. (105), namely, whether $W_x(0) = -1$ and N_y is odd. For both cases, the Wannier-basis inversion matrix element has the same value

$$\langle \{X, k_y\} \mathcal{P} | \{X_1, k_{y,1}\} \rangle = e^{i\xi_{0,0}} [\lambda_y(0) \omega_y]^{-2k_y}. \quad (C27)$$

And we want to relate the FQH amplitude factor $\langle \{j^{X_1, k_{y,1}}\} | \Psi; s, r \rangle$ back to $\langle \{j^{X, k_y}\} | \Psi; s, r \rangle$, but this depends on the inversion transformation $j^{X, k_y} \rightarrow j^{X_1, k_{y,1}}$. As shown in the previous section of this Appendix, we need to discuss two cases in Eq. (107) for the inversion transformation of the 1D index j^{X, k_y} .

First, consider the case where $W_x(0) = 1$ or N_y is even. In this case, $j^{X,k_y} \rightarrow j^{X_1,k_y,1} = -j^{X,k_y}$ under inversion. Also, according to Eq. (94), the shift δ_y is either 0 or $N_y/2$, and thus N_y divides $2\delta_y$. From Eqs. (C26) and (C27) we then have the amplitudes of the inverted state

$$\begin{aligned} & \langle \{X, k_y\} | \mathcal{P} | \Psi; s, r \rangle_{\text{lat}} \\ & = e^{iN_e \xi_{0,0}} [\lambda_y(0) \omega_y]^{-2 \sum k_y} \langle \{-j^{X,k_y}\} | \Psi; s, r \rangle. \end{aligned} \quad (\text{C28})$$

The inversion transformation of the FQH state in Eq. (80) then relates this to the amplitude of another FQH state $|\Psi; \bar{s}, \bar{r}\rangle$, and we can map it back to the corresponding state on lattice $|\Psi; \bar{s}, \bar{r}\rangle_{\text{lat}}$:

$$\begin{aligned} & \langle \{X, k_y\} | \mathcal{P} | \Psi; s, r \rangle_{\text{lat}} \\ & = \zeta_\Psi e^{iN_e \xi_{0,0}} [\lambda_y(0) \omega_y]^{-2 \sum k_y} \langle \{X, k_y\} | \Psi; \bar{s}, \bar{r} \rangle_{\text{lat}}. \end{aligned} \quad (\text{C29})$$

The indices \bar{s} , \bar{r} are defined *uniquely* by Eqs. (78) and (77). The constant ζ_Ψ is the eigenvalue corresponding to $|\Psi\rangle$ of a composite operator [Eq. (75)] and it takes value from ± 1 . The inversion operation thus relates the components of the many-body state $|\Psi; s, r\rangle_{\text{lat}}$ with total momentum [Eq. (69)]

$$(K_x, K_y) = [\kappa_x + sN_e, C\kappa_y + C(r - \delta_y)N_e] \bmod (N_x, N_y),$$

to those of the state $|\Psi; \bar{s}, \bar{r}\rangle_{\text{lat}}$ with total momentum

$$\begin{aligned} (\bar{K}_x, \bar{K}_y) & = [\kappa_x + \bar{s}N_e, C\kappa_y + C(\bar{r} - \delta_y)N_e] \\ & = (-K_x, -K_y) \bmod (N_x, N_y). \end{aligned} \quad (\text{C30}) \quad (\text{C31})$$

thanks to Eqs. (78) and (79) and the fact that N_x divides Nq_x and N_y divides $2\delta_y$ as noted earlier.

The coefficients of the inversion transformation in Eq. (C29) appear to vary for each component, as $\sum k_y$ is different for different components due to umklapp (mod N_y) processes. However, since with inversion $[\lambda_y(0) \omega]^{2N_y} = 1$, according to Eq. (98), the troublesome factor $[\lambda_y(0) \omega_y]^{2 \sum k_y}$ depends only on $\sum k_y \bmod N_y$, and thus *all* the non-zero components $\langle \{X, k_y\} | \Psi; \bar{s}, \bar{r} \rangle_{\text{lat}}$ have the same value of $\sum k_y \bmod N_y$, namely, $-K_y$. This means that the coefficients in Eq. (C29) are actually the same for each component. Therefore, the inversion operator \mathcal{P} indeed brings one state to another *within* the q -fold multiplet,

$$\begin{aligned} & \mathcal{P} | \Psi; s, r \rangle_{\text{lat}} \\ & = \zeta_\Psi e^{iN_e \xi_{0,0}} [\lambda_y(0) \omega_y]^{2C[\kappa_y + (r - \delta_y)N_e]} | \Psi; \bar{s}, \bar{r} \rangle_{\text{lat}}. \end{aligned} \quad (\text{C32})$$

We now proceed to the other case where $W_x(0) = -1$ and N_y is odd. The majority part of the above argument carries over, except that now j^{X,k_y} is mapped to $-j^{X,k_y} - 1$ under inversion. The -1 can be pulled out as a translation T_{cm}^x and absorbed into the state $|\Psi; \bar{s}, \bar{r}\rangle$ [see Eq. (15)]. The amplitudes of the inverted state reads

$$\begin{aligned} & \langle \{X, k_y\} | \mathcal{P} | \Psi; s, r \rangle_{\text{lat}} \\ & = \zeta_\Psi e^{iN_e \xi_{0,0}} [\lambda_y(0) \omega_y]^{-2 \sum k_y} \langle \{X, k_y\} | \Psi; \bar{s}, \bar{r} - 1 \rangle_{\text{lat}}. \end{aligned} \quad (\text{C33})$$

In the current case we have $\delta_y = -1 - \delta_y \bmod N_y$. and thus the state $|\Psi; \bar{s}, \bar{r} - 1\rangle_{\text{lat}}$ has the total momentum of the inversion partner of $|\Psi; s, r\rangle_{\text{lat}}$,

$$(\bar{K}_x, \bar{K}_y) = [\kappa_x + \bar{s}N_e, C\kappa_y + C(\bar{r} - 1 - \delta_y)N_e] \quad (\text{C34})$$

$$= [-\kappa_x - sN_e, -C\kappa_y - C(r - \delta_y)N_e] \quad (\text{C35})$$

$$= (-K_x, -K_y) \bmod (N_x, N_y). \quad (\text{C36})$$

Again, the inversion operator \mathcal{P} brings one state to another *within* the q -fold multiplet,

$$\begin{aligned} & \mathcal{P} | \Psi; s, r \rangle_{\text{lat}} \\ & = \zeta_\Psi e^{iN_e \xi_{0,0}} [\lambda_y(0) \omega_y]^{2C[\kappa_y + (r - \delta_y)N_e]} | \Psi; \bar{s}, \bar{r} - 1 \rangle_{\text{lat}}. \end{aligned} \quad (\text{C37})$$

The index $\bar{r} - 1$ needs careful handling, since $|\Psi; \bar{s}, \bar{r}\rangle$ acquires a phase when $\bar{r} \rightarrow \bar{r} + q/q_x$, as shown in Eq. (19).

Combining Eqs. (C32) and (C37), we have proved Eq. (108).

Appendix D: Recombination of the LLL Orbitals

In this Appendix we prove the recombination formula for the LLL orbitals:

$$\phi_j^v(\tilde{x}, \tilde{y}) = \frac{e^{i(\frac{\pi}{4} - \frac{\theta}{2})}}{\sqrt{N_\phi}} \sum_m^{N_\phi} e^{-i2\pi jm/N_\phi} \phi_m(\tilde{x}, \tilde{y}), \quad (\text{D1})$$

where the orbital wave function $\phi_m(\tilde{x}, \tilde{y})$ is given by Eq. (3), and $\phi_j^v(\tilde{x}, \tilde{y})$ by Eqs. (114) and (118).

Consider the single-particle magnetic translation operator $T(\mathbf{L}_1/N_\phi)$ in the Landau gauge $\mathbf{A} = B\tilde{x}\hat{e}_y$. This operator commutes with $T(\mathbf{L}_1)$ and $T(\mathbf{L}_2)$, and thus is compatible with the periodic boundary conditions in the LLL. From the explicit expressions, we can find the action on the Landau orbitals

$$T(\mathbf{L}_1/N_\phi)\phi_j(\tilde{x}, \tilde{y}) = \phi_{j+1}(\tilde{x}, \tilde{y}), \quad (\text{D2})$$

$$T(\mathbf{L}_1/N_\phi)\phi_j^v(\tilde{x}, \tilde{y}) = e^{i2\pi j/N_\phi} \phi_j^v(\tilde{x}, \tilde{y}). \quad (\text{D3})$$

The second equation shows that the operator $T(\mathbf{L}_1/N_\phi)$ has N_ϕ distinct eigenvalues within the LLL. Since the LLL as a Hilbert space has dimension N_ϕ , each of the N_ϕ eigenspaces of $T(\mathbf{L}_1/N_\phi)$ within the LLL has to be non-degenerate. Moreover, from Eq. (D2) we can construct another state that has the same eigenvalue as $\phi_j^v(\tilde{x}, \tilde{y})$,

$$\begin{aligned} & T(\mathbf{L}_1/N_\phi) \sum_m^{N_\phi} e^{-i2\pi jm/N_\phi} \phi_m(\tilde{x}, \tilde{y}) \\ & = e^{i2\pi j/N_\phi} \sum_m^{N_\phi} e^{-i2\pi jm/N_\phi} \phi_m(\tilde{x}, \tilde{y}). \end{aligned} \quad (\text{D4})$$

Therefore, we must have

$$\phi_j^v(\tilde{x}, \tilde{y}) \propto \sum_m^{N_\phi} e^{-i2\pi jm/N_\phi} \phi_m(\tilde{x}, \tilde{y}). \quad (\text{D5})$$

The proportionality constant cannot depend on (\tilde{x}, \tilde{y}) . It can be fixed by comparing the two sides at $(\tilde{x}, \tilde{y}) = (0, 0)$. We find

$$\phi_j^v(0, 0) = \frac{1}{(\sqrt{\pi}L_1l_B)^{1/2}} \frac{\xi}{\sqrt{N_\phi}} \vartheta_3\left(\frac{j}{N_\phi} \middle| \frac{i\xi^2}{N_\phi}\right), \quad (\text{D6})$$

$$\phi_m(0, 0) = \frac{1}{(\sqrt{\pi}L_2l_B)^{1/2}} \frac{1}{\xi\sqrt{N_\phi}} \vartheta_3\left(\frac{m}{N_\phi} \middle| \frac{i}{\xi^2N_\phi}\right), \quad (\text{D7})$$

where $\xi = \sqrt{L_1/L_2} e^{i(\pi/4-\theta/2)}$, and $\vartheta_3(z|\tau)$ is the third Jacobi- ϑ function,

$$\vartheta_3(z|\tau) \equiv \sum_n^{\mathbb{Z}} e^{i\pi\tau n^2 + i2\pi n z}, \quad \text{Im } \tau > 0. \quad (\text{D8})$$

Using the discrete Fourier transform formula in Ref. 55, we find

$$\vartheta_3\left(\frac{j}{N_\phi} \middle| \frac{i\xi^2}{N_\phi}\right) = \frac{1}{\xi\sqrt{N_\phi}} \sum_m^{N_\phi} e^{-i2\pi j m/N_\phi} \vartheta_3\left(\frac{m}{N_\phi} \middle| \frac{i}{\xi^2N_\phi}\right).$$

The proportionality constant at $(\tilde{x}, \tilde{y}) = (0, 0)$ is then found to be $e^{i(\pi/4-\theta/2)}/\sqrt{N_\phi}$. This proves the recombination formula of the LLL orbitals Eq. (D1).

Appendix E: Proof of Quasi-Isotropy

In this Appendix we generalize the proof in Sec. VII C to cover $C = \pm 1$ with generic values of δ_x and δ_y . The only hurdle compared with the solved case with $C = 1$ and $\delta_x = \delta_y = 0$ is that the states $|\Psi; s, r\rangle_{\text{lat}}$ and $|\Psi; s, r\rangle'_{\text{lat}}$ reside in different momentum sectors [Eqs. (69) and (122)].

We discuss the case of $C = 1$ and $C = -1$ separately.

We find

$${}_v\langle\{j_v^{Y, k_x}\}|\Psi; s', r'\rangle = {}_v\langle\{YN_x - k_x + \delta_x\}|\Psi; s', r'\rangle = e^{i\beta} e^{-i2\pi\sum(YN_x - k_x)\delta_y/N_\phi} {}_v\langle\{YN_x - k_x\}|\Psi; s, r\rangle. \quad (\text{E6})$$

Plugging in the Fourier transform in Eq. (120) gives

$${}_v\langle\{j_v^{Y, k_x}\}|\Psi; s', r'\rangle = e^{i\beta+i\gamma} \frac{1}{\sqrt{N_\phi}^{N_e}} \sum_{\{X\}} e^{-i2\pi\sum k_x X/N_x} \sum_{\{l_y\}} e^{i2\pi\sum l_y Y/N_y} e^{-i2\pi\sum k_x l_y/N_\phi} \langle\{j^{X, l_y}\}|\Psi; s, r\rangle. \quad (\text{E7})$$

Here we have rewritten each sum over m in the Fourier transform as a double sum over all unit cells X and all l_y points in the principal Brillouin zone, and $e^{i\gamma} = e^{-iN_e(\frac{\pi}{4}-\frac{\theta}{2})}$ is a constant phase factor. Then, the core part of $\langle\{k_x, k_y\}|\Psi; s', r'\rangle'_{\text{lat}}$ becomes

$$\frac{1}{\sqrt{N_y}^{N_e}} \sum_{\{Y\}} e^{-i2\pi\sum k_y Y/N_y} {}_v\langle\{j_v^{Y, k_x}\}|\Psi; s', r'\rangle = e^{i\beta+i\gamma-i2\pi\sum k_x k_y/N_\phi} \frac{1}{\sqrt{N_x}^{N_e}} \sum_{\{X\}} e^{-i2\pi\sum k_x X/N_x} \langle\{j^{X, k_y}\}|\Psi; s, r\rangle. \quad (\text{E8})$$

Plugging the above equation into Eq. (123) gives

1. $C = +1$

Comparing Eqs. (69) and (122), we find that the state $|\Psi; s', r'\rangle'_{\text{lat}}$ with (s', r') given by

$$s' = s - \delta_x, \quad r' = r - \delta_y \quad (\text{E1})$$

has the same total momentum as the state $|\Psi; s, r\rangle_{\text{lat}}$. The above equation replaces Eq. (125) in the main text.

We now examine the corresponding FQH states. Substituting in Eq. (17) gives

$$|\Psi; s', r'\rangle = e^{i\beta} (T_{\text{cm}}^y)^{\delta_x} (T_{\text{cm}}^x)^{-\delta_y} |\Psi; s, r\rangle, \quad (\text{E2})$$

where $e^{i\beta} = e^{i2\pi\delta_x(\kappa_x+rN_e)/N_\phi}$ is an inconsequential phase factor. We find the action of T_{cm}^x and T_{cm}^y on $|\{j\}\rangle_v$ by gauge transforming Eq. (115):

$$T_{\text{cm}}^x |\{j\}\rangle_v = e^{i2\pi\sum j/N_\phi} |\{j\}\rangle_v, \quad T_{\text{cm}}^y |\{j\}\rangle_v = |\{j+1\}\rangle_v. \quad (\text{E3})$$

Therefore,

$${}_v\langle\{j\}|\Psi; s', r'\rangle = e^{i\beta} e^{-i2\pi\sum(j-\delta_x)\delta_y/N_\phi} {}_v\langle\{j-\delta_x\}|\Psi; s, r\rangle. \quad (\text{E4})$$

We now examine the lattice amplitudes $\langle\{k_x, k_y\}|\Psi; s, r\rangle'$ obtained by the Wannier mapping. As explained in Sec. VII C, we put all the momenta (k_x, k_y) in the principal Brillouin zone determined by

$$-k_x + \delta_x \in [0 .. N_x), \quad k_y + \delta_y \in [0 .. N_y). \quad (\text{E5})$$

This enables us to use the Wannier mappings j^{X, k_y} and j_v^{Y, k_x} directly.

Eq. (128) with an inconsequential extra factor $e^{i\beta}$.

2. $C = -1$

In this case, we need to find (s', r') such that

$$\begin{aligned}\kappa_x + (s' + \delta_x)N_e &= -\kappa_x - sN_e \pmod{N_x}, \\ \kappa_y + r'N_e &= -(\kappa_y + (r - \delta_y)N_e) \pmod{N_y}.\end{aligned}\quad (\text{E9})$$

Putting in Eqs. (78) and Eq. (79) gives

$$s' = \bar{s} - \delta_x, r' = \bar{r} + \delta_y, \quad (\text{E10})$$

where (\bar{s}, \bar{r}) are related to (s, r) by

$$\langle \{-j\} | \Psi; s, r \rangle = \zeta_\Psi \langle \{j\} | \Psi; \bar{s}, \bar{r} \rangle. \quad (\text{80})$$

Therefore, the FQH amplitudes of the primed states are given by

$$v\langle \{j\} | \Psi; s', r' \rangle = e^{i\beta} e^{-i2\pi \sum (j - \delta_x) \delta_y / N_\phi} v\langle \{j - \delta_x\} | \Psi; s, r \rangle. \quad (\text{E11})$$

We emphasize that the above steps requires the inversion symmetry of the *FQH states* only; there is no requirement on the FCI system.

The following development largely parallels the $C = +1$ case. Putting all (k_x, k_y) in the principal Brillouin zone, we find

$$v\langle \{j_v^{Y, k_x}\} | \Psi; s', r' \rangle = \zeta_\Psi^{-1} e^{i\beta} e^{+i2\pi \sum (Y N_x - C k_x) \delta_y / N_\phi} v\langle \{-Y N_x + C k_x\} | \Psi; s, r \rangle. \quad (\text{E12})$$

Plugging in the Fourier transform in Eq. (120) gives for $C = -1$

$$v\langle \{j_v^{Y, k_x}\} | \Psi; s', r' \rangle = \zeta_\Psi^{-1} e^{i\beta + i\gamma} \frac{1}{\sqrt{N_\phi^{N_e}}} \sum_{\{X\}} e^{i2\pi C \sum k_x X / N_x} \sum_{\{Y\}} e^{-i2\pi C \sum l_y Y / N_y} e^{i2\pi \sum k_x l_y / N_\phi} \langle \{j^{X, l_y}\} | \Psi; s, r \rangle. \quad (\text{E13})$$

And the core part of $\langle \{k_x, k_y\} | \Psi; s', r' \rangle'_{\text{lat}}$ becomes

$$\frac{1}{\sqrt{N_y^{N_e}}} \sum_{\{Y\}} e^{-i2\pi \sum k_y Y / N_y} v\langle \{j_v^{Y, k_x}\} | \Psi; s', r' \rangle = \frac{e^{i\beta + i\gamma}}{\zeta_\Psi} e^{-i2\pi C \sum k_x k_y / N_\phi} \frac{1}{\sqrt{N_x^{N_e}}} \sum_{\{X\}} e^{-i2\pi \sum k_x X / N_x} \langle \{j^{X, k_y}\} | \Psi; s, r \rangle. \quad (\text{E14})$$

Plugging the above equation into Eq. (123) gives Eq. (128) with an inconsequential extra factor $e^{i\beta} / \zeta_\Psi$.

Appendix F: Continuum Limit

We consider the continuum limit of a Chern insulator, $N_x \rightarrow \infty$, $N_y \rightarrow \infty$ with a fixed aspect ratio N_x / N_y . For simplicity, in the following we focus on the case of a square Bravais lattice, with $\mathbf{b}_1 \cdot \mathbf{b}_2 = 0$ and $|\mathbf{b}_1| = |\mathbf{b}_2|$. The formulas in the generic case can be obtained without much extra effort. We define the continuous coordinates $\tilde{x} \in [0, N_x)$, $\tilde{y} \in [0, N_y)$, and the continuous momenta $\tilde{k}_x, \tilde{k}_y \in [0, 2\pi)$,

$$\tilde{k}_x = 2\pi k_x / N_x, \quad \tilde{k}_y = 2\pi k_y / N_y. \quad (\text{F1})$$

Normally, the continuum limit involves sending the unit cell size to zero. To make direct comparison with the formulas in Ref. 15, however, we do not take the limit of the unit cell size going zero, and work instead in a unit system in which $|\mathbf{b}_1| = |\mathbf{b}_2| = 1$.

1. Berry Connection

We show that the discrete connections defined in Eq. (26) reduce to the Berry connection in the usual definition in the continuum limit.

Recall that the Bloch state is given by

$$|\tilde{k}_x, \tilde{k}_y\rangle = \sum_{\alpha} u_{\alpha}(\tilde{k}_x, \tilde{k}_y) |\tilde{k}_x, \tilde{k}_y, \alpha\rangle \quad (\text{F2})$$

$$= \frac{1}{\sqrt{N_x N_y}} \sum_{x, y} \sum_{\alpha} e^{i\tilde{k}_x x + i\tilde{k}_y y} u_{\alpha}(\tilde{k}_x, \tilde{k}_y) |x, y, \alpha\rangle. \quad (\text{F3})$$

The single-particle orbitals are defined by the real-space wave functions.

$$\langle \tilde{x}, \tilde{y} | x, y, \alpha \rangle = \phi_{\alpha}(\tilde{x} - x - \epsilon_{\alpha}^x, \tilde{y} - y - \epsilon_{\alpha}^y). \quad (\text{F4})$$

Here the function $\phi_{\alpha}(\tilde{x}, \tilde{y})$ is centered around $\tilde{x} = \tilde{y} = 0$ and we have made explicit the sublattice shift $\epsilon_{\alpha}^{x, y}$.

We assume that the orbitals are orthonormal in the sense that

$$\langle x, y, \alpha | x', y', \beta \rangle = \delta_{\alpha\beta} \delta_{xx'} \delta_{yy'}. \quad (\text{F5})$$

And in the spirit of tight-binding approximation, we further assume that the orbitals are localized enough such that

$$\begin{aligned}\langle x, y, \alpha | \tilde{x} | x', y', \alpha \rangle &= (x + \epsilon_\alpha^x) \delta_{\alpha\beta} \delta_{xx'} \delta_{yy'}, \\ \langle x, y, \alpha | \tilde{y} | x', y', \alpha \rangle &= (y + \epsilon_\alpha^y) \delta_{\alpha\beta} \delta_{xx'} \delta_{yy'}.\end{aligned}\quad (\text{F6})$$

We can calculate the Berry connection $\mathbf{a} = (a_x, a_y)$ using the usual definition

$$\mathbf{a}(\tilde{k}_x, \tilde{k}_y) = -i \langle u_{\tilde{k}_x, \tilde{k}_y} | \nabla_{\tilde{k}} | u_{\tilde{k}_x, \tilde{k}_y} \rangle, \quad (\text{F7})$$

where the periodic part of the Bloch state is given by

$$|u_{\tilde{k}_x, \tilde{k}_y}\rangle = e^{-i\tilde{k}_x \tilde{x} - i\tilde{k}_y \tilde{y}} |\tilde{k}_x, \tilde{k}_y\rangle. \quad (\text{F8})$$

The result is

$$\begin{aligned}a_x(\tilde{k}_x, \tilde{k}_y) &= -\sum_{\alpha} u_{\alpha}^*(\tilde{k}_x, \tilde{k}_y) (i\partial_{\tilde{k}_x} + \epsilon_{\alpha}^x) u_{\alpha}(\tilde{k}_x, \tilde{k}_y), \\ a_y(\tilde{k}_x, \tilde{k}_y) &= -\sum_{\alpha} u_{\alpha}^*(\tilde{k}_x, \tilde{k}_y) (i\partial_{\tilde{k}_y} + \epsilon_{\alpha}^y) u_{\alpha}(\tilde{k}_x, \tilde{k}_y).\end{aligned}\quad (\text{F9})$$

We assume that the Bloch state $|\tilde{k}_x, \tilde{k}_y\rangle$ is periodic in the \tilde{k}_x direction, and satisfies

$$a_y(\tilde{k}_x, \tilde{k}_y) = 0 \quad (\text{F10})$$

in the \tilde{k}_y direction (similar to the Landau gauge). The Stokes' theorem is applicable, but the non-zero Chern number does not obstruct the construction of a smooth gauge, as we have abandoned the periodic gauge condition in the \tilde{k}_y direction. This is exactly the same boundary condition adopted in Ref. 15.

Since the exponentiated Berry connection restores unitarity in the continuum limit, we can relate its phase to $\mathbf{a}(\tilde{k}_x, \tilde{k}_y)$. To order $\mathcal{O}(1/N_x)$, we have

$$\begin{aligned}\mathcal{A}_x(\tilde{k}_x, \tilde{k}_y) &= \sum_{\alpha} e^{-i2\pi\epsilon_{\alpha}^x/N_x} u_{\alpha}^*(\tilde{k}_x, \tilde{k}_y) u_{\alpha}(\tilde{k}_x + \frac{2\pi}{N_x}, \tilde{k}_y) \\ &\approx 1 - i \frac{2\pi}{N_x} \sum_{\alpha} u_{\alpha}^*(\tilde{k}_x, \tilde{k}_y) (i\partial_{\tilde{k}_x} + \epsilon_{\alpha}^x) u_{\alpha}(\tilde{k}_x, \tilde{k}_y) \\ &\approx e^{i2\pi a_x(\tilde{k}_x, \tilde{k}_y)/N_x}.\end{aligned}\quad (\text{F11})$$

Similarly, to order $\mathcal{O}(1/N_y)$,

$$\mathcal{A}_y(\tilde{k}_x, \tilde{k}_y) \approx e^{i2\pi a_y(\tilde{k}_x, \tilde{k}_y)/N_y}. \quad (\text{F12})$$

In the thermodynamic limit, the above approximate relations become exact.

2. Wilson Loops

Define the phase angle (polarization)

$$\theta(\tilde{k}_y) = \int_0^{2\pi} d\tilde{p}_x a_x(\tilde{p}_x, \tilde{k}_y) \quad (\text{F13})$$

The Wilson loop along a fixed \tilde{k}_y is given by

$$W_x(\tilde{k}_y) = e^{i\theta(\tilde{k}_y)}. \quad (\text{F14})$$

The Bloch state $|\tilde{k}_x, \tilde{k}_y + 2\pi\rangle$ is connected to the state $|\tilde{k}_x, \tilde{k}_y\rangle$ by a gauge transform. Specifically, since we assume $a_y(\tilde{k}_x, \tilde{k}_y) = 0$, we have

$$\begin{aligned}W_y(\tilde{k}_x) &= \exp\left[i \int_{\tilde{k}_y}^{\tilde{k}_y+2\pi} d\tilde{p}_y a_y(\tilde{k}_x, \tilde{p}_y)\right] |\tilde{k}_x, \tilde{k}_y + 2\pi\rangle \\ &= |\tilde{k}_x, \tilde{k}_y + 2\pi\rangle.\end{aligned}\quad (\text{F15})$$

The gauge transform is thus given explicitly by

$$|\tilde{k}_x, \tilde{k}_y + 2\pi\rangle = [W_y(\tilde{k}_x)]^* |\tilde{k}_x, \tilde{k}_y\rangle. \quad (\text{F16})$$

The Wilson loop $W_x(\tilde{k}_y)$ is gauge invariant. Naively, one might expect that the phase angle $\theta(\tilde{k}_y)$ is also periodic. However, in the continuum limit, this is *not* true. As explained in Sec. III C, when \tilde{k}_y gradually increases by 2π , $W_x(\tilde{k}_y)$ winds around the unit circle at the origin of the complex plane. The winding number in the clockwise direction is given by the Chern number C . Since we assume the smooth gauge for the Bloch states, $\theta(\tilde{k}_y)$ must be smooth as well. Therefore, we have the quasi-periodic condition¹⁵

$$\theta(\tilde{k}_y + 2\pi) = \theta(\tilde{k}_y) - 2\pi C. \quad (\text{F17})$$

In the light of Eq. (F16), this can also be understood as

$$\theta(\tilde{k}_y) \rightarrow \theta(\tilde{k}_y) - 2\pi C \quad (\text{F18})$$

under the gauge transformation

$$|\tilde{k}_x, \tilde{k}_y\rangle \rightarrow [W_y(\tilde{k}_x)]^* |\tilde{k}_x, \tilde{k}_y\rangle. \quad (\text{F19})$$

3. Maximally Localized Wannier States

In the continuum limit (which unfortunately cannot be used to compute overlaps with the exact ground states from numerical diagonalization on the finite-size lattice), the projected position operator $\hat{\mathcal{X}} = P\hat{x}P$ becomes unitary. Therefore, the eigenstates $|X, k_y\rangle$ of $\hat{\mathcal{X}}$ (the unitary part of $\hat{\mathcal{X}}$) are just the eigenstates of $\hat{\mathcal{X}}$, the 1D *maximally* localized Wannier states. The change in the gauge condition in the \tilde{k}_y direction does not affect the form of the Wannier states, as the construction is performed independently at each \tilde{k}_y . We can rewrite the definition in Eq. (32) using the continuum variables,

$$|X, \tilde{k}_y\rangle = \frac{1}{\sqrt{N_x}} \sum_{\tilde{k}_x}^{N_x} \exp \left[-i\tilde{k}_x X + i\tilde{k}_x \frac{\theta(\tilde{k}_y)}{2\pi} - i \int_0^{\tilde{k}_x} d\tilde{p}_x a_x(\tilde{p}_x, \tilde{k}_y) \right] |\tilde{k}_x, \tilde{k}_y\rangle. \quad (\text{F20})$$

This expression is exactly the same as in Ref. 15. The center position of this state can be related to the phase angle by $\theta(\tilde{k}_y)$

$$\langle X, \tilde{k}_y | \tilde{x} | X, \tilde{k}_y \rangle = X - \frac{\theta(\tilde{k}_y)}{2\pi}. \quad (\text{F21})$$

We now move on to discuss the gauge transform of these Wannier states. This is where the current discussion diverges from Sec. III and Ref. 15. Consider a gauge transformation

$$|\tilde{k}_x, \tilde{k}_y\rangle \rightarrow e^{i\eta(\tilde{k}_x, \tilde{k}_y)} |\tilde{k}_x, \tilde{k}_y\rangle. \quad (\text{F22})$$

The Berry connection transforms by

$$\mathbf{a}(\tilde{k}_x, \tilde{k}_y) \rightarrow \mathbf{a}(\tilde{k}_x, \tilde{k}_y) + \nabla_{\tilde{k}} \eta(\tilde{k}_x, \tilde{k}_y), \quad (\text{F23})$$

and thus

$$\int_0^{\tilde{k}_x} d\tilde{p}_x a_x(\tilde{p}_x, \tilde{k}_y) \rightarrow \int_0^{\tilde{k}_x} d\tilde{p}_x a_x(\tilde{p}_x, \tilde{k}_y) + \eta(\tilde{k}_x, \tilde{k}_y) - \eta(0, \tilde{k}_y). \quad (\text{F24})$$

In particular, for $\tilde{k}_x = 2\pi$,

$$\theta(\tilde{k}_y) \rightarrow \theta(\tilde{k}_y) + \eta(2\pi, \tilde{k}_y) - \eta(0, \tilde{k}_y). \quad (\text{F25})$$

This is consistent with Eq. (F18). Putting all of these together, we find that

$$|X, \tilde{k}_y\rangle \rightarrow e^{i\eta(0, \tilde{k}_y)} |X - \frac{1}{2\pi} [\eta(2\pi, \tilde{k}_y) - \eta(0, \tilde{k}_y)], \tilde{k}_y\rangle. \quad (\text{F26})$$

This is *fundamentally different* from the transformation in the periodic, non-smooth gauge on a lattice [Eq. (39)]: in addition to acquiring a phase, the Wannier state may hop to a different unit cell upon a gauge transformation. The transformation given in Eq. (F26) differs from that of Ref. 15.

The discrepancy between Eq. (39) and Eq. (F26) comes from the smooth gauge condition. Due to the winding motion, the argument angle of $W_x(\tilde{k}_y)$ is multi-valued by nature. At finite size, we require $\lambda_x(k_y)$ to be the N_x -th root of $W_x(k_y)$ with argument angle in $(-2\pi/N_x, 0]$. This corresponds to confining the argument angle of $W_x(k_y)$ to the branch $(-2\pi, 0]$. In the continuum limit,

$$[\lambda_x(k_y)]^{k_x} = [W_x(k_y)]^{k_x/N_x} \rightarrow [e^{i\theta(\tilde{k}_y)}]^{k_x/(2\pi)}. \quad (\text{F27})$$

The smooth gauge condition in the continuum requires $\theta(\tilde{k}_y)$ to be smooth as well, and thus makes it impossible to fix $\theta(\tilde{k}_y)$ to $(-2\pi, 0]$.

4. Curvature Fluctuations

We now derive the connection between Wannier states, the continuum analogue of Eq. (52). Similar to Eq. (F7), we use the periodic part of $|X, \tilde{k}_y\rangle$ and calculate

$$\tilde{a}_y(X, \tilde{k}_y) \equiv -i \langle X, \tilde{k}_y | e^{i\tilde{k}_y \tilde{y}} \partial_{\tilde{k}_y} e^{-i\tilde{k}_y \tilde{y}} | X, \tilde{k}_y \rangle. \quad (\text{F28})$$

From Eq. (F20), we obtain

$$\tilde{a}_y(X, \tilde{k}_y) = \partial_{\tilde{k}_y} \Phi_y(X, \tilde{k}_y) + \frac{1}{2\pi} \int_0^{2\pi} d\tilde{k}_x \left[\frac{\tilde{k}_x}{2\pi} \partial_{\tilde{k}_y} \theta(\tilde{k}_x, \tilde{k}_y) - \int_0^{\tilde{k}_x} d\tilde{p}_x \partial_{\tilde{k}_y} a_x(\tilde{p}_x, \tilde{k}_y) + a_y(\tilde{k}_x, \tilde{k}_y) \right]. \quad (\text{F29})$$

Here we have used the limit $\frac{1}{N_x} \sum_{k_x}^{N_x} \rightarrow \frac{1}{2\pi} \int_0^{2\pi} d\tilde{k}_x$ to make the notations coherent. Recall that $a_y(\tilde{k}_x, \tilde{k}_y) = 0$, the third term in the bracket vanishes, while the first two terms can be related to the Berry curvature

$$f_{xy}(\tilde{k}_x, \tilde{k}_y) = \partial_{\tilde{k}_x} a_x(\tilde{k}_x, \tilde{k}_y) - \partial_{\tilde{k}_y} a_y(\tilde{k}_x, \tilde{k}_y). \quad (\text{F30})$$

We end up with

$$\tilde{a}_y(X, \tilde{k}_y) = \partial_{\tilde{k}_y} \Phi_y(X, \tilde{k}_y) + \frac{1}{2\pi} \int_0^{2\pi} d\tilde{k}_x \int_0^{\tilde{k}_x} d\tilde{p}_x \left[f_{xy}(\tilde{p}_x, \tilde{k}_y) - \bar{f}_{xy}(\tilde{k}_y) \right], \quad (\text{F31})$$

where the average Berry curvature $\bar{f}_{xy}(\tilde{k}_y)$ is defined by

$$\bar{f}_{xy}(\tilde{k}_y) = \frac{1}{2\pi} \int_0^{2\pi} d\tilde{k}_x f_{xy}(\tilde{k}_x, \tilde{k}_y). \quad (\text{F32})$$

Similar to the discrete case, the fluctuation of Berry curvature appears in the connection between adjacent Wannier states, even more sharply than the finite-size formula in terms of $W_{\blacksquare}(k_x, k_y)$ and $\bar{W}_{\blacksquare}(k_x, k_y)$.

We stop the exposition of the continuum case here, as the rest of the construction could be obtained directly by taking the continuum limit of the finite-size formulas.

Appendix G: Comments on Qi's Prescription

In this Appendix we discuss issues in Ref. 15 that we have found while trying to extend the prescription to the torus geometry.

The original proposal was to map the eigenstates of the projected position operator in the gauge $a_y = 0$ to the states in the LLL, and use these Wannier states to build the *cylinder* FQH states on a lattice. One would expect a similar construction would hold for the *torus* FQH states. As pointed out in the main text, the subtle points are that we need to apply the phase fix discussed in Sec. III A to restore orthogonality of the Wannier states, and that we have to modify the Wannier-LLL index mapping according to Eq. (43).

Based on the observation that the Wannier center shift by one unit cell when \tilde{k}_y increases by 2π , Eq. (3) in Ref. 15 claimed that $|X, \tilde{k}_y + 2\pi\rangle = |X + C, \tilde{k}_y\rangle$. However, as pointed out in Appx. F 2, we can think of $k_y \rightarrow \tilde{k}_y + 2\pi$ as the gauge transform in Eq. (F19), and thus the Wannier state $|X, \tilde{k}_y + 2\pi\rangle$ is given by Eq. (F26),

$$|X, \tilde{k}_y + 2\pi\rangle = [W_y(0)]^* |X + C, \tilde{k}_y\rangle. \quad (\text{G1})$$

Ref. 15 missed the extra factor $[W_y(0)]^*$.

This seemingly innocent problem is actually catastrophic, unless $W_y(0) = 1$. It is directly responsible for the low overlap between the constructed many-body state and the ground states for several important FCI models examined in Sec. VI A. Assuming $|X, \tilde{k}_y + 2\pi\rangle = |X + C, \tilde{k}_y\rangle$ as in Ref. 15, we can limit k_y to a *single* Brillouin zone when building the $N_x N_y$ Wannier states.

Consider the simplest case with Chern number $C = +1$ and the shift parameter $\delta_y = 0$. The principal Brillouin zone is given by $(k_x, k_y) \in [0 .. N_x) \times [0 .. N_y)$. We need to implement of the gauge condition $a_y = 0$ on the lattice. The lattice analogue of $a_y = 0$ is setting the exponentiated connection $A_y = 1$. As pointed out in Sec. III B, we only need to enforce this condition along $k_x = 0$. Namely, we should fix the phase of $|0, k_y + 1\rangle$ relative to $|0, k_y\rangle$ by requiring $A_y(0, k_y) = 1$. Starting from the Bloch state at $(k_x, k_y) = (0, 0)$, this can be done recursively in the interior of the principal Brillouin zone till we reach the boundary $(k_x, k_y) = (0, N_y - 1)$. This introduces a *jump* in the phase of $A_y(0, k_y)$ at the

boundary of Brillouin zone. The Berry connection along $k_x = 0$ is given by $A_y(0, k_y) = A_y(0, k_y + N_y)$ and

$$A_y(0, k_y) = \begin{cases} 1 & \text{if } k_y \in [0 .. N_y - 1), \\ W_y(0) & \text{if } k_y = N_y - 1. \end{cases} \quad (\text{G2})$$

The value of $A_y(0, N_y - 1)$ reflects the relative phase of the Bloch state at $(0, N_y)$ as fixed by the periodic boundary and the (gauge-invariant) Wilson loop. We emphasize that $A_y(0, N_y - 1)$ is the connection between the Bloch states at momenta $(0, N_y - 1)$ and $(0, 0)$, rather than the states at $(0, N_y - 1)$ and $(0, N_y)$; the value of $A_y(0, N_y - 1)$ in Eq. (G2) is not in conflict with $a_y = 0$.

In this particular gauge of Bloch states, the original construction amounts to Eq. (32) with $e^{i\Phi_y(X, k_y)} = 1$. The analysis in Sec. IV C shows that for this choice of $e^{i\Phi_y(X, k_y)}$, the resulting many-body wave function is indeed translationally invariant, in agreement with the claim in the original paper.¹⁵ However, the connection between adjacent Wannier states $\langle X, k_y | \hat{Y} | X', k'_y \rangle \propto A_y(0, k_y)$ changes abruptly at the Brillouin zone boundary $k_y = N_y - 1$. Unless $W_y(0) = 1$, this strong k_y dependence sets the Wannier states apart from the Landau orbitals, as shown in Sec. IV B, and destroys the FQH character of the constructed lattice trial state, in accordance with the numerical results presented in Sec. VI A.

We now check the inversion symmetry. Putting $e^{i\Phi_y(X, k_y)} = 1$ in Eq. (99), we have

$$e^{i\xi_{0, k_y}} \mathcal{P} |X, k_y\rangle = \begin{cases} |-X, -k_y\rangle & \text{if } W_x(k_y) = 1, \\ |-X - 1, -k_y\rangle & \text{otherwise.} \end{cases} \quad (\text{G3})$$

Recall that the sewing matrix elements $e^{i\xi_{0, k_y}}$ are related to the Berry connections. Plugging Eq. (G2) into Eq. (87), we find

$$e^{i\xi_{0, k_y}} = \begin{cases} e^{i\xi_{0, 0}} & \text{if } k_y = 0 \bmod N_y, \\ W_y(0) e^{i\xi_{0, 0}} & \text{otherwise.} \end{cases} \quad (\text{G4})$$

Restricted by the inversion symmetry, $W_y(0)$ can be ± 1 . If $W_y(0) = 1$, then all the analysis of *our proposal* in the main text can be reused to show that the original prescription in this case preserves the inversion symmetry on the many-body level. If $W_y(0) = -1$, however, the constructed many-body wave function breaks inversion symmetry. The reason is very simple: since $|X, k_y\rangle$ receives a different coefficients upon inversion depending on whether $k_y = 0 \bmod N_y$, different components of the many-body wave function transforms differently under inversion. We expect the degree of the inversion breaking to decrease as the system size increases.

It should be obvious that the above problems in original proposal is not limited to the case $C = 1$ and $\delta_y = 0$; it erupts whenever $W_y(0) = -1$.

Finally, we note that in a related paper,²² a slightly modified formula for the 1D localized Wannier states were proposed for a generic gauge condition on a_y . In our notations, the updated formula reads

$$|X, \tilde{k}_y\rangle = \exp \left[i\tilde{k}_y \frac{\theta_y}{2\pi} - i \int_0^{\tilde{k}_y} d\tilde{p}_y a_y(0, \tilde{p}_y) \right] \frac{1}{\sqrt{N_x}} \sum_{\tilde{k}_x}^{N_x} \exp \left[-i\tilde{k}_x X + i\tilde{k}_x \frac{\theta(\tilde{k}_y)}{2\pi} - i \int_0^{\tilde{k}_x} d\tilde{p}_x a_x(\tilde{p}_x, \tilde{k}_y) \right] |\tilde{k}_x, \tilde{k}_y\rangle. \quad (\text{G5})$$

Here the real number θ_y is defined by

$$\theta_y = \int_0^{2\pi} d\tilde{p}_y a_y(0, \tilde{p}_y). \quad (\text{G6})$$

The exponential prefactor in Eq. (G5) was introduced to fix the gauge choice between the Wannier states at different \tilde{k}_y .²² Judging by appearance, the formula may look similar to ours [Eqs. (32) and Eq. (63)] at first sight. However, further scrutiny reveals a fundamental difference. The continuum formalism in Refs. 15 and 22 requires a smooth gauge that is periodic in the \tilde{k}_x direction. Stokes' theorem then dictates that the gauge cannot be periodic in the k_y direction. In particular, $a_y(0, \tilde{p}_y)$ is not periodic. Therefore, the phase $e^{i\theta_y}$ is *not* the Wilson loop along $\tilde{k}_x = 0$ and is *not* gauge invariant. We can actually remove the added exponential prefactor in Eq. (G5) altogether, by going back to the $a_y = 0$ gauge. Therefore, the updated formula for the Wannier state in Ref. 22 is actually no different from the original one in Ref. 15, and they suffer from the same problem detailed earlier.

Appendix H: Overlap between Random Vectors

Consider two random unit vectors sampled independently and uniformly from the vector space \mathbb{C}^d . We are interested in the probability distribution of the absolute

square of the inner product (the overlap) between them. We seek an expression for the probability $p_d(u)$ for the overlap to be larger than u .

Since the absolute square does not see the relative phase between the two vectors, we only need to study \mathbb{R}^d . The uniform sampling of unit vectors in \mathbb{C}^d corresponds to the uniform sampling *by area* over S^d , the unit $(d-1)$ -dimensional sphere surface embedded in \mathbb{R}^d . We build a Cartesian coordinate system (x_1, x_2, \dots, x_d) with the x_1 axis pointing in the direction of one of the two vectors. Then we can see clearly that $p_d(u)$ is just two times the surface area of the hyperspherical cap on S^d of height $(1 - \sqrt{u})$, divided by the surface area of S^d . Using the hyperspherical polar coordinates, we find that

$$p_d(u) = \frac{2S_{d-1}}{S_d} \int_{\sqrt{u}}^1 dx (1-x^2)^{(d-3)/2}, \quad (\text{H1})$$

where S_n is the surface area of S^n , given by

$$S_n = \frac{n\pi^{n/2}}{\Gamma(\frac{n}{2} + 1)}. \quad (\text{H2})$$

This can be evaluated using numerical quadrature. We note that at large d , the probability $p_d(u)$ to have overlap higher than u is *exponentially* small, bounded from above by

$$\mathcal{O}[(1-u)^{(d-1)/2}]. \quad (\text{H3})$$

-
- ¹ F. D. M. Haldane, Physical Review Letters **61**, 2015 (1988).
² D. N. Sheng, Z.-C. Gu, K. Sun, and L. Sheng, Nature Communications **2**, 389 (2011).
³ T. Neupert, L. Santos, C. Chamon, and C. Mudry, Physical Review Letters **106**, 236804 (2011).
⁴ N. Regnault and B. A. Bernevig, Phys. Rev. X **1**, 021014 (2011).
⁵ J. Venderbos, S. Kourtis, J. van den Brink, and M. Daghofer, Physical Review Letters **108**, 126405 (2012).
⁶ Y.-F. Wang, Z.-C. Gu, C.-D. Gong, and D. N. Sheng, Physical Review Letters **107**, 146803 (2011).
⁷ Y.-L. Wu, B. Bernevig, and N. Regnault, Physical Review B **85**, 075116 (2012).
⁸ R. B. Laughlin, Physical Review Letters **50**, 1395 (1983).
⁹ B. A. Bernevig and N. Regnault, Physical Review B **85**, 075128 (2012).
¹⁰ H. Li and F. D. M. Haldane, Physical Review Letters **101**, 1010504 (2008).
¹¹ B. A. Bernevig and F. D. M. Haldane, Physical Review Letters **100**, 246802 (2008).
¹² B. A. Bernevig and F. D. M. Haldane, Physical Review Letters **101**, 246806 (2008).
¹³ A. Kol and N. Read, Phys. Rev. B **48**, 8890 (1993).
¹⁴ G. Möller and N. Cooper, Physical Review Letters **103**, 105303 (2009).
¹⁵ X.-L. Qi, Physical Review Letters **107**, 126803 (2011).
¹⁶ F. D. M. Haldane, Phys. Rev. Lett. **55**, 2095 (1985).
¹⁷ S. Kivelson, Physical Review B **26**, 4269 (1982).
¹⁸ N. Marzari and D. Vanderbilt, Physical Review B **56**, 12847 (1997).
¹⁹ R. Yu, X. L. Qi, A. Bernevig, Z. Fang, and X. Dai, Physical Review B **84**, 075119 (2011).
²⁰ S. A. Parameswaran, R. Roy, and S. L. Sondhi, ArXiv e-prints (2011), 1106.4025.
²¹ M. O. Goerbig, The European Physical Journal B **85** (2012).
²² M. Barkeshli and X. L. Qi, ArXiv e-prints (2011),

- 1112.3311.
- ²³ Y.-F. Wang, H. Yao, Z.-C. Gu, C.-D. Gong, and D. Sheng, *Physical Review Letters* **108**, 126805 (2012).
- ²⁴ T. Hughes, E. Prodan, and B. Bernevig, *Physical Review B* **83**, 245132 (2011).
- ²⁵ A. Alexandradinata, X. Dai, and B. A. Bernevig (2012), unpublished.
- ²⁶ K. Sun, Z. Gu, H. Katsura, and S. Das Sarma, *Physical Review Letters* **106**, 236803 (2011).
- ²⁷ B. A. Bernevig, T. L. Hughes, and S.-C. Zhang, *Science* **314**, 1757 (2006).
- ²⁸ E. Tang, J.-W. Mei, and X.-G. Wen, *Physical Review Letters* **106**, 236802 (2011).
- ²⁹ X. Hu, M. Kargarian, and G. A. Fiete, *Physical Review B* **84**, 155116 (2011).
- ³⁰ J. A. Nelder and R. Mead, *The Computer Journal* **7**, 308 (1965).
- ³¹ S. H. Simon, E. H. Rezayi, N. R. Cooper, and I. Berdnikov, *Physical Review B* **75**, 075317 (2007).
- ³² N. Regnault, B. Bernevig, and F. Haldane, *Physical Review Letters* **103**, 016801 (2009).
- ³³ A. Sterdyniak, N. Regnault, and B. A. Bernevig, *Physical Review Letters* **106**, 100405 (2011).
- ³⁴ B. A. Bernevig and N. Regnault, *ArXiv e-prints* (2012), 1204.5682.
- ³⁵ J. K. Jain, *Phys. Rev. Lett.* **63**, 199 (1989).
- ³⁶ G. Moore and N. Read, *Nuclear Physics B* **360**, 362 (1991).
- ³⁷ N. Read and E. Rezayi, *Physical Review B* **59**, 8084 (1999).
- ³⁸ T. Liu, C. Repellin, B. A. Bernevig, and N. Regnault, *ArXiv e-prints* (2012), 1206.2626.
- ³⁹ F. Wang and Y. Ran, *ArXiv e-prints* (2011), 1109.3435.
- ⁴⁰ Y. F. Wang, H. Yao, C. D. Gong, and D. N. Sheng, *ArXiv e-prints* (2012), 1204.1697.
- ⁴¹ S. Yang, Z. C. Gu, K. Sun, and S. Das Sarma, *ArXiv e-prints* (2012), 1205.5792.
- ⁴² M. Trescher and E. J. Bergholtz, *ArXiv e-prints* (2012), 1205.2245.
- ⁴³ Z. Liu, E. J. Bergholtz, H. Fan, and A. M. Laeuchli, *ArXiv e-prints* (2012), 1206.3759.
- ⁴⁴ T. Neupert, L. Santos, S. Ryu, C. Chamon, and C. Mudry, *Physical Review B* **84**, 165107 (2011).
- ⁴⁵ L. Santos, T. Neupert, S. Ryu, C. Chamon, and C. Mudry, *ArXiv e-prints* (2011), 1108.2440.
- ⁴⁶ T. Neupert, L. Santos, S. Ryu, C. Chamon, and C. Mudry, *ArXiv e-prints* (2012), 1202.5188.
- ⁴⁷ B. Estienne, N. Regnault, and B. A. Bernevig, *ArXiv e-prints* (2012), 1202.5543.
- ⁴⁸ Y. M. Lu and Y. Ran, *ArXiv e-prints* (2011), 1109.0226.
- ⁴⁹ J. McGreevy, B. Swingle, and K. A. Tran, *ArXiv e-prints* (2011), 1109.1569.
- ⁵⁰ X. G. Wen, *Phys. Rev. Lett.* **66**, 802 (1991).
- ⁵¹ X.-G. Wen, *Phys. Rev. B* **60**, 8827 (1999).
- ⁵² D. Yoshioka, B. I. Halperin, and P. A. Lee, *Physical Review Letters* **50**, 1219 (1983).
- ⁵³ D. Yoshioka, *The Quantum Hall Effect (Springer Series in Solid-State Sciences)* (Springer, 2010), ISBN 364207720X.
- ⁵⁴ F. D. M. Haldane, *Phys. Rev. Lett.* **51**, 605 (1983).
- ⁵⁵ M. Ruzzi, *Journal of Mathematical Physics* **47**, 063507 (2006).
- ⁵⁶ It is always possible to line up \mathbf{L}_2 with the \hat{e}_y axis for a torus of any aspect ratio.
- ⁵⁷ Notice that the original treatment in Ref. 16 put an additional factor of $(-1)^{pq(N_e-1)}$ in the formula, but this is not necessary for our purposes: (κ_x, κ_y) are defined by Eq. (7). Our choice can be regarded as an alternative labeling aimed to simplify the formulas in this paper, at the cost of the identity of (κ_x, κ_y) as true momentum.
- ⁵⁸ We emphasize that the operators S_x and R_y are defined in the continuum. In contrast to the discussions in Ref. 9, here we do not add a lattice pinning potential to the FQH setup. Were we to do that, S_x and R_y would not be legitimate translation operators as they contain one-body translations that are a fraction of a unit cell size. We bridge the FQH and the FCI sides through the properties of the second-quantized amplitudes, without directly migrating the continuum translation operators and their algebra to the lattice.
- ⁵⁹ A notable special case is when q divides N_y . Since $\text{GCD}(N_y, q) = \text{GCD}(pN_y, q) = N_y N_{0x}/N = q/q_x$, in this case we have $q_x = 1$, and thus $S_x = (T_{\text{rel}}^x)^\dagger$ and $R_y = T_{\text{cm}}^y$. Hence, the original q -fold states diagonal in $(T_{\text{rel}}^x, T_{\text{cm}}^y)$ are already the simultaneous eigenstates of S_x and R_y without any recombination.
- ⁶⁰ We thank F.D.M. Haldane for stressing the importance of this point to us.
- ⁶¹ The non-unitary connection $\mathcal{A}_a(k_x, k_y)$ ($a = x, y$) may vanish on a very small lattice. This problem is most pronounced on an $N_x \times N_y = 2 \times 2$ lattice with inversion symmetry. In this case, all the four Bloch states are inversion eigenstates. The connection \mathcal{A}_a between two Bloch states vanishes when the two states belong to different inversion eigenvalues. We do not consider such pathological cases in our treatment.
- ⁶² Arguably we could also use the aspect ratio as a variational parameter. We leave this for future work.
- ⁶³ The absolute value of $\langle X, k_y | \hat{Y} | X', k'_y \rangle$ does not depend on the choice of the phase $e^{i\Phi_y(X, k_y)}$. It is given by $|\mathcal{U}_y(k_y)|$.
- ⁶⁴ In the case of many occupied bands, the inversion operator is a matrix, but in the absence of additional symmetries in 2D, it can always be represented in a diagonal $[U(1)]^{N_{\text{occupied}}}$ form.²⁴
- ⁶⁵ The two-orbital model is not included in the 6×3 calculations, because this model does not have a gapped topological ground state at this lattice size.
- ⁶⁶ Notice that this quantity cannot be generalized to the case with more than one state in a momentum sector, for example the Laughlin FCI state on a 6×3 lattice, as the absolute value operation breaks the orthogonality between the degenerate states at the same momentum.
- ⁶⁷ Even when the C_4 symmetry is present in the hopping amplitudes locally, the lattice aspect ratio has to be fixed to specific values (square, for example) for the symmetry to survive at finite size.